IONTOPHORETIC STUDIES OF VISUAL NEURONS IN *DROSOPHILA MELANOGASTER*

Thesis by

Robert Lewis Powers

In Partial Fulfillment of the Requirements

for the Degree of

Doctor of Philosophy

California Institute of Technology

Pasadena, California

1979

(Submitted May 22, 1979)

To the loving memory of my mother,

Mrs. Mary Louise Lewis Powers

August 3, 1920

December 17, 1975

ACKNOWLEDGMENTS

I am deeply grateful to Professor G. D. McCann for his generous support and guidance during the course of my graduate study. I thank also Dr. K.-I. Naka and Dr. D. H. Fender for their important contributions, both professional and personal.

This thesis would not have been possible without the high level of competence of the members of the laboratory in which the work was conducted. The names of Mr. Dan Aranovich, Mr. Al Broers, Mr. Ben Ellert, Mr. Ron Fargason, and Mr. Dale Knutsen are found throughout the following text. To these people I offer special thanks for their outstanding contributions to the research environment and for their continuing assistance to my work. I thank also Mrs. Evelyn Johnson for her always gracious help.

I thank Dr. A. J. Hudspeth for his care and help in drafting the final manuscript. I thank Kathy Lewis, whose competence and patience in typing the final version will be evident to the reader.

I appreciate the assistance of many more people mentioned here. The invaluable contributions of Mr. A. Chodos, Dr. D. Cohen, Ms. S. Garcia, Mr. F. Hayes, Dr. Susanne Hering, Dr. R. Larkin, Dr. R. Pierantoni and Dr. M. Shippey are documented in the thesis. I thank Dr. M. Hyson for the use of his graphics materials. Mr. Larry White has contributed programming support. Dr. C.-F. Wu has been helpful in many discussions.

I am indebted to Dr. W. L. Pak, Dr. S. Benzer and Miss Eveline Eichenberger for preparing flies. I thank in particular Dr. Mike Wilcox, who demonstrated to me the preparation of Drosophila for recording.

The California Institute of Technology provides a stimulating environment for the conduct of one's work. I thank the Institute for its

support and for the opportunity of being associated with it.

Finally, I wish to express the thanks that are the most deeply felt, to Mrs. Nancy Carroway.

ABSTRACT

The physiology of single cells in the visual system of the fly Drosophila melanogaster is studied by intracellular recording. Iontophoresis or current passage from the micropipette is used in two distinct ways. The first of these is to yield a short injection of free calcium ion into the photoreceptor or primary sensory neuron. Iontophoresis of Ca^{++} is shown to have a pronounced but reversible effect upon the receptor potential response to light input. The transient change is characterized by gain suppression and phase delay to sinusoidal stimuli. The phase delay is expressed at 10.0 Hz and higher. These changes are, however, dependent upon the genotype of the animal. Two single-gene mutants of this fly have been identified as having lesioned or altered physiology in the visual receptors. The location of the lesions is in the casual pathway after photon absorption by the photopigment and before ion permeability changes are effected at the plasma membrane. The norp A^{H52} mutant responds to Ca^{++} injection in a manner similar to that of wild type. The trp mutant, however, has a much prolonged recovery period. The recovery, when finally begun, is characterized by a transient phase advance with respect to the normal response. To this author's knowledge this is the first description of a phase advance in a visual cell potential that does not involve manipulation of the light stimulus.

A physiological model for phototransduction is developed to account for the results of Ca^{++} injection and the new distinction in receptor function based upon genotype. This model incorporates both intracellular Ca^{++} and mitochondrial energy in the early events of the visual sensory

process. A study of mathematical models developed to account for the time scale of the recovery to injection concludes that the photoreceptor sequesters free Ca^{++} following an injection. This conclusion is consistent with the physiological model for phototransduction.

Iontophoresis is used in a second way in a study of membrane properties of both photoreceptors and second-order neurons of the visual system. Small currents are passed into the cells simultaneously with the application of Gaussian white noise light stimulation. The Wiener kernels obtained for the intracellular potential are used as sensitive assays of the dynamics of membrane resistance changes following light input. The photoreceptor membrane conductance is approximately a linear function of light intensity for the stimuli used. By contrast the monopolar neurons of the Drosophila visual system, which are proximal to the primary sensory cells, exhibit an active voltage dependence in the response.

TABLE OF CONTENTS

Chapter I

INTRODUCTION AND BACKGROUND

Introduction

Of considerable interest in recent years has been the problem of visual excitation in photoreceptors. Specifically, effort has been applied to elucidating that presumed mechanism, known as phototransduction, by which light-induced isomerization of photopigment chromophores results in selective conductance change at the plasma membrane of these primary sensory neurons. One of the most fruitful approaches to this problem has been that of genetic dissection of the Drosophila visual system. This thesis addresses primarily the application of genetic dissection and intracellular technique to the problem of phototransduction in the visual cells of this Dipteran.

Chapter I reviews the parts of visual science relevant to the conduct of the work presented here. These have been organized into three fields: phototransduction in the invertebrates, the role of calcium in photoreception, and genetic dissection of Drosophila. The first chapter then concludes with a rationale for the experiments which brings to bear these three disciplines.

Chapter II is a detailed description of the materials and methods used. This includes a discussion of the preparation of the fly for recording and descriptions of the light stimulus and the electrophysiological equipment and techniques. The chapter concludes with two remarks concerning the special difficulties associated with Drosophila as a preparation for intracellular studies.

The third chapter presents the results obtained from experiments in which Ca^{++} is injected into individual Drosophila photoreceptors. The

results demonstrate a new distinction in the physiology of these primary sensory cells based upon the genotype of the tissue. Chapter IV then develops a model for photoreceptor function which is based on the results of the previous chapter. A central feature of the model is that both free intracellular Ca^{++} and mitochondrial energy are utilized early in the phototransduction process. Chapter V presents theoretical models for the intracellular Ca^{++} concentration that would be obtained in the typical iontophoretic experiment. The conclusion derived from the evaluation of these models is in substantial agreement with the physiological model of Chapter IV.

The final chapter presents and discusses the results of small current iontophoretic experiments on both photoreceptors and second-order visual neurons in Drosophila. The white noise technique is used here as a sensitive assay for variation in response. The methods applied distinguish membrane properties between these two retinal cell types.

The following work applies iontophoretic technique in two very different ways. Manipulation of intracellular ionconcentration and of plasma membrane current both are used to yield a greater understanding of the physiology of neurons in the Drosophila visual system.

Phototransduction in the Invertebrates

Perhaps the central question in the discipline of visual excitation is the existence of a chemical messenger or transmitter mediating the transduction process, that is, communicating the information of rhodopsin ismerization to permeability changes at the plasma membrane. A great deal of circumstantial evidence has been accumulated for several photoreceptors arguing for the efficacy of the transmitter model (Cone, 1973; Hochstein, Minke & Hillman, 1973). In a 1971 abstract, Yoshikami and Hagins first proposed the model for vertebrate photoreceptors wherein free ionized calcium acts as a diffusible intracellular transmitter. Both rod disks and cone interstitial space are presumed to sequester Ca^{++} from the cytoplasm in the dark and to release it down its electrochemical gradient in the light. Free Ca^{++} then diffuses intracellularly to other portions of the plasma membrane there binding to Na^{+}-channels and reducing the dark current (Yoshikami & Hagins, 1973; Hagins & Yoshikami, 1974). The role of Ca^{++} as a diffusable transmitter in vertebrates is consistent with its known diffusion coefficient in muscle cytoplasm and its calculated apparent binding to sarcoplasmic reticulum (Cone, 1973). Intramembrane diffusion of rhodopsin itself has been suggested as a possible initial mechanism of light-induced Ca^{++} transport in frog (Cone, 1972).

There is evidence that Ca^{++} acts as an intracellular transmitter in some hyperpolarizing invertebrate systems as well. Light-induced hyperpolarization in the Aplysia neuron R2 is mediated by a K^{+} conductance increase mechanism which is mimiced by injection of Ca^{++} (Brown & Brown, 1973). Pressure injection of Ca^{++}-EGTA buffer with adequately small free

Ca^{++} reversibly blocks the photoresponse, and illumination of pigmented granules in these cells stimulates release of Ca^{++} (Brown, Baur & Tuley, 1975). In Pecten distal photoreceptor, which also hyperpolarizes to light through modulation of K^+ permeability (p_{K^+}), treatment with metabolic poisons expected to interfere with ATP production (Baker, 1972), and hence also with ATP-dependent mitochodrial Ca^{++} sequestration, reversibly mimics the dependence of membrane potential in the light on external $[K^+]$ (Gorman & McReynolds, 1974).

The case for Ca^{++} transmission in invertebrates is however less well established for the p_{Na^+}-modulating systems. One of the recommendable aspects of the Yoshikami-Hagins model is that fundamentally the same physiology is required of Ca^{++} at the inner surface of the plasma membrane for depolarizing invertebrate as for vertebrate cells, that it block Na^+-channels (Hagins, 1972). However, this would apparently exclude the free cytoplasmic Ca^{++} from involvement in the early events of the photoreceptor process in the depolarizing cells. Indeed, a great quantity of evidence has been developed that Ca^{++} modulates light sensitivity in the photoreceptors of Limulus, Balanus, and honey bee drone after the peak of the receptor potential transient, and therefore after the initial events of phototransduction.

Cyclic nucleotides have also been proposed as transmitters. Externally applied cyclic adenosine monophosphate (cAMP) protected from phosphodiesterase activity reversibly depolarizes the Limulus lateral photoreceptor (Miller, Gorman & Bitensky, 1971), though iontophoretic injection yields inconsistent results (Miller, 1973). Unprotected application behaves

similarly, reducing membrane resistance, but increasing the light response latency, a result which would not be expected from a substance mimicing the effects of light (Wulff, 1971).

Corroborative data have been obtained from a frog rod outer segment (ROS) preparation (Bownds & Brodie, 1975). After being shaken from the retina, individual ROS in various saline solutions swell at rates that reflect p_{Na^+} of the plasma membrane; these rates are decreased by illumination. In the presence of agents expected to inhibit cyclic nucleotide phosphodiesterase, dark swelling rates are markedly increased. Thus presumed increased activity of cyclic nucleotide leads to increased p_{Na^+}, a result consistent with what would be predicted from the Limulus work. The role proposed for cAMP as a transmitter in photoreceptors is supported by evidence developed in other tissues, particularly secretory systems. Here, cAMP is a 'second messenger' usually associated with subsequent enzyme activation and a Ca^{++} requirement (Rasmussen, 1970). Nevertheless, the evidence remains inconclusive: the identity of a transmitter in any p_{Na^+}-modulating photoreceptive system has yet to be demonstrated.

The issue of a transmitter in photoreceptors was developed concurrently (Fuortes & Hodgkin, 1964) with the proposal by Wald, Brown and Gibbons (1963) that light-induced isomerization of vertebrate rhodopsin yields an enzymatically active metarhodopsin. Thus, enzymatic amplification of the information of photon capture would provide the gain (Hagins, 1965, 1972) necessary to account for the quantum-order sensitivities of several systems. As a more modern example, a light-induced phosphorylation of a frog ROS preparation rhodopsin has been shown to be proportional to the degree of

bleach (Bownds, Dawes, Miller & Stahlman, 1972). Further, the fact that the action spectrum for the phosphorylation reaction parallels the absorption spectrum of the pigment suggests that rhodopsin is at least strongly coupled to a kinase catalyzing the reaction, if not itself displaying such activity in the bleached state. But the time course of the phosphorylation in both frog and cow (Kühn, Cook & Dreyer, 1973) are far too slow to mediate the primary response to light, so the system must be relegated to a possible role in sensitivity adjustment of the receptor cell.

Enzyme-like activity has been proposed for the turtle cone at the ion gating step of the transduction process. Removal of particles blocking conductance paths by an autocatalytic reaction as the first step in a cascade of first-order systems models the Fuortes-Hodgkin (1964) shortening of time scale for this system (Baylor, Hodgkin & Lamb, 1974). Of course there is nothing in the model to require that all or any of its steps be mediated by chemical systems. Indeed, the general question of the involvement of chemical reactions in the primary phototransduction process, excluding subsequent modulation of sensitivity, remains nearly as problematical today as in earlier days of Limulus work, when it was shown that some ATP-dependent component of the light repsonse of lateral photoreceptor could be reversibly poisoned while maintaining resting potential and conductance (Borsellino & Fuortes, 1968). Since in this particular case it would appear that mitochondrial Ca^{++} sequestration had been interrupted, the results are consistent with the experiment's addressing physiology at the membrane, and not prior events in the light response.

In the absence of detailed models of transduction, normally occurring physiological phenomena which arguably reflect more closely underlying mechanisms than the receptor potential itself may acquire particular significance. Such an opportunity has been provided by the discrete wave or quantum bump process familiar in arthropods: Limulus (lateral eye: Adolph, 1964, Fuortes & Yeandle, 1964; ventral photoreceptor: Millecchia & Mauro, 1969a), Locusta (Scholes, 1964), Musca (Kirschfield, 1966), and Drosophila (Wu & Pak, 1975). Several properties already demonstrated of this process have recommended it as an attractive assay for events occurring in the normal pathway of phototransduction. Foremost among these is of course its remarkable sensitivity, the threshold of the light-elicited process being limited by the quantal nature of the stimulus and by effective photopigment absorption (Fuortes & Yeandle, 1964).

Although the voltage noise associated with high rates of bump production displays usually pronounced adaptation to increasing stimuli, the results obtained from voltage-clamping of the dark-adapted Limulus ventral photoreceptor spontaneous process are consistent with the light response data (Millecchia & Mauro, 1969b). If the spontaneous wave and light-induced voltage noise processes are identical, this would support the conclusion of Dodge, Knight and Toyoda (1968) that light-elicited bumps sum to form the receptor potential. However, these processes in Limulus may not be identical, spontaneous waves being smaller on the average than those that are evoked by light (lateral eye, brief flash: Srebro & Behbehani, 1971; ventral photoreceptor, steady light: Yeandle & Spiegler, 1973). Nevertheless, the processes are statistically independent in ventral photoreceptor (Yeandle & Spiegler, 1973) and the large bump process is virtually

independent of clamped membrane potential (Behbehani & Srebro, 1974). This last contradicts the hypothesis that ventral eye large discrete waves derive from regenerative membrane properties, although the results may be colored by possible resistive coupling of the membrane surface to extracellular medium via glial processes (Millecchia & Mauro, 1969a). Complicated membrane grounding may also be an important factor in a controversy over adaptational properties of ventral photoreceptor. Whether bumps sum linearly (Lisman & Brown, 1975a) or nonlinearly (Srebro & Behbehani, 1974) to lights within a log unit of threshold may profoundly affect statistics of the data. A fundamental distinction may be drawn between the claims: evidence for the first was obtained under voltage clamp, and the second not.

Lateral eye large bumps are more likely to depend on nonlinear membrane behavior (Dowling, 1968; Srebro & Behbehani, 1971). It has been conjectured that the large bumps are supported by several contiguous microvilli excited by an individual microvillus' permeability change (Behrens & Krebs, 1976). Since dark adaptation increases the area of mutual contact within a rhabdomere, such a model would predict that bumps in the dark-adapted preparation be larger than those under steady lights. Further, loss of microvilli apposition with increasing light could help subserve the decreases in both duration and amplitude of bumps (Dodge et al., 1968).

Further evidence for the discrete wave process' being closely coupled to mechanisms of absorption and phototransduction has been obtained in the thermal studies of Srebro and Behbehani (1972). Assuming that the

rate of bump production follows the Arrhenius relation for a rate reaction:

$$k = ze^{-\frac{E}{RT}},$$

where k is the first-order rate constant, z the frequency or collision factor, and E the activation energy, these authors obtained an apparent activation energy of E = 48.6 kcal/mole for the lateral photoreceptor spontaneous process, and values not significantly different from zero for the light-induced process. As they point out, this first figure and the apparent spontaneous Q_{10} = 19 are quite high for physiological systems. However, since the light-induced values are so low, these authors argue that the underlying reaction is that of photopigment isomerization. To reproduce their argument, the energy for isomerization is ordinarily supplied by photons of high energies (E = 54 kcal/mole about the photopigment maximum absorption wavelength). Thus, a thermally-induced process dependent upon isomerization would be expected to show a similarly high activation energy in the dark. Conversely, in the light, photochemical reactions show virtually no dependence on temperature (Hecht, 1921) so the process is released from the previous constraint on activation. Since the data for the light-induced process are obtained as a difference between the stimulus-coincident and the spontaneous rates, the low activation energies obtained in the light probably reflect events in bump production subsequent to isomerization. This particular evidence does not evaluate the pathway of the discrete wave process within the domain of phototransduction proper, that is, after isomerization and prior to membrane conductance change. However, several competing models for spontaneous bump production which are governed by reactions of lower Q_{10}'s

are seen as inconsistent. Aqueous diffusion is hence doubtful as a candidate for the source of the spontaneous discrete wave process in this preparation. On the other hand, the rate-limiting step for the light-induced process may well be either diffusion of a transmitter or chemical reaction with a low activation energy.

The quantum bump process in Drosophila does not exhibit any of the complications so far described for Limulus. Wu and Pak (1975) have demonstrated that the light-elicited bumps at very low intensities look very much like those that are spontaneous, being 0.2 − 1 mV in height. No consistent change in shape could be detected to differing wavelength stimulation for individual cells. Further, the action spectrum of bump production is indistinguishable from that of both the ERG and intracellular light response data; therefore, the bumps very likely sum to form the receptor potential.

Calcium and Photoreception

The Yoshikami-Hagins model for Ca^{++} activity in photoreceptors is expressed best in fig. (1.1), which is taken directly from Hagins (1972). Hagins posited a mechanism for Ca^{++} activity in invertebrate photoreception that is fundamentally similar to the vertebrate case. The model applies to the p_{Na^+}-modulating photoreceptors, so does not include those photosensitive p_{K^+} systems mentioned above. Though not operating as a primary transmitter from the pigment-bearing to the conductance-mediating portions of membrane, it is supposed that Ca^{++} ions, having been gated into the cell during the photoresponse, then bind to light-coupled Na^+-channels

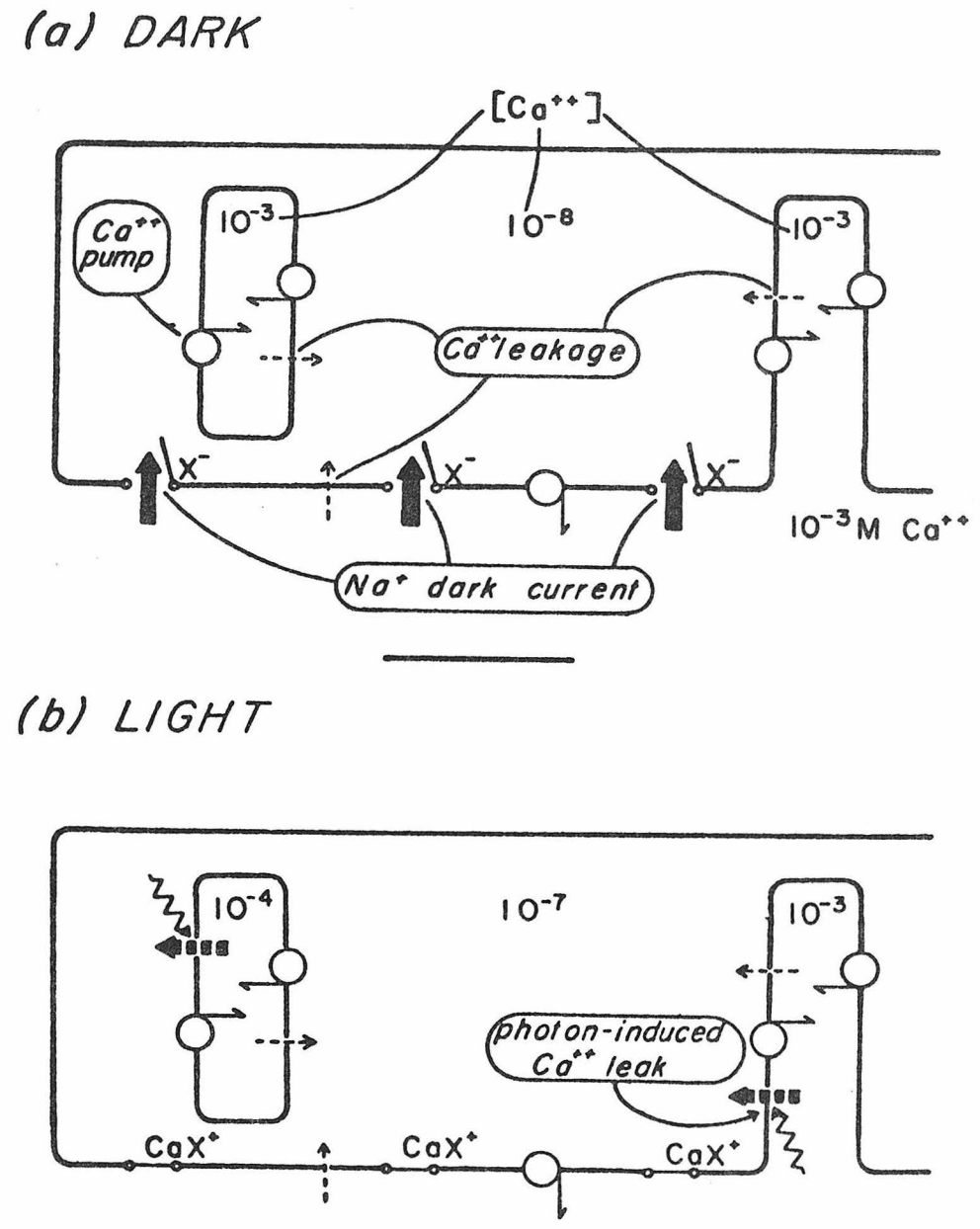

Figure 1.1. The Yoshikami-Hagins model for calcium function in vertebrate photoreceptors. Rod disks are represented on the left, and cone plasma membrane invaginations on the right. For the invertebrate case the model specifies that intracellular Ca^{++} reduces the increased Na^{+} current in the light. This figure is copied directly from Hagins (1972).

from the inside. The apparent affinity of the Na^+ permeability sites for Ca^{++} then is a factor in determining p_{Na^+}. This mechanism would be responsible for controlling adapted membrane potential in the light and perhaps responsivity as well.

The applicability of the Yoshikami-Hagins model to invertebrates is predicated on the hypothesis that intracellular Ca^{++} activity ($a_{Ca^{++}}$) increases in the light. Direct evidence for this has been demonstrated in Limulus ventral eye and Balanus lateral ocellus using the luminescence of injected aequorin as an assay for $[Ca^{++}]_{in}$ (Brown & Blinks, 1974). In these photoreceptors maximum aequorin response elicited by light is found to be a function of both the stimulus intensity and interstimulus interval in the expected manner. Further, it is shown in Limulus that the peak response is elicited during the decay of the receptor potential transient and after the peak of the light-induced current (LIC). The position of this peak coincides with the time of maximum sensitivity in this cell, measured as peak current per incident photon when clamped to the dark-adapted resting potential (Lisman & Brown, 1975a). The aequorin luminescence is found to decay after the peak, and for injections that do not independently alter the responsivity of the cell, the time constant of this decay is measured as low as 330 msec. If in fact the decay of luminescence reflects the kinetics of $[Ca^{++}]^2$ (Baker, 1972) during light and not activation of some unknown inhibitors of the aequorin reaction, then instantaneous internal $a_{Ca^{++}}$ cannot be the determinant of photosensitivity. Brown and Blinks proposed that this role is allocated to sites with high affinity for Ca^{++}. The apparent dissociation constant for Ca^{++} binding to Na^+ membrane carriers in rods and cones has been estimated by

Cone (1973) to be in the range $10^{-8} - 10^{-6}$ M. Therefore, the suggestion that high-affinity sites determine sensitivity is compatible with the notion that these sites are the membrane Na^+-channels.

At least in the dark, Balanus photoreceptors exhibit inward and outward currents consistent with this view. Assuming that current is proportional to the number of membrane carriers binding Na^+, the relationship between current and $[Ca^{++}]_{out}$ is predicted by the condition that Na^+ and Ca^{++} bind competitively to the same sites, with $k_{Ca^{++}} << k_{Na^+}$ (Brown, Hagiwara, Koike & Meech, 1970). In the light, replacing of Ca^{++} with Mg^{++} in the bathing medium increases the amplitude of the plateau phase of the receptor potential more than that of the transient. Under these same conditions, a cell clamped to resting potential shows marked increases in both phases of the LIC. Although internal $a_{Ca^{++}}$ is almost certainly coupled to $[Ca^{++}]_{out}$, it will be seen that evidence from such perfusion data may still be explained by assuming that the site of competition is at the extracellular surface of the membrane (i.e. Lettvin, Pickard, McCulloch & Pitts, 1964). However, in virtually Ca^{++}-free media the dependence of the reversal potential on $[Na^+]_{out}$ remains far less than the Nernst prediction for Na^+ permeability alone. After controlling for K^+ and Cl^-, the authors, therefore, suggested that Ca^{++} may carry at least some fraction of the LIC.

This situation may be contrasted with that in Limulus ventral photoreceptor, where change in both p_{K^+} and $p_{Ca^{++}}$ may be important in the light response (Brown & Mote, 1974). For Na^+ bath concentrations near to that of normal artificial seawater (ASW) this receptor, when maintained in a

constant state of light adaptation, behaves nearly as a Na^+ electrode, but its deviation for low $[Na^+]$ is consistent with contribution of K^+ to the LIC. In low-Ca^{++}SW, the plateau phase of the Limulus receptor potential is enhanced relative to the transient (Lisman & Brown, 1972b). Both phases of the LIC can nevertheless be distinguished under these circumstances. Even when the membrane potential is clamped to levels more positive than the reversal potential the LIC has transient and sustained components (Millecchia & Mauro, 1969b). Therefore, Ca^{++} conductance may contribute to the LIC (Lisman & Brown, 1972a) independently of any Na^+-Ca^{++} exchange mechanism (Baker, 1972). Whether or not such an exchange contributes to the photoresponse of these cells is as yet undecided (Hanani & Hillman, 1976). But the evidence in Balanus certainly does not exclude Na^+-dependent Ca^{++} entry as the unique vehicle of LIC not due to p_{Na^+}-modulation.

Evidence relating depolarizing photoreceptor responsivity to internal $a_{Ca^{++}}$ has been obtained with intracellular injections. Fein and Lisman (1975) injected approximately $2 \cdot 10^{-4}$ mole Ca^{++} into the Limulus ventral photoreceptor. They estimated a decrease in sensitivity of about 0.9 log unit at the injection site, and 0.2 log unit 80 μ away immediately after the iontophoresis was terminated. These figures are consistent with localized light adaption seen in these cells. Further, progressive decrement of receptor potential transient with respect to the plateau, characteristic of change in adaptive state, is associated with these injections (Lisman & Brown, 1972b). These lines of evidence indicate that a rise in intracellular $a_{Ca^{++}}$ mimics the desnsitizing effects of light.

Injection of the Ca^{++} chelating agent EGTA into Limulus photoreceptor tends to flatten both the receptor potential and the LIC, in each case lessening the decay of transient to plateau. The degree to which the receptor potential displays monophasic response to a step of light is correlated with the maximum of the aequorin response (Brown & Blinks, 1974). EGTA injection both protects the photoreceptor from LIC sensitivity decrement after conditioning lights and renders the LIC plateau a more linear function of log light intensity (Lisman & Brown, 1975b). Pressure injection of Ca^{++}-EGTA buffers produces similar effects in the current records. Increasing $[Ca^{++}]$ in these buffers increases the absolute threshold of response.

These data are consistent with the model that Ca^{++} is gated into the cell during the decay of the transient. Iontophoresis of Na^{++} into Limulus photoreceptors yields similar results to that of Ca^{++} in ASW (Lisman & Brown, 1972b), though up to 50 times as much molar quantity is needed. This similarity varies directly with $[Ca^{++}]_{out}$: in low-Ca^{++} SW no diminution in receptor potential is seen with the injections used. This and other evidence has led these authors to hypothesize that Ca^{++} entry during prolonged light is stimulated by increasing $[Na^{+}]_{in}$.

A Na^{+}-Ca^{++} exchange mechanism has been proposed for the photoreceptor of the honeybee drone. The resting potential of this cell is governed primarily by $p_{K^{+}}$, partly by $p_{Na^{+}}$ (Fulpius & Baumann, 1969). Replacement of Na^{+} by $TrisH^{+}$, however, indicates that the light response, particularly the initial spike, is mediated largely by $p_{Na^{+}}$. In low-Na^{+} the plateau is diminished more than the transient. Decreasing $[Ca^{++}]_{out}$ broadens the transient and raising it results in the opposite. Pressure injection of

EGTA into these cells reversibly abolishes the decay of the transient (Bader, Baumann & Bertrand, 1976). Further, a distinct plateau phase can be reinstituted after injection by increasing the average power level of the stimulus. Injection of Ca^{++}-EGTA buffer, $[Ca^{++}] = 3.3 \cdot 10^{-6}$ M, mimics the changes in response seen after strong illumination: the slow phase of the receptor potential is shortened and its maximum diminished.

The initiation of a faster off-response to pulses of bright light in the bee following Ca^{++}-EGTA injection might suggest similar properties of the on-response of the slow phase, in this case of course marked by the spike. This compares with a similar observation in Limulus, wherein the latency of onset of both receptor potential and LIC is diminished following Ca^{++} iontophoresis (Brown & Lisman, 1975). These results are seen to be consistent with the Fuortes-Hodgkin model for the light-adapted ventral eye.

The details of Ca^{++} physiology in depolarizing invertebrate photoreceptor response, and consequently the extent to which the Yoshikami-Hagins model is correct, remain problematical. As seen above, evidence has favored a role for Na^{+}- dependent Ca^{++} entry. There is no evidence to exclude in any of these preparations a Na^{+}-independent Ca^{++} component of LIC. Ultrastructural work has demonstrated an increase in dark-adapted over light-adapted material in the numbers of Limulus mitochondrial granules expected to sequester Ca^{++} (Behrens & Krebs, 1976). Thus, energy-dependent contribution to Ca^{++}-mediated photosensitivity is a definite possibility.

Genetic Dissection of 'Drosophila'

The genetic dissection of Drosophila was proposed by Benzer (1967)

originally as a tool by which one could study the physiological basis of behavior. His work demonstrated that sex-linked heritable deficiencies in phototaxis could be induced. Phototaxis is the behavioral response in these animals upon sudden illumination; wild type flies walk toward the source of light. Specifically, Benzer suggested that single-gene mutations could be isolated, each of which could represent an individual lesion at some step in the coupling of stimulus to response. Phototactic mutants, that is, mutants with an altered behavioral phenotype in this response to illumination, may carry physiological deficiencies at any point in the processes of photoreception, brain processing or motor output. Discovering where the lesion is then leads to demonstrating the degree of its necessity to the behavioral response.

Soon after Benzer's paper X-chromosome (tan) and III-chromosome (ebony) mutants which displayed abnormal electroretinogram (ERG) phenotypes were isolated by deficient phototactic response (Hotta & Benzer, 1969; Pak, Grossfield & White, 1969). These authors proposed that single-gene alterations could be employed in the study of photoreception itself. Several such mutants, mostly X-chromosome, have now been isolated and are reviewed by Pak (1975). The lesioned physiology then may prove valuable in illuminating normal or wild type function, typically by processes of elimination. The elegant morphological version of this process is that of mosaicism, wherein the autonomy of gene expression to some tissue may be tested (Hotta & Benzer, 1970, 1972). The Drosophila nervous system has been investigated at several locations using this general approach, including thoracic ganglion pacemaker units (Ikeda & Kaplan, 1970a,b), neuromuscular junction of both the adult (Ikeda, Ozawa & Hagiwara, 1976) and larva (Jan

& Jan, 1977), and the adult eye in various aspects: Photopigment disposition among receptor cells (Harris, Stark & Walker, 1976), phototransduction, and the integrative or motor output of the visual system (Heisenberg & Götz, 1975).

Two Drosophila mutants have been identified by Pak and Pinto (1976) as being of particular interest with respect to phototransduction. The receptor potentials of both of these animals exhibit unusual properties of the quantum bump process. The X-chromosome mutant no receptor potential A (norp A)(alleles x-(12,13,16); Pak, Grossfield & Arnold, 1970) exhibits normal photoreceptor membrane resting potential and resistance in the dark. However, the corneal-negative component of the ERG is severely decremented and the on- and off-transients are absent. That the lesion is localized to the photoreceptor population is confirmed by intracellular records (Alawi, 1972; Alawi, Jennings, Grossfield & Pak, 1972). Now that forty alleles have been isolated (Pak & Pinto, 1976), the degree of decrement available for this mutant extends from marginal to virtually complete abolition of response. Although the eye of one of the most severely affected alleles, norp A^{P12}, contains approximately one-third of the normal complement of photopigment, this pigment behaves normally in vitro to spectral difference absorption paradigms designed to test rhodopsin and metarhodopsin interconversion (Ostroy, Wilson & Pak, 1974).

Perhaps the most immediate expected consequence of gene alteration is protein difference. Thus, the eye of norp A shows protein differences that are seen as concentration exchange in two protein subunits separated on SDS gel (Ostroy & Pak, 1973). In the mutant eyes the amount of a protein of apparent molecular weight 51,000 is increased, while the amount

of another of molecular weight 46,000 is decreased. Since the photopigment complement for norp A^{P12} is normal in its relative composition, the protein difference detected must reflect a genetic lesion at a location following photon absorption in the phototransduction process. Further, the degree of protein and ERG differences for various alleles are comparable (Ostroy & Pak, 1974).

Temperature sensitivity in the ERG waveshape has been shown for the norp A^{H52} allele (Deland & Pak, 1973). At 17° C the ERG of flies raised at 19° is normal, but at 33° the transients are eliminated and the sustained component reduced. This effect is reversible up to that temperature sufficient to fully suppress the response. Exposure at this temperature through time then eliminates recoverability. The evidence is consistent with a norp A^{H52}-altered protein undergoing conformational change affecting photoreceptor membrane conductance. In this connection, temperature sensitive paralysis in shi^{tsi} has been attributed to reversible blockage of neuromuscular transmission; temperature-dependent change of the subsynaptic muscle receptor protein was suggested by Ikeda, et al. (1976) for this mutant. Thus it is likely that protein is somehow involved in the Drosophila phototransduction process, in a role that is of course not yet understood.

There is evidence that this role involves the latency of bump production (Pak, Ostroy, Deland & Wu, 1976), and perhaps the efficiency of production as well. The intracellular receptor potential of norp A^{H52} shows an abnormally long delay and a far less pronounced off-effect than seen in the wild type control, with a slow decay to dark resting potential.

Bump records show an unusually wide dispersion after a dim light flash. From inspection of the records and calculation of the autocorrelation function for the induced voltage noise, the authors argue that the typical bump shape itself has remained unaffected by the mutation. Assuming that bumps are statistically independent events, invariance of the autocorrelation between two noise records is necessary if not sufficient to imply that the shape of the average bump remains unchanged.

The other phototransduction mutant, trp, was first described by Cosens and Manning (1969) as a III-chromosome recessive. The ERG of this animal exhibits a greatly attenuated sustained corneal-negative component, and its responsivity to subsequent flashes is decremented with respect to wild type. That this reflects repolarization of the retinula cells in steady light to near resting potential has been confirmed in the intracellular preparation (Minke, Wu & Pak, 1975b). This decay is seen for stimuli bleaching less than 3% of the rhodopsin complement. Light-induced voltage noise remains undiminished during the saturated portion of the response to increasing light intensity. Autocorrelation of the noise demonstrates that average bump shape is similarly unaffected, implying that the genetic lesion probably degrades efficiency of light-coincident bump production for intensities one log unit above threshold. Further, a form of prolonged depolarizing afterpotential (PDA), which reflects conversion of rhodopsin to metarhodopsin in the wild type fly (1-6) cells (Minke, Wu & Pak, 1975a), is expressed in the mutant cells primarily as prolonged voltage noise. It is elicited by intense blue light and rescinded by orange stimulation just as the normal PDA. The implication is that repolarization of trp retinula cells is due to alteration in the photoreception process at some stage

after photon capture. Indeed, since induction and elimination of the mutant PDA is essentially identical to that in wild type, any light-induced transmitter-releasing processes subsequent to pigment change (Hochstein et al., 1973) should remain intact as well. Therefore, it must be the case that the trp genetic lesion is expressed after the putative transmitter release.

Rationale

The availability of Dipteran systems with lesioned phototransduction provides an otherwise inaccessible probe into the physiology of the visual sensory cells. Since expression of the single gene involved must be restricted to at most a few proteins, this probe is probably highly specific to some part of the transduction process. The fact that only two such mutants have been isolated so far supports the assumption of specificity.

In order to demonstrate that the transduction path has been lesioned at least one obvious precondition must be fulfilled, that the lesioned path be continuous from photon capture to that point at which light-coupled response may be demonstrated. Some years ago that point would have been ERG measurement; the limit is now intracellular recording with fine-tipped glass micropipettes. Presently a more sensitive and unassailable proof of in vivo neural activity does not exist. In this connection, the demonstration by Alawi (1972) that the virtually unresponsive cells of norp A^{P12} (his x-12) have normal resting potential and nearly normal membrane resistance first isolated the expression of the allele to a nonlethal alteration of receptor function. Prior to this evidence it was

possible that only a fraction of the receptors in x-12 remained alive and contributing to the ERG.

It is perhaps unfortunate that the respiratory requirement of the Drosophila retina is so severe. Thus an in vivo retinula cell preparation analogous to the vertebrate ROS system has not been developed. Tissue hardness of this retina is in this sense a mixed blessing. While providing a resilient substrate for mechanical cell penetration, the physical structure virtually assures that cells will never be separated in a controlled bath by gentle agitation.

Another respect in which the study of Drosophila is limited is really the concatenation of all the techniques that are unavailable for fly visual studies. In a field dominated by Limulus ventral photoreceptor the fly is indeed at a severe disadvantage. This single sensory cell is nearly as large as one entire side of the Drosophila retina. Recording the light-induced current requires at least two simultaneous penetrating electrodes, one for recording and one for the voltage clamp feedback, preferrably separated by some distance so as to minimize coupling. Isolation of the various components of this current requires control over bath ion concentrations. Permeability of the membrane to the several ionic species is estimated usually by plotting the reversal potential as a function of external concentration and comparing with the Nernst prediction for steady state Donnan equilibrium (Katz, 1966).

None of these multi-electrode or bath techniques is available for the Drosophila retina. All the intracellular data recorded must be read from the same pipette through which current is passed. Since electrode resistances are so high and variable, the passive bridge balance as

described in 'Materials and Methods' is inaccurate for current changes of more than 0.01 nA, too small to render a quantitative difference in membrane response.

In all experimental situations trade-offs are made and hopefully understood. Within the limitations for Drosophila explicitly presented above, the genetic dissection of this animal provides variables on photoreception unavailable in any other animal.

The role of Ca^{++} in invertebrate photoreception has been thoroughly reviewed in this chapter. Indeed, its importance is being recognized in a growing number of physiological systems besides the classic synaptic transmission (Carafoli & Crompton, 1978), some of which involves binding by protein in nervous tissue (Mullins & Brinley, 1977). Since the most likely target of single gene alteration in any system is protein change, Ca^{++} binding of the affected protein is also likely to be changed. Proteins undergo conformational changes upon binding Ca^{++} that are global in nature and not simply local to the particular ligands involved (Williams, 1977). Since the entire protein is involved in the loss of energy upon binding, the apparent dissociation constants should be altered by the genetic expression.

In view of the general importance of Ca^{++} to the physiological regulation, and in particular its demonstrated importance to photoreception in other systems, manipulation of the intracellular Ca^{++} concentration of the Drosophila photoreceptor should enhance the genetic probe already in place. Since the available mutants have lesions that are isolated to the bump process familiar in arthropods, expected differences in Ca^{++} binding by proteins in the path of phototransduction should help decompose the bump

process itself.

Chapter II

MATERIALS AND METHODS

Preparation

Animals used for electrophysiological recording in this study were of the species Drosophila melanogaster raised in our laboratory under high humidity at approximately 20°C. The stocks were bred in 8 dram glass vials on Storr's fly medium (Pak, Hartl & Götz, 1974). New stocks were prepared at four-day to two-week intervals, depending upon the supply needed, by depositing usually two non-virgin females into fresh bottles. Among the mutants maintained were white and trp;w obtained from the laboratory of Dr. S. Benzer and norp A^{H52};w obtained from the laboratory of Dr. W. L. Pak. White flies were of the Canton S strain. Flies selected for recording were females usually older than one day post-emergence and younger than that time when signs of age appeared, probably about two weeks post-emergence. Egg-laying females were preferred since they provided the largest amount of retinal tissue of those individuals in a given population.

All flies used in this study carried the white eye color on the first chromosome (Lindsley & Grell, 1967). White eliminates the retinal screening pigments among the retinula cells and hence increases the apparent sensitivity to light. Utilizing the white background is standard procedure in fly retinal studies where the spatial properties of the light stimulus are not significant. Henceforth, unless otherwise specified, the white background will be assumed, even when discussing wild type photoreception.

The norp A^{H52} allele is a temperature-sensitive mutant (Deland & Pak, 1973) as we have described in the previous chapter. All experiments reported here were done in a room whose temperature did not exceed about 25°C. This is within the permissive range, that is, cooler than that

temperature at which the electroretinogram (ERG) is abolished. This allele was chosen because it is one of the most responsive of the norp A's.

Whole animals were prepared for recording in a manner similar to that demonstrated in the Cold Spring Harbor laboratory course description, 'Neurobiology of Drosophila' (Pak, et al., 1974). After light anesthesia with CO_2 the fly was immobilized ventral side up on a glass cover slip by application of waxes with a heated wire. A petri dish filled with ice provided an adequate heat sink for this procedure. First the wings were affixed in their normal "walking" position with soft dental wax, then the dorsal surface of the thorax was affixed with a mixture of bees wax: rosin, 3:1. The dental wax was used in places where maleability and speed of application were important, and the bees wax mixture where the hydrophobic character of the rosin was required. Following these initial steps the legs were individually joined to wax walls built up on either side of the preparation. The abdomen was partially immobilized by depositing wax between the dorsal surface and the wings. In this last step it is critical to avoid touching the fourteen abdominal spiracles which terminate the tracheal respiratory system (Ferris, 1950, p. 410). Occasionally in preparations given to large abdominal contractions dental wax was applied to the ventral surface and the legs as well. The head was then secured to the thorax with a slight dorsal rotation and the proboscis immobilized. In securing the head, it is critical again to avoid touching the two anterior thoracic spiracles (Ferris, 1950, p. 399). A razor blade section vibrated by a speaker cone was used to slice away a small section of the ventral side of the cornea of the right eye. Beadle's ringer (Ephrussi & Beadle, 1936; Wu & Pak, 1975) was immediately

applied to the fresh insult and the cover slip positioned on the experimental set-up inside a chamber continuously perfused with moist air. The preparation was judged acceptable if, among other measures, the exposed retina was neither overly desicated nor subject to excessive heamolymph movement (Arnett, 1971).

Light Stimulus

The light source used in all experiments to be described was a glow tube (Sylvania R1131C) operated at 260 V by pulse-width modulation as shown in fig. 2.1. An amplified sawtooth signal (nominally 6.67 KHz) from an 8038 was applied to the inverting side of a 311 comparator. The desired input signal was connected to the non-inverting side. The output of the 311 was then amplified in two forward-biased NPN transistor stages. In this way the voltage applied across the glow tube was pulsed, the ratio of the times when on to the times when off being linearly related to the intended intensity output. Gain and offset of the amplified sawtooth signal were permanently adjusted so as to obtain maximum linear modulation of the input signal as monitored at the 318 output. The frequency components of the stimulus of the order of $10^2 - 10^3$ KHz by far exceed the frequency discrimination of any biological visual system. This type of operation of the glow tube avoided the red spectral shift of the light output for straightforward voltage modulation characteristic of these tubes at low intensities. The design is due to Mr. D. Aranovich. A similar curcuit has been referred to in an abstract (McDonald, 1960).

Light stimuli were delivered to the preparation directly to the front of the head. A 3-log unit neutral density wedge and a **Balzers** 491 nm filter were placed in the optical path. This blue filter was

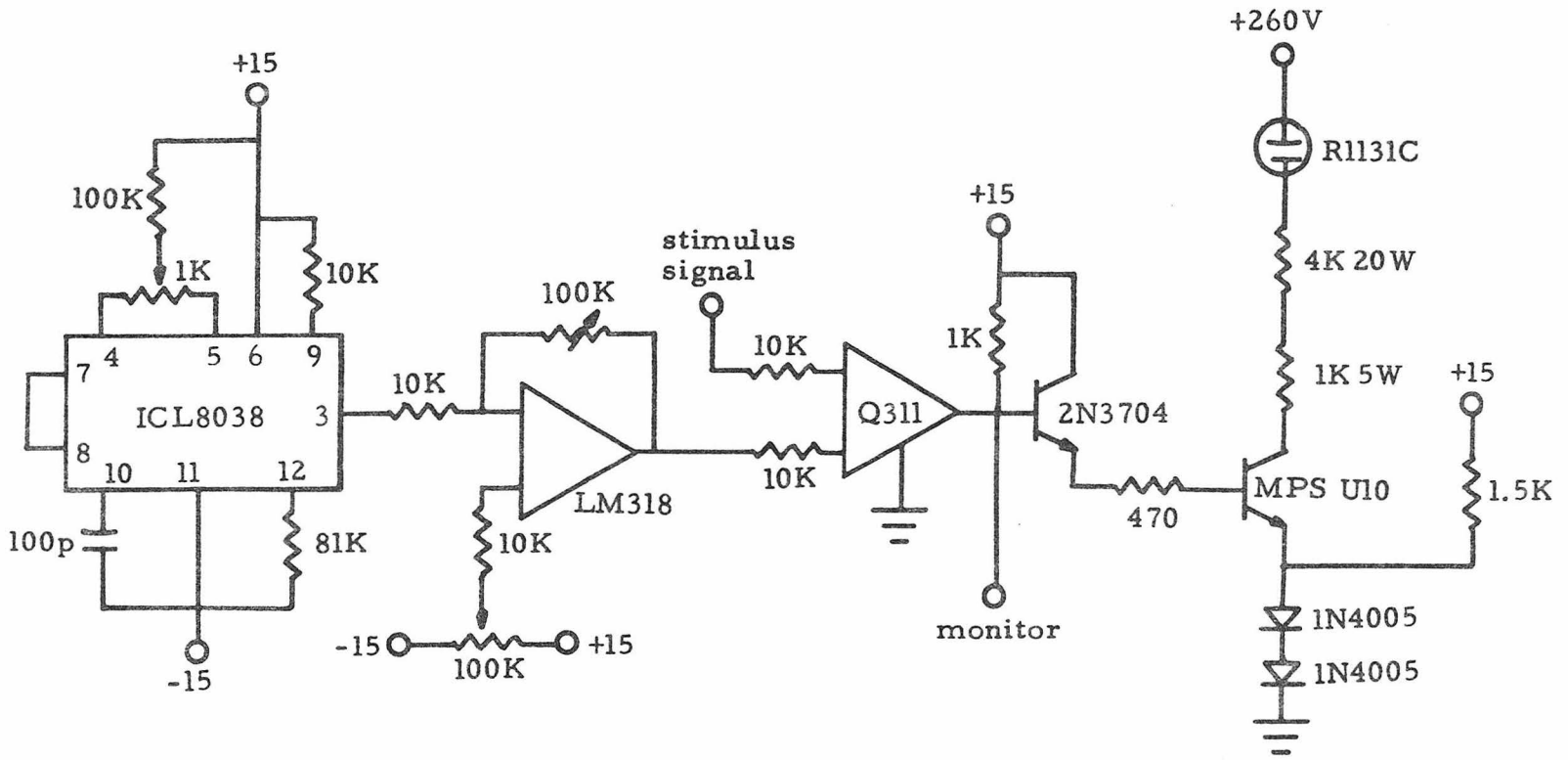

Figure 2.1. Glow tube pulse-width modulator. A nominal 6.67 KHz sawtooth signal is compared with the intended stimulus signal by the 311. The R1131C glow tube current is then either fully on or fully off. Low-pass filtering of the light intensity output by visual systems provides the intended linear light stimulus. The design is due to Mr. D. Aranovich.

chosen since it lies close to the maximum of the absorption spectrum of Drosophila rhodopsin at 480 nm (Ostroy, Wilson & Pak, 1974). The eye of the animal was focused to a 2 mm diameter disk, and the maximum incident intensity was $1.07 \cdot 10^{10}$ phot $cm^{-2} sec^{-1}$ at 491 nm. A light-sensitive diode (United Detector Technology, PIN 3DP) which provided all the stimulus data was placed in the light path. The current output of the diode was fed to a 741 operational amplifier in a standard ammeter configuration.

The light intensity was calibrated by a light-sensitive diode (United Detector Technology, PIN 10UV) placed at the level of the focused stimulus. The diode was coupled to an amplifier (United Detector Technology, Model 101A). For the unattenuated white stimulus at maximum intensity, that is, with no intervening spectral filter, output of the amplifier at the low sensitivity setting was 0.429 V. Output at the high sensitivity setting for the 491 nm stimulus at maximum intensity was 0.388 V.

For the sinusoidal light stimulation experiments the log frequency spectrum was divided evenly by three values per decade. Hence, frequencies used were 1.0, 2.15, 4.64, 10.0, 21.5, 46.4 and 100 Hz, although responses for the last of these frequencies were particularly attenuated. Average intensity at 491 nm was 0.4 that of the maximum, or $4.3 \cdot 10^{9}$ phot cm^{-2} sec^{-1}. Depth of modulation was approximately $80^{o}/o$ of the maximum intensity range.

For white noise stimulation a single channel white noise generator constructed by Mr. D. Aranovich was used. The output was filtered at 100 Hz; the resulting stimulus was distributed in Gaussian fashion about the mean of 0.4 maximum intensity. Autocorrelation of the stimulus was half-maximal at a time shift of 3 msec. With the intervening 491 nm filter, the Wiener stimulus power delivered to the preparation was typically

$1.9 \cdot 10^{13}$ $phot^2$ $cm^{-4} sec^{-1}$. Since photons have the units of energy, this power should be distinguished carefully from the intensity power of the light. The calculation was done as follows. Maximum light intensity corresponded with a voltage shift of 7.93 V from the dark level as finally digitized. The power level computed for the digitized stimulus was typically about $1.03 \cdot 10^{-5}$ sec. Hence,

$$1.03 \cdot 10^{-5} \cdot \text{sec} \left[\frac{1.07 \cdot 10^{10} \text{ phot cm}^{-2} \text{sec}^{-1}}{7.93} \right]^2 = 1.9 \cdot 10^{13} \text{ phot}^2 \text{cm}^{-4} \text{sec}^{-1}.$$

Microelectrodes

Light-evoked responses were recorded by means of glass micropipettes. Pyrex tubing (type 7740, 9 mm O.D., 7 mm I.D.) were pulled out to approximately 1 mm O.D. capillary tubing by a vertical oven device constructed by Mr. A. W. Broers. A previously pulled capillary was inserted into the tubing for this procedure so that the resulting capillaries contained a continuous filament inside. Sections of these capillaries were pulled on a Takahashi Model EH-12 horizontal puller kindly lent by Dr. K.-I. Naka. The pipette tips were inspected with a microscope, and acceptable tips were usually beyond the resolving power at x40 magnification. Microelectrodes constructed by these methods have tip dimensions of the order of 0.1 μ (Naka, Inoma, Kosugi & Tong, 1960; Tomita, 1969). These micropipettes were then stored dry until ready for use, usually not longer than one day. Immediately before mounting on the experimental set-up they were filled with an appropriate electrolyte solution with a syringe. The convex surface presented to the solution by the filament interior to

the capillary greatly facilitates rapid and complete filling. In the absence of residual bubbles a low resistance path is guaranteed from the tip to the shank of the electrode.

During the course of the work undertaken with Drosophila, five saline solutions were employed. In addition to 2M potassium citrate and 2M KCl, three stock solutions were used specifically for iontophoresis. For Ca^{++} injections, 38.04 g (0.1 mole) ethyleneglycol-bis-(β-aminoethyl-ether)N,N'-tetraacetic acid (EGTA) was added to 100 ml H_2O, or some small multiple thereof. This suspension was measured at pH 3-4. During continuous stiring and intermittent cooling, pH was brought to 7.0 by the addition of sufficient $Ca(OH)_2$. Since the affinity of EGTA for Ca^{++} is pH-dependent (Schmid & Reilley, 1957), increasing with pH, this rough titration is precipitous after about pH 6. There was nearly always an overshoot. Adjustment with HCl and $Ca(OH)_2$ then yielded the desired stock at pH 7.0. EGTA injections utilized this same stock except that extreme care was taken not to bypass pH 7.0, and therefore not to add Cl^- ions. The solution used in this case had pH 7.1. For Mg^{++} injections, 29.57 g (0.1 mole) ethylenediamine-tetraacetic acid (EDTA) was added to 100 ml H_2O and sufficient $Mg(OH)_2$ added to bring the pH to 7.0. Occasionally the precipitate in the Ca^{++}-EGTA mixtures was filtered out, but this did not seem to make any difference in the usability of their electrodes. For most of the experiments described here, these three stock solutions were diluted by 9 parts of the non-ionic detergent Triton X-100 (1%) , used principally for solubilizing proteins from cell plasma membranes. This lowered the typical electrode resistance which was of the order of 500 MΩ, particularly during and after current passage. The reduced viscosity with detergent would be expected to

lessen solution-glass surface forces and to enhance mixing at the tip of the electrolyte and intracellular tissue fluid.

Silylation

A brief description of a project attempting to silylate the interior of the micropipettes is in order here. The dilution of the electrolyte with detergent was employed primarily in response to the problems presented by electrodes whose resistance would become excessive, especially during and after current passage. Silylation constituted a prior response to this same difficulty. Treatment of the interior of micropipettes with silicon compounds is commonly used for ion-selective electrodes (Walker, 1971, 1976). In this application the purpose in their use is to render the interior glass surface hydrophobic. This accommodates filling approximately the first 200 μ of the tip with an organic liquid ion exchanger. The organic phase then acts as a membrane with selective ion permeability between the aqueous phases of the intracellular fluid and the electrolyte of the pipette. Given the ionic composition of the electrolyte, the intracellular activity of the ion selected by the particular exchanger may be calculated by a modified Nernst equation from the known potential developed at the shank of the electrode.

It was hoped that treatment of the pipettes used in this work with the same silicon compounds might prevent binding of the Ca^{++} to the glass. In this case no organic phase is permitted; despite the expected hydrophobic character of the internal treated surface the aqueous phase should be continuous throughout the pipette typ. Two basic silylation procedures were attempted. The first procedure involved treatment with differing

concentrations of dimethyldichorosilane ($(CH_3)_2SiCl_2$), a compound commonly used for ion-selective electrode silylation, carried by several organic solvents. The silane was introduced by touching the open end of the shank momentarily to a droplet of solution. Capillary action provided by the interior filament transmitted the solution to a region typically of a few hundred microns at the tip. Dipping of the tip itself into the droplet, though preferable in that it would afford greater control of the amount of solution introduced, proved ineffective for these pipettes. Subsequent heat treatment presumably binds the silane to the interior surface and serves to eliminate the solvent. The heat employed was necessarily more gentle than that usually applied in ion-exchanger preparation since it was critical to preserve the tip size and shape in this work.

With some experience with this first approach, it became apparent that physical clogging of the tip after filling with the aqueous Ca^{++} electrolyte presented a capricious difficulty, even when visual inspection of the tip under the microscope revealed no sign of blockage prior to the aqueous fill. There is the possibility that a rehydrolysis of the surface after exposure to the electrode water could result in an accumulation of polymer at the tip (Dr. M. Shippey, personal communication). Dimethyldichlorosilane presents two weakly bound chlorines, the ligands to which are available for reducing two hydroxyl groups at the glass surface. Polymer chains of dimethylsilicones could result from the silicon ligands coupling end to end. The second compound tried was therefore hexamethyldisilazane (HMDS) ($((CH_3)Si)_2NH$), which upon reducing hydroxyl groups on the surface would present only one ligand to silicon. If this bond were

subsequently broken silicon-based polymers would not be expected to result by this mechanism. HMDS was employed just as the description above in concentrations of $0.1^{o}/o$ - $0.3^{o}/o$ in dry toluene. Some injections were accomplished with electrodes prepared with HMDS, one such record of which is to be found in the next chapter, but physical obstruction of the tip remained a problem.

On the basis of this experience with the two silanes specified, it appears that silylation of the interior of fine-tipped micropipettes is unobtainable if a reliably continuous aqueous phase is required through the tip. Physical obstruction of the tip with material following treatment with dimethyldichlorosilane and HMDS have been encountered in other laboratories (Dr. J. L. Walker, personal communication).

Transport Number

Current injection for the purposes of material deposition is characterized primarily by the transport number of the electrode. The simplest analytical determination of the transport is given by the ratio,

$$\frac{JzF}{I},$$

where J is the ion flow, z the absolute value of the valence, F the Faraday constant, and I the current (Chowdhury, 1969). J is an empirical factor which may differ widely for different pipette types, including different glasses used in the capillary construction, as well as for different electrolytes and external solutions. Disposition of the tip in membranous structures may also be an important factor.

Reuben, Brandt and Grundfest (1974) determined the transport number

for their Ca^{++} iontophoresis electrodes to be 0.20 ± 0.032 s.d. Currents of known amplitude and duration were passed from pipettes containing a known $^{45}Ca^{++}$ activity, and the resultant label in the saline receiving the material was assayed by scintillation counting. The electrolyte was specified as 100 mM Ca-Tris-EGTA. The pipettes were intended for iontophoresis into single muscle fibres of the crayfish and carried up to 1 μA for as long as 30 minutes. Fein and Lisman (1975) used similar microelectrodes to impale Limulus ventral photoreceptor. However, the microelectrodes used in the study described here for use in Drosophila intracellular work are undoubtedly finer-tipped than those used in these previous studies in muscle and ventral photoreceptor. This difference is reflected in the current capacity of the electrodes. The maximum current carried by the Drosophila pipettes filled with the Ca^{++}-EGTA buffer as described above was always the current used, typically 2 nA. This is approximately three orders of magnitude less than that for the crayfish study. The interior of all the glass pipettes binds Ca^{++} and therefore probably retains a net charge during iontophoresis that would oppose cation entry to the tip from the shank side of the electrode. The electrical conductance would be nonlinearly related to the tip cross-sectional area in that its slope would decrease with decreasing area. Therefore it is not unreasonable to assume a transport number for the Drosophila Ca^{++} microelectrodes at least an order of magnitude less than that demonstrated for the crayfish electrodes. Consequently we estimate a transport number of approximately 1°/o for most of the Ca^{++} pipettes of this study.

Two attempts to quantitate directly the transport number of the Ca^{++} electrodes may be described here. Injections of up to 100 ncoul were made into 20 µl droplets of sterile-room prepared 0.1 N HNO_3. The droplets were deposited on 1" sterile teflon disks immediately prior to electrode positioning and current passage, and sterile technique was observed on the electrophysiological set-up as far as possible. With a transport number identically equal to 1.0, the expected total amount of Ca^{++} to be passed into the droplet is $5 \cdot 10^{-13}$ mole. Standards were also prepared of 1000 ppb (parts per billion) Ca^{++} to 1 ppb in sterile 0.1 N HNO_3. An amount of $5 \cdot 10^{-13}$ mole Ca^{++} in this volume of acid is equivalent to approximately 159 ppb Ca after drying. The prepared sample droplets were removed from the teflon disks and placed in the beam path of a Varian Techtron Model 63 carbon rod atomizer (Ms. S.D. Garcia, Dr. S. V. Hering, personal communications). Droplets of 20 µl of the standards were handled in a similar manner. The droplets are first vaporized in an open chamber, then atomized with a carbon-carbon arc. The data read out is absorption of light at 422.7 nm through time following the onset of the atomizing potential as assayed by a Varian Techtron type AA-5 spectrophotometer. The amount of Ca^{++} to be detected is near the resolving power of this instrument. The absorption response was erratic at the high voltage setting required to atomize this relatively light metal. This was the case for all the standards at or below 100 ppb.

The second attempt involved the same range of droplet concentrations, this time dried onto 1" carbon disks. The disks were then carbon-coated and mounted in the beam path of an electron probe X-ray microanalyzer (EPMA) (Mr. A. A. Chodos, Dr. S. V. Hering, personal communications).

The beam itself is under the control of a PDP-8/L operating with the FOCAL language. The output data of this instrument operating in the wavelength dispersive mode are the numbers of detected X-ray emissions; for calcium the detector is set for 3.36 Å radiation. The system was programmed to scan the region of each dried drop on the disk in a square raster and display the number of such detections on the paper output in a similar raster. The droplet positions could not be assessed from this data for 100 ppb samples. Since the disk substrate must be transparent to the electron beam the carbon disks were required. This presented a varigated surface to the focused beam which resulted in scattered X-ray emission. The emission angle is dependent upon the angle at which the electron beam enters the sample. Brown, Baur and Tuley (1975) used a related electron microprobe system to demonstrate that Ca^{++} is released from granules in Aplysia giant neurons upon illumination. To ensure that their preparation contained measurable levels of calcium, these authors added 10 mM $CaCl_2$ to the fixative.

Electrophysiological Recording

After positioning the cover slip with the fully prepared fly on the experimental apparatus, the micropipettes were, one at a time, filled with the appropriate electrolyte, mounted on the vertically driven micromanipulator (Prior), and lowered by hand with the coarse adjustment through the corneal wound into the receptor layer. A platinum wire from the noninverting side of the pre-amplifier (Transidyne General, MPA-6) made electrical contact with the electrolyte. The indifferent was a

tungsten wire previously etched to a point by current passage in sodium nitrite and mounted on a Narishige extracellular manipulator. This electrode was inserted into either a leg or the thorax of the animal. The inverting side of the pre-amplifier received the indifferent. The relationship of the pre-amplifier to the preparation is schematized in the upper right portion of fig. 2.2.

After confirmation of the characteristic waveform of the ERG potential of the retina, the indifferent was moved from its neutral position to make contact with the fluid of the eye at the most unobtrusive corner of the wound. Since the preparation was electrically isolated from the table by the cover slip on which it was waxed, the only preparation ground was via the extracellular electrode. No impedance matching problems were encountered with this arrangement. All data recorded therefore represent extracellular retinal potentials subtracted from the intracellular response. Data recorded in this manner more truly reflect the transmembrane potential of the given unit than if the reference had been at an electrically neutral site.

To reduce noise in the recording set-up the shielded pre-amplifier was mounted directly on the top of the micromanipulator. This minimized the distance between the top of the pipette and the FET base. Intracellular penetrations were obtained by advancing the micromanipulator carefully by hand through the retina with the fine adjustment while intermittently bypassing the negative capacitance feedback of the MPA-6. The 3.9 sec interval trigger pulses from a 555 in a pulse train configuration were passed through a foot switch to a 555 in a one-shot configuration. This pulse activated a relay mounted inside the MPA-6, temporarily short-circuiting the resistance defining the degree of capacitance

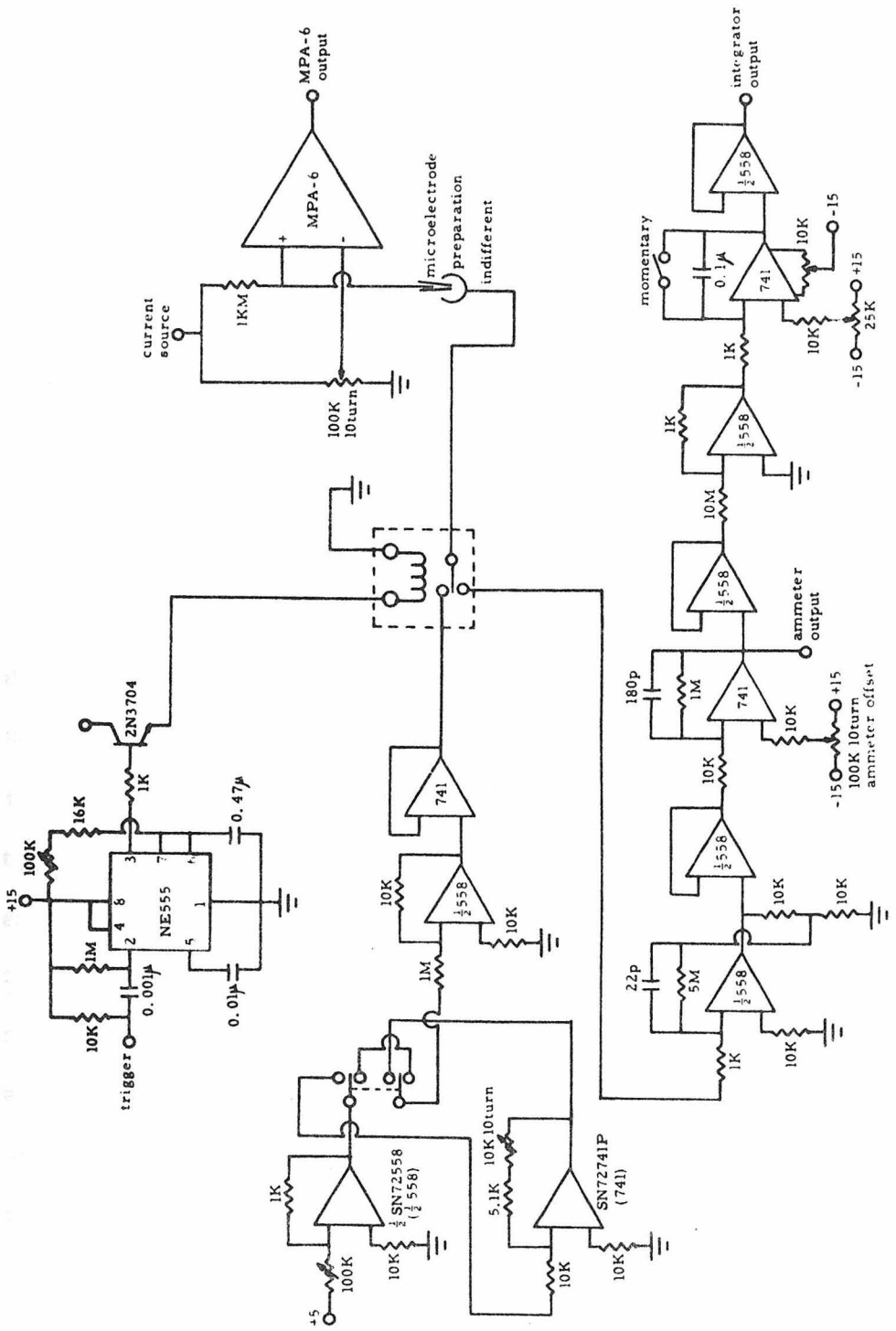

Figure 2.2. Electrophysiological recording schematic. Trigger pulses applied to the 555 in the one-shot configuration at the top add 10 mV pulses to the indifferent potential. The MPA-6 pre-amplifier and passive bridge was mounted on the micromanipulator directly above the recording pipette. The ammeter and integrator section is shown below.

compensation. This causes the feedback loop to oscillate at a frequency dependent upon electrode resistance during the period the compensation is being maximized. Since the noninverting input is being driven under these circumstances by the feedback loop, this voltage oscillation with respect to the inverting input drives alternating current through the electrode tip. While the exact mechanical stresses induced at the tip by this procedure are not well understood, the result is that penetrations of cells may be obtained. It was found that short bursts no longer than 20 msec were the most effective in holding photoreceptors after penetration. For the high resistance pipettes used this typically resulted in only two or three oscillations.

The pulse train 555 triggered also the primary oscilloscope sweep, showing both the stimulus pulse and the AC-coupled output of the pre-amplifier. This light pulse was delivered approximately 0.1 sec after delivery of the capacitance oscillation. In this way a tentative penetration could be identified immediately, providing enough time to disengage the foot switch. Worthwhile penetrations were identified in wild type flies primarily by the light response and only secondarily by a sudden drop in potential. Indeed, it was often the case that the apparent potential would increase suddenly when a unit was obtained. While there can be no doubt that the resting potential is always negative, the stresses induced on the pipette tip by its progress through this hard tissue usually induced wide fluctuations in the DC level. Often the stress induced by a small advancement would be relieved by the pre-amplifier oscillation, as registered in DC potential shifts. Alawi (1972) measured the resting potential for white-eyed Drosophila photoreceptors to be 21.5 mV ± 5.7 s.d. His penetrations were accomplished by jolting the

preparation by an unspecified method.

The basic electronic set-up for recording with current injection is shown in fig. 2.2. The path from the micropipette to the indifferent electrode formed one leg of a passive bridge. This bridge could be balanced so that an external voltage applied at the position labelled "current source" would not register a potential difference at the inputs of the MPA-6. For most work reported here, the balance was set for a 400 M dummy resistance between the non-inverting input and the indifferent. The 100 K potentiometer at the buffer input was mounted on the micro-manipulator as well. Therefore, in order not to disturb the mechanical stability of the electrode tip placement in the tissue, no attempt was made to rebalance the bridge subsequent to obtaining an intracellular response. In cases where data were taken during a continuous current injection, the output of the pre-amplifier was adjusted with a DC offset. Since the maximum currents used for such continuous injections were only ±0.5 nA, the pre-amplifier output did not saturate.

Currents fed through the 1 KM resistor (MDX-400, Victoreen Instrument Co.) were measured with a 741 operational amplifier in an ammeter configuration followed by an operational amplifier buffer. An analogue integrator provided with a momentary discharge of the capacitor and a high precision offset at the non-inverting input followed the ammeter. Immediately prior to an iontophoresis which was to be integrated and recorded, the integrator was zeroed and stabilized with these features. Since the electrode resistances were so high, and more particularly since following a large iontophoresis with a Ca^{++}-EGTA or Mg^{++}-EDTA pipette these resistances varied through time in an individual manner, the ammeter

in all such records was interrupted automatically at approximately 3.9 sec intervals for approximately 0.05 sec and a calibration pulse was applied to the indifferent. As shown in fig. 2.2, the length of the interruption was determined by a 555 in a one-shot configuration which activated a relay. The DPDT switch in the upper left-hand side of fig. 2.2 was meant to make negative calibration pulses available for possible hyperpolarizing unit recordings, but was rarely used. The positive pulse was adjusted by a 10-turn 10 K potentiometer to yield a 10 mV signal across the inputs of the MPA-6 when a 400 M dummy resistance replaced the microelectrode, as when the current injection bridge was balanced.

Data Analysis

During most experiments three channels of data were amplified, DC offset, and recorded on analogue tape with an Ampex tape drive. These channels were:

i) the output of the photosensitive diode,

ii) the output of the pre-amplifier, and

iii) the output of the ammeter integrator.

These channels were observed as needed on oscilloscopes. In addition, the nonintegrated ammeter output was monitored in the appropriate experiments, and the light stimulus and electrophysiological response channels were plotted on a Gulton TR-722 dual channel paper recorder at a speed of 1 mm/sec for data identification. The three recorded channels were subsequently digitized and stored on digital magnetic tape by the LAB data collection system operating on a DEC PDP-11, implemented by Mr. B. M. Ellert and Mr. W. D. Knutsen. Channels i) and ii) were sampled at a rate

of 0.001 sec and iii) was sampled at 0.01 sec. All data collected under LAB are compatible with file manipulation and numerical calculation by GAS, which itself may be optionally under the command of GHOST, both operating on the PDP-11 and implemented by Mr. W. D. Knutsen. All calculations made on the data were accomplished with the GAS system.

For the purposes of Fourier-transforming the stimulus and response data through time to obtain gain and phase information, a Fortran subroutine package was written enabling the user to create in a Fortran byte array the syntax required for controlling GHOST. This enables the user to introduce contingencies into GHOST manipulation which may be implemented while the user is away during a long GHOST run. The GHOST procedures called in this manner controlled GAS-implemented fast Fourier transforms of 1.024 sec sections of data, did the appropriate manipulations to obtain normalized gain and phase data points for each time segment, and deposited these data into new GAS data sets at positive times corresponding to time after the current was turned off in the raw data. The 10 mV calibration pulses running throughout these records were identified visually and their times of occurrence recorded in DOS files in a format compatible with Fortran input. Avoiding these calibration pulses in the records was a particular goal necessitating the writing of a GHOST syntax package capable of handling such contingencies. Another important contingency was variation in data set length, or the amount of time taken to specify full recovery of the receptor potential. A limit in GAS of the number of data sets that can be stored at any one time on the DIVA disk required a piecemeal approach to data analysis for long records.

The subroutine package for controlling GHOST was used by other

programs to deposit the byte syntax into DOS files. Each GHOST procedure call was followed by '^0' characters. A program PSPEC written by Mr. W. D. Knutsen was then used to write the contents of the DOS file onto paper tape, replacing each occurrence of '^0' by the 'control.0' character which suppresses GAS output to the terminal. Use of the paper tape to control GAS then enables the user to monitor the progress of GHOST procedure calls while suppressing the interactive GAS commands.

Some further processing was found necessary to obtain the Fourier records as presented in the next chapter. Since the calibration pulses were continuous throughout, the Fortran main program generating GHOST syntax determined three 1.024 sec blocks between each pulse with exceptions made at the beginning and end. When the calculated data were then deposited into the new GAS data sets, this left many of the one-second time positions corresponding to calibration pulses empty. These positions were subsequently filled by the average of the neighboring data. Using the GAS input-output package GASIO and modified versions of GSUMDUMP, written by Mr. W. D. Knutsen, the GAS data with intermittent empty positions were written into DOS files, processed under FORTRAN, then redeposited on tape as new GAS data sets. The experimental trade-off made in maintaining the continuous calibration while accepting intermittent loss of data was worthwhile for this system.

Two Remarks

Some general comments concerning Drosophila recording may be made here. It was discovered during the course of this intracellular work that recording from those Drosophila mutants chosen was extraordinarily

difficult, much more so than in the ordinary white-eyed preparation. The decremented light-responsiveness of these animals rendered much less clear during the experiment the condition of the particular region of retina in which the electrode tip resided. This interfered with the experimenter's assessment of the condition of the entire animal, a judgement that is of critical importance to data acquisition in a preparation dependent upon active respiration. While the electrode is advanced in a well-functioning wild type retina during pulse train stimulation, small on- and off-deflections of the recorded potential result from differences in ERG strength with respect to the placement of the indifferent. This is an important indication of preparation viability that was largely unavailable for the mutants. Further, it was more difficult to assess whether a unit had been penetrated, and, once penetrated, how responsive and how likely to be maintained.

Another general observation that can be made in retrospect concerns the time of year for recording from the Drosophila eye. The best recordings were made during the winter months of December through February. The worst time for this work seems to be the summer months. In particular, when ERG's were checked on summer flies that had been fully waxed down to the cover slip but whose retinas had not been violated by the speaker cone-coupled razor, these ERG's were frequently fully responsive. But after the cut was made on those same flies, the ERG was typically nearly absent. Some decrement is expected after the cut, but the summer flies seemed especially vulnerable to complete visual function destruction by it. All data for norp A and for wild type low light intensity injections were collected during the summer. However,

the trp injection work was done in December and February. This author has been unable to confirm these seasonal observations with others. Whether due to chance or to uncontrolled factors related to the southern California location, the seasonal differences exerted a profound influence on the progress of this intracellular work.

Chapter III

RESULTS

Introduction

This chapter describes the intracellular data obtained from Drosophila photoreceptors following iontophoresis of Ca^{++}. Wild type and the two phototransduction mutants norp A and trp are the preparation material. Both pulse and sinusoidal light stimulation are used. Pulse stimulation data show a new 'injection-insensitive' component of response. For sinusoidal stimulation both wild type and norp A exhibit transient gain suppressions at all frequencies tested and phase delays at 10.0 Hz and above following iontophoresis. The trp data exhibit a much prolonged gain suppression with respect to the other two animals. Further, gain recovery in trp photoreceptors is accompanied by a transient phase advance at 10.0 Hz instead of a delay.

EGTA and Mg^{++} Iontophoresis

Manipulation of the intracellular Ca^{++} concentration was attempted by two iontophoretic techniques, injection of EGTA and of Ca^{++}. Negative iontophoresis from the EGTA-injecting pipettes prepared as described in 'Materials and Methods' produced no change in the receptor potential that could be distinguished from negative iontophoresis from a 2 M KCl pipette. The similarity of the data obtained for EGTA and Cl^- makes it likely that the large negative currents used, typically 5 nA, provided in both cases a quickly recovering artifact due only to the current. While both EGTA and EDTA are known to cross cell membranes (Fischbach & Nelson, 1977), it may well be that much of the current for the EGTA pipette was carried by intracellular cations. Transport numbers for anions through microelectrode

tips smaller than 0.5 μ may be close to zero (Agin, 1969). Chapter VI describes white noise input results during continuous negative current passage. This is a much more sensitive assay for the effects of iontophoresis alone on the response.

Similarly, positive iontophoresis from Mg^{++}-EDTA and 2 M KCl electrodes yielded no significant change in receptor potentials. This is an important control for the Ca^{++} iontophoresis since the results for this cannot be attributed to an artifact from current passage alone. Indeed, the current capacity of both the Mg^{++} and K^{+} pipettes far exceeded the typical Ca^{++} pipette, and the lower resistance was fully utilized. The cation transport number for these other pipettes must also be much greater. Mg^{++} is the most likely cation to compete with Ca^{++} for binding to intracellular proteins (Williams, 1977) and for replacing it in virtually any physiological system. Therefore the negative result with the Mg^{++}-EDTA pipette shows high specificity of the results obtained in this chapter for Ca^{++}.

Pulse Response Recovery A

Figure 3.1 shows raw data from recordings and injections from a Drosophila photoreceptor with a Ca^{++}-EGTA pipette. Since the record is from preliminary work along the lines of Ca^{++} injection several differences exist between the conditions under which these data were taken and the more productive experimental situation as described in 'Materials and Methods' for subsequent work. Light stimuli for these records are 0.2 sec pulses of white light from dark level at approximately 4 sec intervals; no spectral or neutral density filter intervened in the optical path between

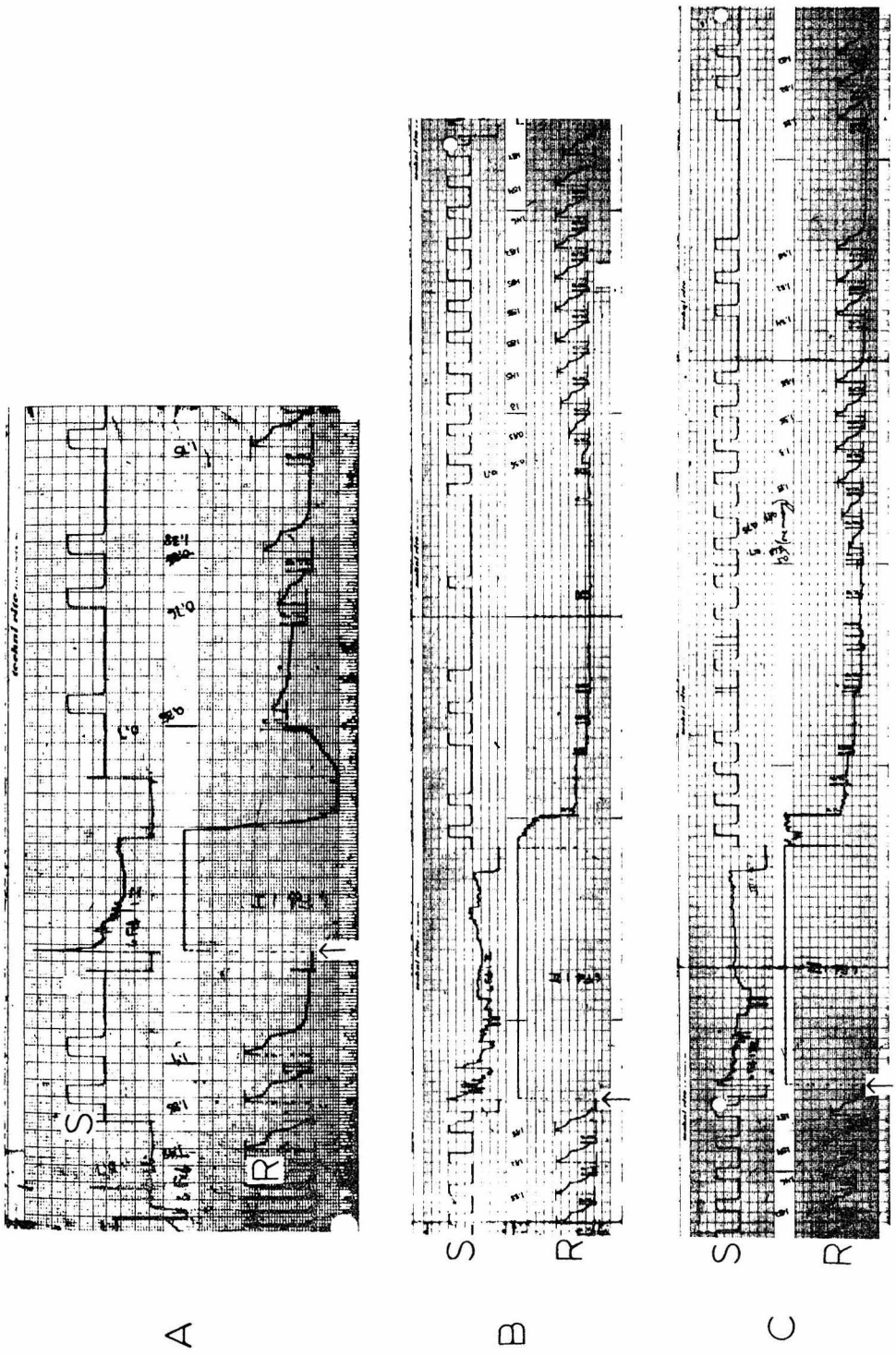

Figure 3.1. Paper records from three Ca^{++} injections into the same wild type photoreceptor. The light stimulation (S) is one pulse 0.2 sec in duration every 4 sec. Receptor potentials (R) are preceeded by 10 mV calibration pulses. The arrows indicate the initiation of current injection. Total currents passed are A) 0.973 ncoul, B) 2.88 ncoul, and C) 4.32 ncoul.

the glow tube and the preparation, although the stimulus was still focused to a 2 mm spot at the position of the fly. The data depicted in fig. 3.1 are photographed directly from the paper record from the Gulton dual trace unit. The Gulton was modified to an automatic recording speed operation; normally running at 1 mm/sec, the speed was switched to 25 mm/sec for about half a second when a trigger pulse indicated that the electrode calibration and light stimuli pulses were about to be delivered. In this way, good time resolution of the data could be obtained without wasting paper. **Apparent non-uniformities in the stimulation rate shown are due only to** difficulties in the various triggering mechanisms for the recorder.

This cell accepted three Ca^{++} injections as shown in the three pairs of records; the unit was lost upon a fourth attempt. The electrolyte in this case was the straight Ca^{++}-EGTA stock solution undiluted by 1% Triton X-100. The lower records (R) for each pair are the recorded pre-amplifier output. Each receptor potential is preceded by first a momentary artifact in this channel from triggering the higher recorder speed and then the calibration pulse applied to the indifferent. The upper records (S) for each pair begin with records of the light stimuli from the current-monitored photodiode. After preliminary pulses the upper trace was switched (at the arrows indicated) to the ammeter output following the indifferent and the recorder engaged at 25 mm/sec. After a short baseline for zero current had been established, positive iontophoresis began for varying lengths of time. The erratic upper trace for this period during which the pre-amplifier saturates represents the nonstationary maximal current passed by the pipette. Immediately following the recision of current the upper trace was returned to the

light monitor and the Gulton returned to the automatic speed mode. The total current passed into the unit was estimated after completion of the experiment by Xeroxing the raw data, cutting out the portions of the ammeter output records above baseline, and weighing these papers. The estimated integrals so obtained were 0.973 ncoul, 2.88 ncoul, and 4.32 ncoul for the first through third, respectively.

Several factors contributed to the difficulty in this experimental operation. Among these were the physical requirements on the experimenter in manipulating both the Gulton unit and current injection while maintaining stable recording in the photoreceptor. Further, as the ammeter output indicates, the resistance of pipettes with straight Ca^{++}-EGTA stock was extremely unstable during injection; dilution of the electrolyte with non-ionic detergent in subsequent work alleviated some of this characteristic problem.

The maximum height of the receptor potential for each response after the injections was measured by hand and is presented in fig. 3.2 as a function of the number of flashes after injection. The abscissa time excursion is based on the estimate of 4 sec for each pulse interval. The ordinate is measured in mV, where the 10 mV calibration pulse normalizes the data; the use of these calibration pulses will be more fully discussed below where data with better time resolution is presented. The receptor potential height for all three injections into this unit follows an approximately sigmoid time course. This result, in addition to the observation that the shape of the receptor potential returns eventually to nearly the original, indicates that the effects of Ca^{++} iontophoresis into these units are under ideal conditions completely reversible. This is of course an

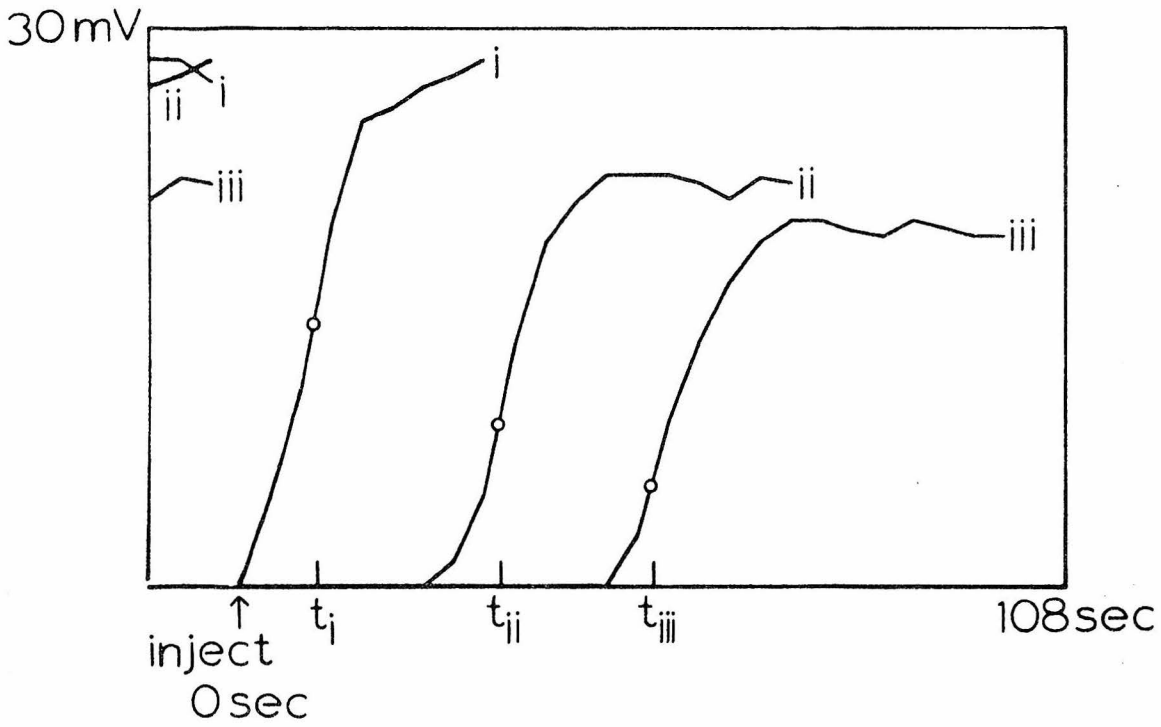

Figure 3.2 Receptor potential heights from fig. 3.1 following injection. Traces i), ii), and iii) correspond to parts A), B), and C) of fig. 3.1, respectively. Prior to injection, three control data points are displayed for each trace. The ordinate scale is based on the 10 mV calibration pulse heights; the abscissa scale is based on the inter-pulse interval of 4 sec. Circles indicate the inflection points of the sigmoid recoveries.

important point in comparing the results of a series of injections into the same unit.

For the second and third injections the recovery follows a quiescent period where the potentials are virtually unmeasurable on the upper record. The circles on the curves of fig. 3.2 indicate the approximate inflection points for the sigmoid shape; these points are reasonably canonical for each of the recoveries and are labeled t_i, t_{ii}, t_{iii}. Thus each injection has associated two numbers, one the current integral and one the approximate time of inflection of receptor potential maximum. Two independent numbers may now be calculated from these six,

$$\frac{2.88 - 0.973}{t_{ii} - t_i} \text{ ncoul/sec} = 7.87 \cdot 10^{-2} \text{ ncoul/sec}$$

$$\frac{4.32 - 0.973}{t_{iii} - t_i} \text{ ncoul/sec} = 7.56 \cdot 10^{-2} \text{ ncoul/sec} .$$

That these numbers are comparable demonstrates the viability of the cell during this recording. Their approximate value may reflect the rate of Ca^{++} extrusion through the plasma membrane assuming the time of current passage is short compared to the time scale of recovery. Indeed, the second and longest injection lasts 4.4 sec, less than $t_{ii} - t_i \approx 14$ sec. The use of the numbers obtained for this unit in determining an extrusion rate for Ca^{++} will be more fully discussed in Chapter V when models of the Ca^{++} concentration within the photoreceptor are presented and the attendant parameters are nondimensionalized.

The numbers so obtained for this unit require at least two conditions be fulfilled. The cell must recover from three injections and the current integrals must have a reasonable spread. This is the only unit obtained

in this study in which both conditions have been met. Viability after the third injection is evident from the shape of the final receptor potentials, although there is some decrement in maximal response. The ratio of the current integrals is approximately 1:2:4.

The time scale to recovery of this unit exceeds that of the typical wild type units to be discussed below. The largest integrated current for these data, that of the third injection, is approximately that used for most subsequent recordings. The electrode used for this unit may have had a higher transport number for Ca^{++} ion than those of later work. This pipette contained approximately ten times the Ca^{++} concentration of the pipettes prepared according to 'Materials and Methods'. This would tend to delay response recovery.

The similarity of the curves in fig. 3.2 suggests that the intracellular free Ca^{++} concentration as a function of time is close for all three recoveries, after time translations which make the sigmoids overlap. It will be argued in Chapter V that diffusion and extrusion of Ca^{++} ion alone are insufficient to explain the time course of recovery of the records obtained in this study. Therefore a third mechanism is introduced, sequestration and release of ion by immobile intracellular sites, where the release rate is small with respect to that of immobilization. A large capacity for sequestration would govern the free Ca^{++} concentration in such a way that the qualitative results of fig. 3.2 would be expected. Successively higher injections essentially load the intracellular sites with successively higher bound concentrations.

Pulse Response Recovery B

While the shape of the receptor potential changes during the recovery, as is apparent from the data, it is difficult to make accurate measurements on the paper record. Therefore the data for the next series of pulse response experiments were collected onto magnetic tape as described in 'Materials and Methods'. Further, the 491 nm interference filter was used which effectively lowered the intensity of the incident light. Therefore the receptor potentials shown in all subsequent records are taken below the intensity necessary to produce distinct transient and plateaux phases. Since the results of injection are just as apparent at the lower intensity as with the unattenuated stimulus, it was decided that the better definition of the incident spectrum and intensity well justified the intensity loss.

Figure 3.3 shows sections of the digitized record of another wild type unit recorded with a Ca^{++}-EGTA pipette which was silylated with 0.3°/o HMDS in toluene as described in 'Materials and Methods'. The electrolyte was the stock buffer diluted by two parts 1°/o Triton X-100. This electrode has unusually high current passing ability; approximately 4 ncoul was injected in 0.6 sec.

Prior to the onset of each light pulse is the calibration pulse applied across the indifferent and adjusted previously to 10 mV when a 400 M resistance replaces the microelectrode in the current path as described in 'Materials and Methods'. While not impossible, it is at least very inconvenient to continuously monitor the electrode resistance. This is particularly true when working with Drosophila in that the preparation is so delicate. Much that in other preparations would be described as

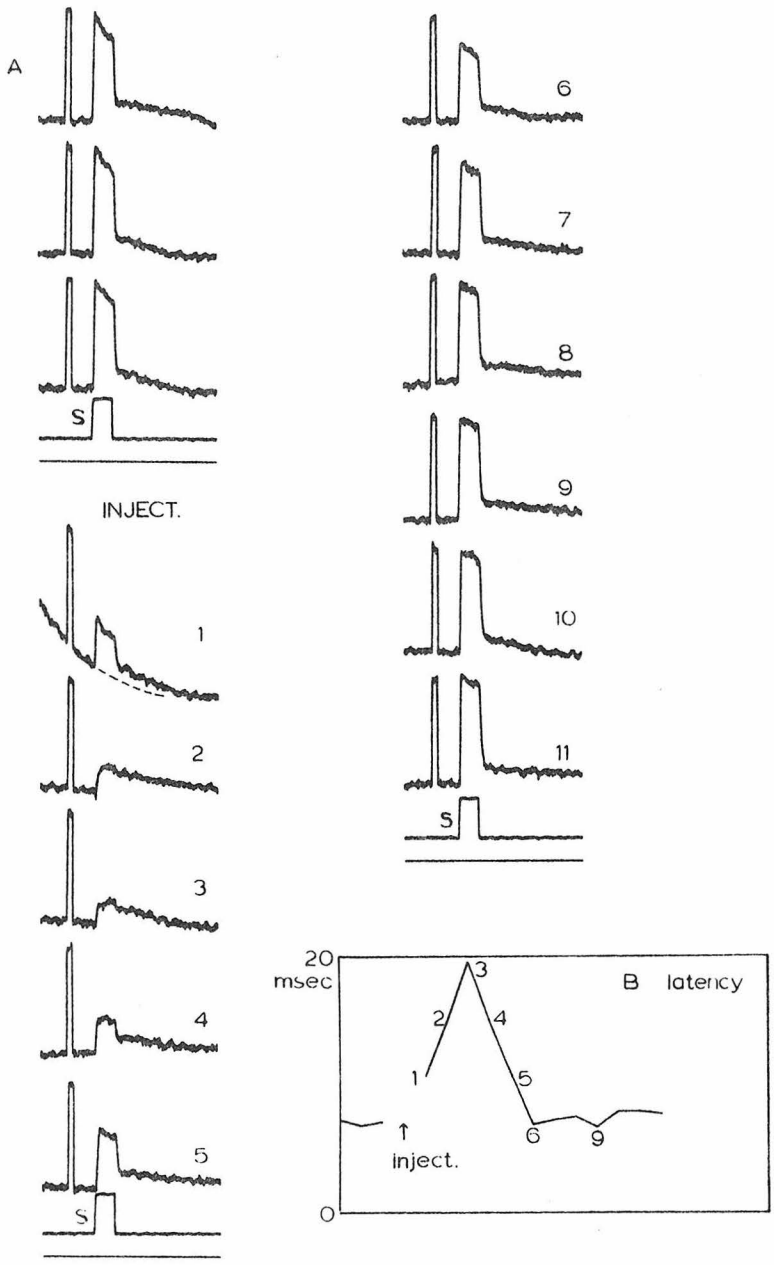

Figure 3.3. A) Receptor potentials before and after Ca^{++} injection. Trace (S) indicates the 180 msec maximum intensity light pulse at 491 nm delivered at 3.9 sec intervals. Clearly visible are the 10 mV calibration pulses preceeding each receptor potential. B) Latencies of the receptor potentials of part A). The numbers correspond to the individual post-injection responses.

experimental convenience becomes experimental necessity in this small Dipteran. Therefore the calibration pulses, while not exactly 10 mV in height for any given electrode, approximate this value sufficiently to provide both an indication of the state of the electrode after a strong injection and a reasonable voltage measure to which the recorded receptor potential may be compared.

The first post-injection response has a maximum height of 4.1 mV, which exceeds those responses for the next twelve seconds. Further, the shape of this first depolarization is much like a control response in miniature, as contrasted with the next three pulse responses. This is reflected in the latency of response plotted as a function of time for this unit. Therefore, while the first response is reduced in absolute value, it took a matter of at least 2 sec for the injection to be fully expressed in the shape of response. This result is masked in all subsequent records to be described, in part because the requisite time for current passage sufficient to elicit changes in response was longer by a second or two. The fortuitous circumstances of this unusual microelectrode combined with the timing of current passage with respect to the train of light stimuli enabled this result. Further, use of pulses of light provides a convincing response even when superposed on a rapidly changing DC level of the pre-amplifier output. Had sine or other more complicated stimuli been delivered here it would have been difficult to eliminate the contamination of the measured data due to the approximately exponential baseline.

The response of this cell to Ca^{++} iontophoresis is evidence for an

effect of lowered intracellular pCa distinct from that predicted by the Yoshikami-Hagins model for Ca^{++} involvement in photoreception. This model specifies a simple blockage of Na^{+} channels in the plasma membrane from the inside of the cell. The first post-injection response of fig. 3.3 is nearly compatible with this view, since additional blockage of available light-coupled conductance channels would be expected to reduce the receptor potential multiplicatively. The latency of the first response is nearly identical to that of the fifth, but total depolarization of the former is about three-quarters that of the latter.

The first five post-injection responses are qualitatively different from the controls, and thus cannot be explained by simple reduction of membrane conductance. It is likely that by the time of the second response, 3.9 sec after the first, some additional event or events in the phototransduction process have been altered by lowered pCa. It is the recovery of this event that is measured in most of the experiments reported in this chapter.

With the possible exception of the unit of fig. 3.1, in none of the wild type cells that recovered in the present study was light-responsiveness completely eliminated by Ca^{++} iontophoresis. Thus, it is possible that the Ca^{++}-sensitive event is either incompletely suppressed in these experiments or can be bypassed in the phototransduction process.

The somewhat pedestrian advantage of pulse train stimulation during a period of moving baseline has been exploited in fig. 3.3 in suggesting the dotted curve underneath the first recovery response. After the off-repolarization of the cell in all the control responses for this cell there is an 'after-potential' which decays more slowly to resting potential.

This after-potential was observed first by Alawi (1972) for the white-eyed Drosophila mutant. It is evident from the data presented in fig. 3.3 that this component of the response is preserved throughout the recovery from Ca^{++} iontophoresis. While the evidence for its preservation in the first response rests upon the suggested baseline, this component is clearly maximal for the next response. Therefore, in sharp contrast to the major stimulus-coincident portion of the response this component is largely injection-insensitive. This last is the case only to the extent that the decremented component is sufficiently large to support the after-potential at the falling edge of the pulse stimulus. Other pulse train stimuli experiments show clearly that in units given to similar after-potentials the stimulus-coincident portion of the maximally suppressed response during recovery is always sufficient to support an undiminished after-potential. This suggests that these two components of low pCa pulse response are identical. It will be argued in the next chapter that this single component derives drom coupling to other cells and therefore does not reflect a truly 'Ca^{++}-insensitive' component of the receptor potential.

The observation that the first post-injection receptor potential is much faster than the subsequent responses indicates further that the Ca^{++}-sensitive event is engaged by iontophoresis with some delay. This delay may be due either to an inherent property of the event or to the time required for free Ca^{++} ion to diffuse inside the photoreceptor over sufficient length and at sufficient concentrations to be effective.

Wild Type Sinusoidal Response Recovery

While change in shape of the pulse response through time following Ca^{++} injection has been demonstrated, the type of nonstationary analysis utilized is limited by the need to collect time domain data that best characterize the receptor potential. Large pulse responses are advantageous in this respect. This necessitates the relatively slow pulse train rate for this rapidly light-adapting Dipteran photoreceptor. In the frequency domain however, with stimulus power sharply peaked at a given frequency, the response can be characterized by gain and phase continuously throughout the nonstationary period. Since the respiration of Drosophila photoreceptors requires that the whole animal remain intact for recording, the measured intracellular response of these cells is often noisy. Abdominal contraction in otherwise healthy preparations often gives rise to random excursions in the potential being recorded. The automatic filtering of stimulus and response components implied by Fourier domain calculations reduces the error that would otherwise be incurred in the time domain. Hence frequency domain analysis was selected as the approach most likely to discriminate among injection recoveries of the photoreceptors of wild type and the selected mutants.

Figures 3.4 - 3.5 depict both the raw data and the processed Fourier records for a wild type photoreceptor that was injected five separate times with positive current from a Ca^{++}-EGTA micropipette. This cell is exemplary in that during continuous recording the unit accepted and fully recovered from this number of injections. Figure 3.5b shows two pulse responses of this unit, the first recorded before the first injection and

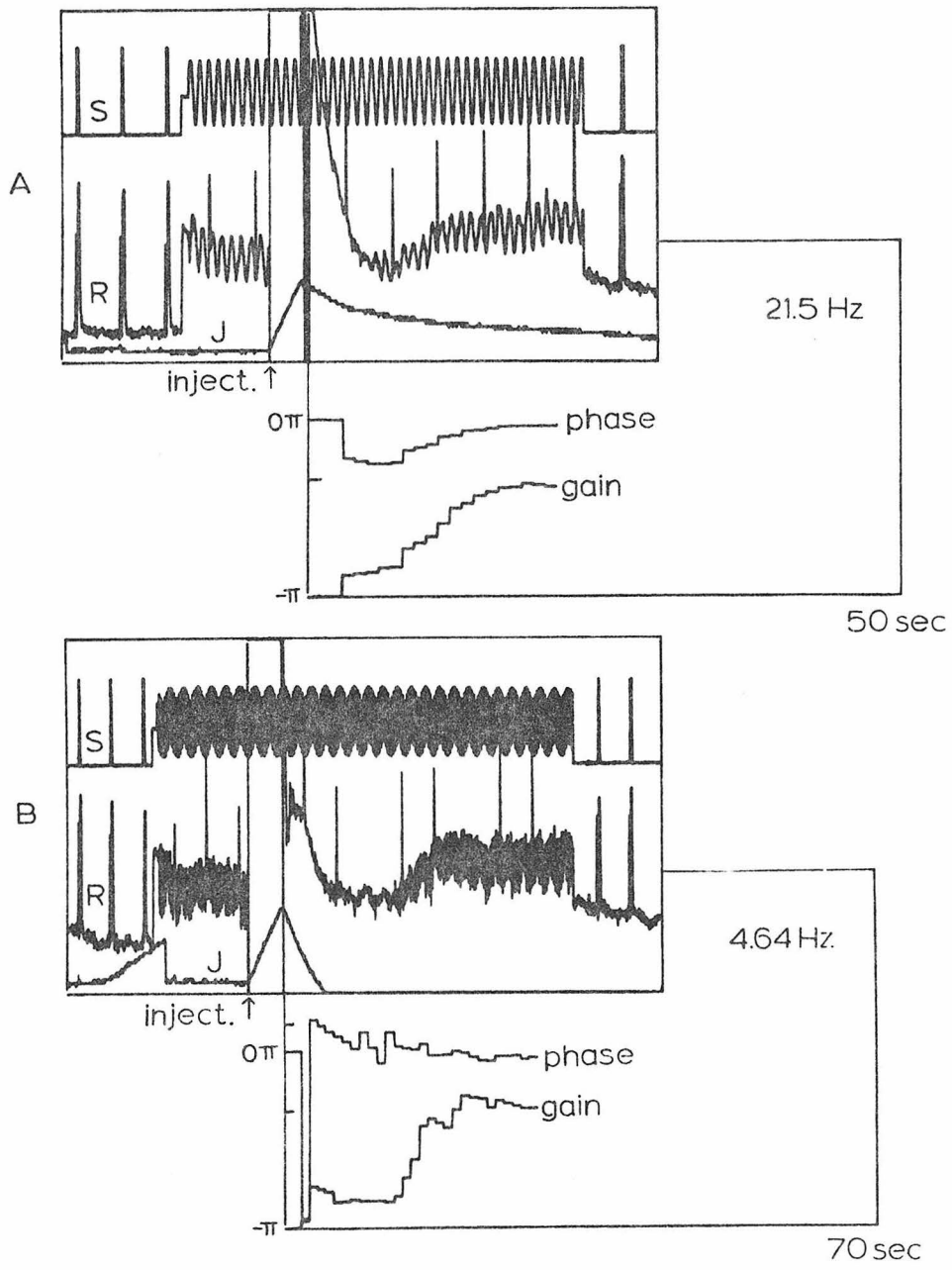

Figure 3.4. Sinusoidal response recoveries of a single wild type photoreceptor following Ca^{++} injection. Light stimuli at 491 nm and 0.4 maximum intensity are A) 21.5 Hz and B) 4.64 Hz. Normalized gain and relative phase of the response (R) with respect to the stimulus (S) are shown in the adjacent graphs following the recision of current. The 0π and $-\pi$ designations refer to the phase difference from control. The single tick mark visible in the adjacent graph of A) defines the control gain of 1.0. The upper tick mark of the adjacent graph of B) defines the negative of the control phase.

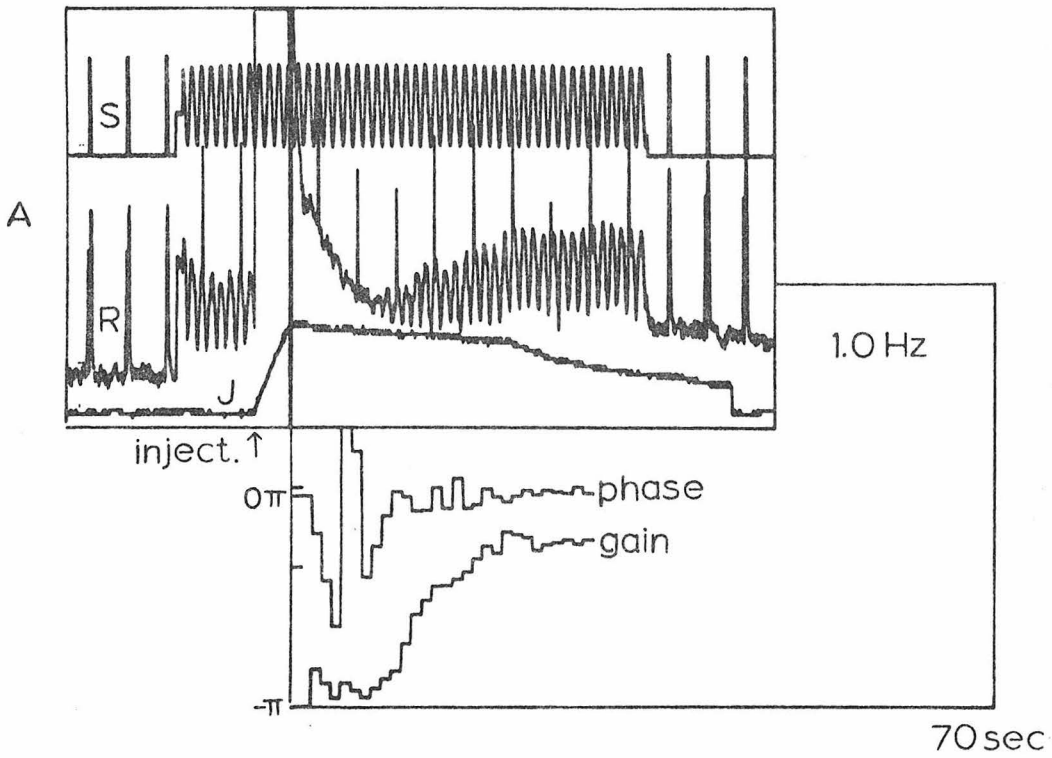

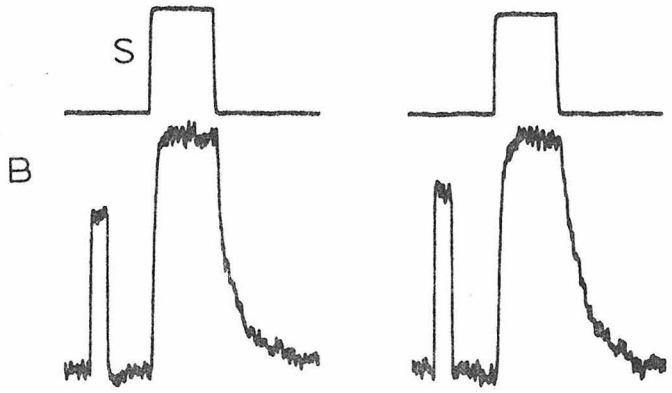

Figure 3.5. A) Sinusoidal response recovery at 1.0 Hz of the photoreceptor of fig. 3.4. B) Pulse response receptor potentials to 170 msec pulses before the first injection and after the fifth injection.

the second recorded after the fifth injection. The records on the top of this figure are of the stimulus data pulses 170 msec in duration from dark to maximum intensity at 491 nm. The records below are the recorded intracellular response. The calibration pulse height has increased somewhat after the fifth injection indicating that electrode resistance has decreased. The pulse response is indeed comparable after the fifth injection to that of the control. The delay of the depolarization on-response is in both cases 8 msec. Differences are seen in the lessened total depolarization, the rounded shoulder of the on-response, and the increased latency of the off-repolarization. However, such response decrement is to be expected in intracellular data of such small units over a few minutes of recording, particularly when current is used.

In the three presentations before the pulse comparisons, the time scale is considerably compressed in that they are each 50 or 70 sec in width. The uppermost trace (S) in fig. 3.4a is the light monitor data, with pulses every 3.9 sec before sinusoidal stimulation at 21.5 Hz. The data below show the intracellular response (R). Just visible are the calibration pulses before each pulse response. Running the entire length of the figure is the integrated current record (J). At the left-hand side of fig. 3.4b may be seen a large jump discontinuity downward in the integrated current. This identifies the zeroeing of the current integral by momentary discharge of the integrating capacitor as described in 'Materials and Methods'.

After the third pulse in this fig. 3.4a, the light stimulus is switched to the sinusoid, the cell depolarizes and light-adapts to the new average intensity, and control or pre-injection sine data is collected

by which to normalize the subsequent calculations. It is important to point out here that the data for both light stimulus and response, because of the sampling rate of the graphics on the CRT used, are aliased in both presentations of fig. 3.4. Figure 3.5a is not aliased in this manner since 1.0 Hz is compatible with display for the 70 sec time frame. Nevertheless, the aliased pictures give a good indication of the true amplitudes.

After two calibration pulses superposed on the sinusoidal response in fig. 3.4a the positive iontophoresis begins and lasts 2.68 sec for a total injection of 3.3 ncoul as documented by the current integral. The time of injection is bracketed in this figure by vertical lines in the response data, narrow at the onset and heavier at the offset of current. The pre-amplifier frequently oscillated in this manner upon instantaneous switching of maximal current. Following recision of current there is frequently an exponential discharge in the integrating capacitance of the J trace, more particularly evident in fig. 3.4b. This is not taken to weaken the validity of the integral obtained since the climb of its value is linear in most acceptable records. Sometimes electrodes were given to sudden resistance changes during regular recording in the absence of current. These changes were not immediately evident in calibration pulse height but enough to provide an apparent offset of the input to the integrator. Such situations were not permitted to interfere with intracellular data collection; if the current integral could be zeroed and remained steady for a few seconds before an injection, as fig. 3.4b illustrates, the experiment proceeded.

The pre-amplifier record itself saturates during the injection. This DC level returns within a few seconds after the current is turned off. The calibration pulses are applied continuously to the indifferent and six are evident in the sine response in fig. 3.4a after the injection. The fact that the heights of the first one or two after current passage are comparable to those before injection demonstrates that electrode resistance has not been markedly altered by the current. Before the DC level of the pre-amplifier has fully declined the response of this cell is already recovering between the first and second such pulses. Between the second and third pulses the average depolarization of the cell is increasing. Since the record of this phenomenon is contaminated by readjustment of the pre-amplifier output, quantification of the extent of DC potential change is difficult to obtain. However, it is apparent that an injection-stimulated hyperpolarization of the cell from the otherwise light-adapted transmembrane potential is the simplest explanation for the local minimum at the second post-injection pulse. Figure 3.4b is a more graphic illustration of the hyperpolarization in that the receptor potential recovery is delayed with respect to that of fig. 3.4a, and so is less likely to be contaminated by the strong exponential decay of the pre-amplifier output. Most good Ca^{++} injection recoveries obtained during sinusoidal stimulation that are delayed in this manner show some relative hyperpolarization.

Some observations may be made here as well about the permanent upward drift of the entire recorded response after injection evident in all three presentations. When the sinusoidal light stimulation is finally returned to pulses, the recorded resting potential is higher than the resting potential recorded prior to injection. This is due in

part to the higher state of light adaptation of the cell from the sinusoid average intensity, and this contribution is reflected in the slow repolarization of the resting potential between the final pulses as dark adaptation proceeds. However this relative depolarization is not enough to account for the difference with the control potential, the same difference between control and final sinusoidal responses. This discrepancy may be attributed to a change in the junction potential at the tip of the electrode, that potential developed between the electrolyte and intracellular fluid owing to surface effects of the glass (Agin, 1969). Following current passage it is likely that the ionic composition of the tip region itself undergoes some unspecified change that results in a new junction potential. Since this potential is simply additive to the data collected, the efficacy of the measured response still rests on the demonstrated viability of the cell, as in fig. 3.5b.

Nearly always after a cell was lost in a recording session with a Ca^{++} pipette, the electrode was 'cleaned out' by alternating maximal current passage of both polarities in the extracellular fluid. In this way, usable electrodes could be maintained during a pass through the retina. The steady state potential was frequently observed to decrease following this procedure. This lends support to the hypothesis regarding a change in ionic composition of the tip from intracellular current passage. Since the composition of the extracellular space is expected to be very different from that of intracellular spaces (higher pK, lower pNa, lower pCa in the extracellular space) the junction potential of the fine tip would differ in these environments.

Pictured below the raw sine records in figs. 3.4 - 3.5 are the fully

processed gain and phase calculations on the same time scale, the phase data above and the gain below. These plots begin at that time at which the current is turned off. These results are normalized to calculations made for raw data before the injection. Prior to injection, three blocks of 1.024 sec were selected, avoiding of course the calibration pulses, and control gain and phase were determined in absolute numbers by averaging among the three. The gain following injection is divided by the control gain; the phase following injection has subtracted from it the control phase modulo 2π. The visible tick mark in fig. 3.4a indicates normalized gain of 1.0. The vertical scale for the lower plots applies only to the phase. A phase datum above 0.0 indicates phase advance with respect to the control. An additional tick mark visible in fig. 3.4b indicates the negative of the absolute control phase. Therefore, the distance between this mark and phase of 0.0, where all the phase plots initiate, defines the upper physical limit on the response phase; phase data in excess of this value must be attributable either to noise not coupled to the stimulus or to values differing from those indicated by units of 2π. In addition, large excursions in phase data as shown in early history of the recovery of fig. 3.5a may correspond to crossings of the $\pm\pi$ limits.

Figure 3.6 shows the processed records for all five injections into this cell covering the range of light stimulation from 1.0 Hz to 21.5 Hz. The chronological order of the injections is indicated by the number in the upper-right corner of each graph. These records illustrate both the success of the experiment as well as the difficulty inherent in its interpretation due to the delicate conditions under which it is undertaken.

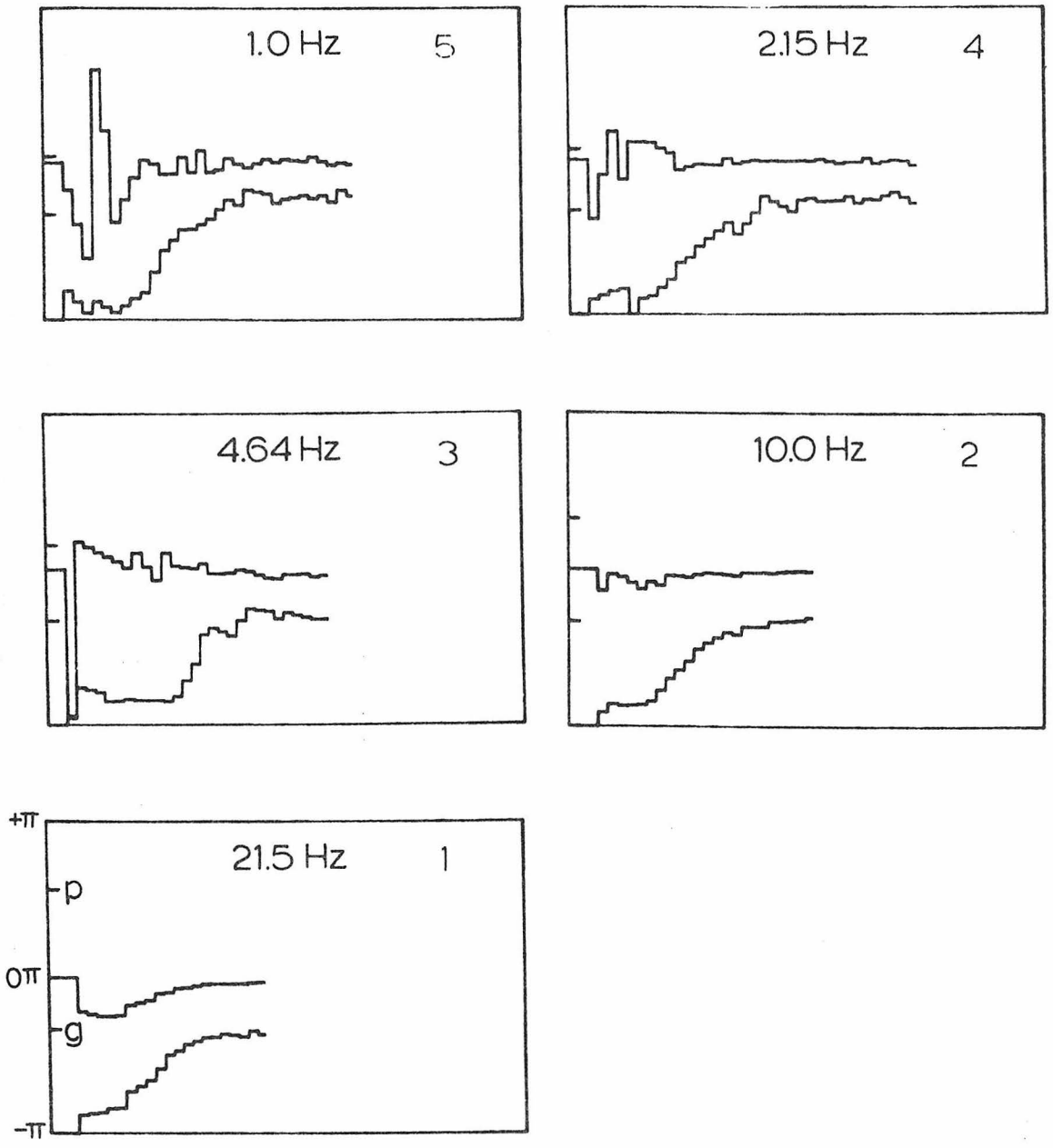

Figure 3.6. Processed gain and phase records for the five recoveries of the cell of figs. 3.4 and 3.5. Chronological order of the injections is indicated in the upper right-hand corner of each graph. The tick marks labeled 'p' and 'g' in the lowest graph are the control phase and gain values, respectively. The labels $+\pi$, 0π, and $-\pi$ on the vertical axis of this graph refer to the relative phase. Each graph is 50 msec in length.

The calculated gains uniformly undergo a dramatic suppression in the early recovery. This period is characterized by approximately steady gain normalized to 0.1 - 0.3. Then follows a gain advance whose onset is identifiable to within certainly a few seconds. The subsequent recovery proceeds typically on the order of 10 sec, but may be more or less precipitous. In general, early injection gain recoveries proceed more rapidly than later ones. Thus the gain recoveries from the first three injections into this unit have a sharper sigmoid shape than those from the final two.

The processed phase records also exhibit transient changes during recovery that return eventually to the control values. There is a significant and constant phase delay at 21.5 Hz; the maximum phase shift is approximately -0.25π. The time course of the phase parallels that of the gain even to the extent that the time of onset of the phase recovery is identical to the onset of gain recovery. This observation, in addition to the fact that the maximally suppressed gain is fully 20% that of the control, supports the contention that the phase data reflect light-coupled response throughout. The phase data at 10.0 Hz undergo less of a shift than at the higher frequencies, but the direction of change, delay instead of advance, is the same.

The phase shift of this cell corresponds formally to a delay of 5.8 msec, comparable to the actual increments in delay of the second and fourth pulse responses of the cell of fig. 3.3, which are each 7.8 msec. Whether the sinusoidal response reflects an actual delay of some mechanism involved in the response is not addressed by the present methods. Since

it was necessary to optimize the signal to noise ratio, stimulus power was restricted to a single narrow region of the Fourier domain.

The phase data at the lower frequencies show excursions up into the unphysical region. In only one of these (fig. 3.4b at 4.64 Hz) is there a consistent trend in the phase response. The time of unphysical phase for this injection comes soon after the current is turned off, just after the raw receptor data inexplicably remains at a high DC value. This is the same injection that exhibits unusual behavior of the current integral. It is possible that during the period of this third injection and recovery the tip of the pipette was marginally positioned inside the cell in the sense that good contact with the volume of cytoplasm was not being well maintained. In view of the slight phase delay at 10.0 Hz for this unit, no coherent pattern of phase change may be ascertained from the lower frequencies. In none of the later three injections is there a good indication from the phase records of the time of onset of gain advance.

Further Injections into Wild Type Units

Figures 3.7 - 3.10 show processed records for several other injections into wild type units all integrated to approximately 4 ncoul and recorded under the same conditions. Stimulation frequencies are from 4.64 Hz to 46.4 Hz. The figures are organized so that each horizontal row represents data from the same cell. Therefore, each of these cells except the single one of fig. 3.10 at 46.4 Hz recovered from at least two injections. As in fig. 3.6, the number of the injection is indicated for each graph, each of which covers a time of 50 sec. In general, the observations made above for

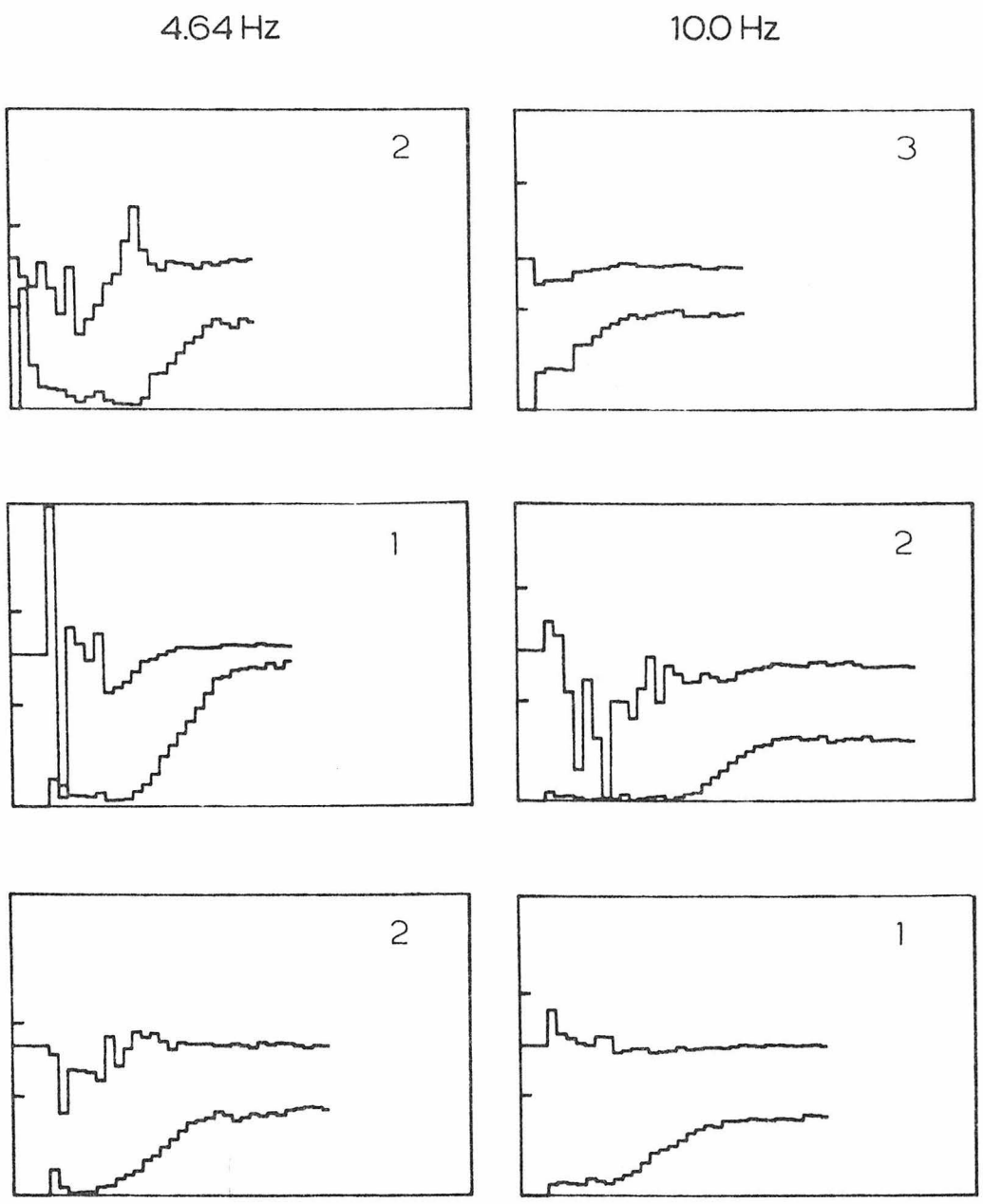

Figure 3.7. Processed gain and phase recoveries for three wild type photoreceptors following Ca^{++} injection. Each horizontal row represents two records for each cell during 491 nm light stimulation, 0.4 maximum intensity, at 4.64 Hz and 10.0 Hz. Chronological order of the injections for each unit is indicated in the upper right of each 50 sec graph. Scales and tick marks are identical to those of fig. 3.6.

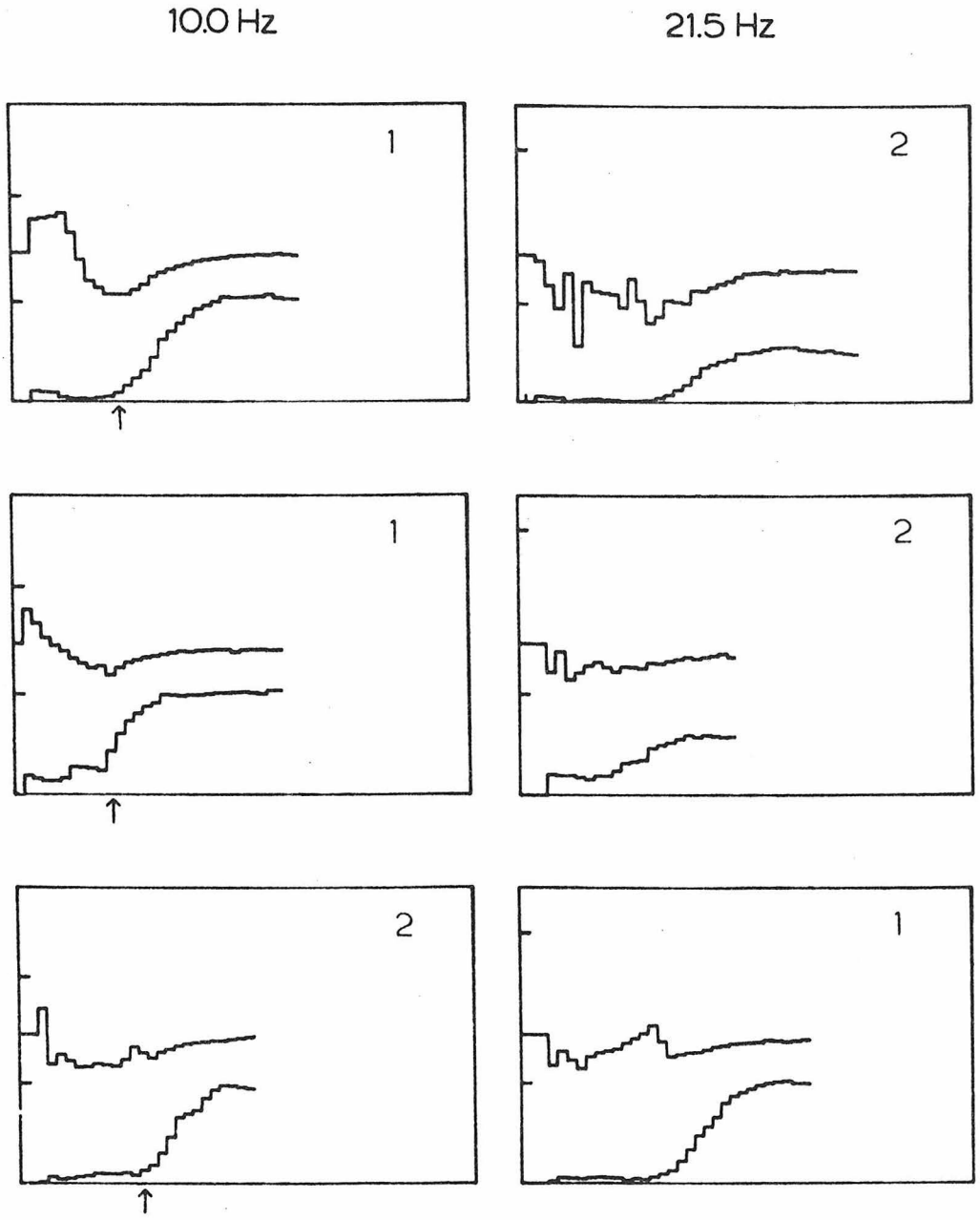

Figure 3.8. Wild type data at 10.0 Hz and 21.5 Hz, with the same format as fig. 3.7. Arrows in the 10.0 Hz records indicate the inception of gain recovery; data before the arrows is used in fig. 3.15.

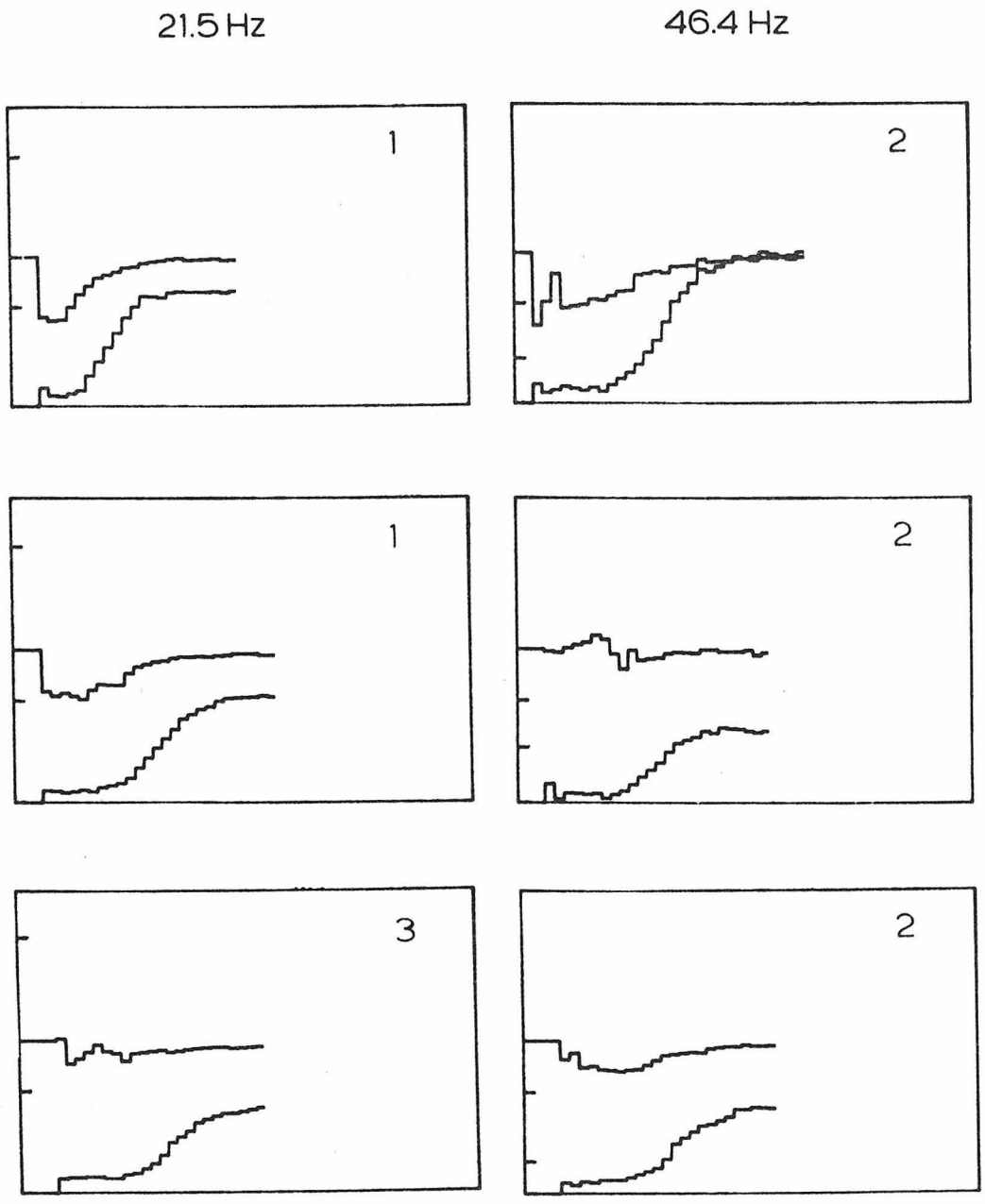

Figure 3.9. Wild type data at 21.5 Hz and 46.4 Hz, with the same format as fig. 3.7.

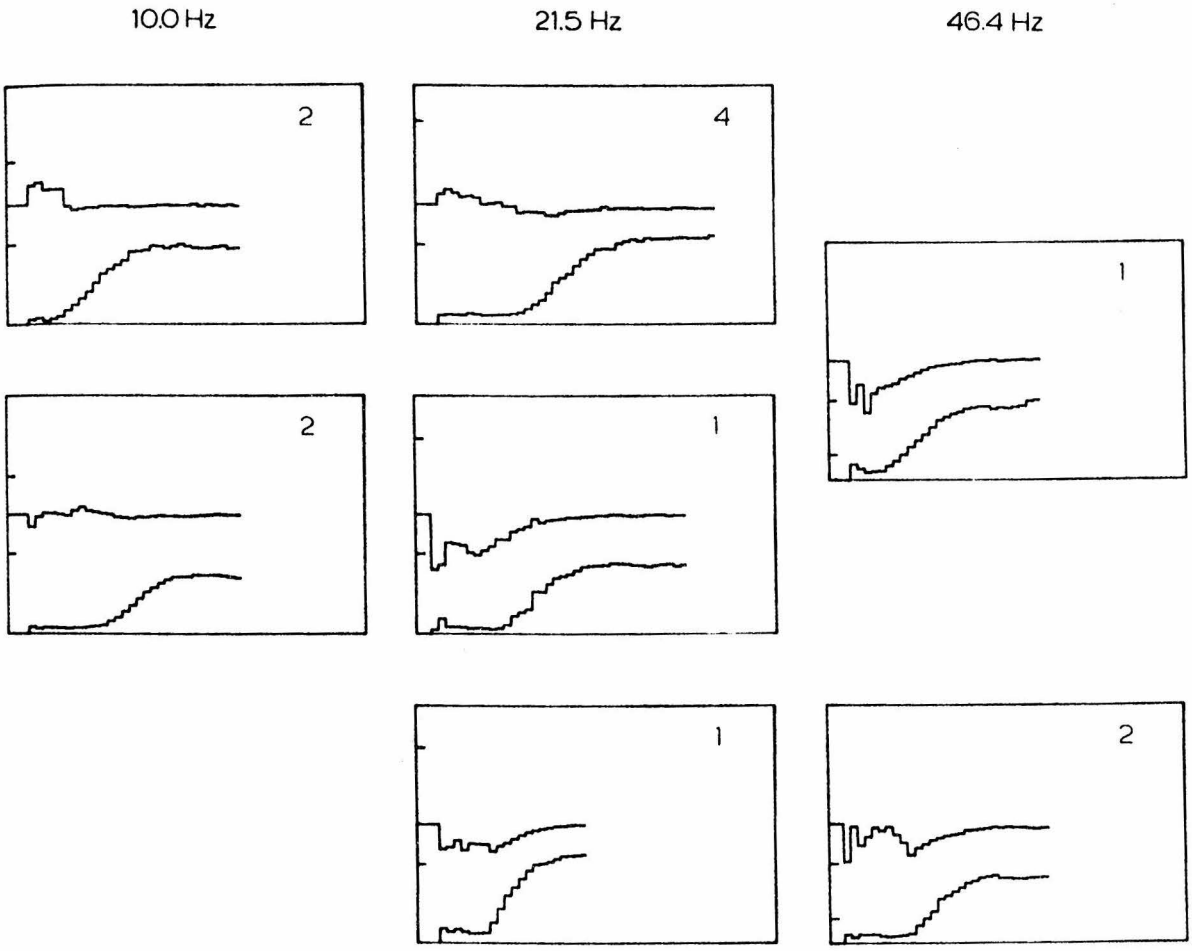

Figure 3.10. Wild type data at 10.0 Hz - 46.4 Hz. Recoveries of four units is presented, three from the horizontal rows and one single-injection record at 46.4 Hz. Otherwise the format is the same as for fig. 3.7. The control phase tick marks for the 46.4 Hz records indicate the true stimulus phase minus 2π.

the cell for which the raw data have been shown hold for these injections as well. There is a period of gain quiescence followed by a well defined initiation of recovery. Both the length of quiescence and length of recovery are of the order of 10 sec. The phase may extend to the unphysical region during the former period but typically settles to a delay which follows gain recovery back to the pre-injection value. As might be expected, single units often have similar recovery patterns for frequency pairs, although the constantly changing disposition of cell viability and of the penetration seal provides obvious exceptions to this rule.

Figure 3.11 shows results from the lower frequency range 1.0 - 4.64 Hz, and fig. 3.12 shows data obtained under identical recording conditions at 4.64 - 21.5 Hz,but with the intensity of stimulation reduced by 0.9 log unit. Phase data at the lower frequencies are in general more noisy than that for the higher frequencies,in part because there are fewer cycles over which to average; note that it is the log frequency range that has been divided evenly and not the linear range. No consistent trend is evident for the lower frequency phases. With the single exception of the middle cell of fig. 3.7 at 4.64 Hz, the phase delay in the response below 10.0 Hz appears to be largely unaffected by low intracellular pCa. This is true as well at the lower intensity. Since all the data obtained at this lower intensity for 46.4 Hz are extremely noisy, only the range 4.64 Hz - 21.5 Hz is shown in fig. 3.12.

Injection into 'norp A' Units

The injection results of selected norp A^{H52} records are presented in

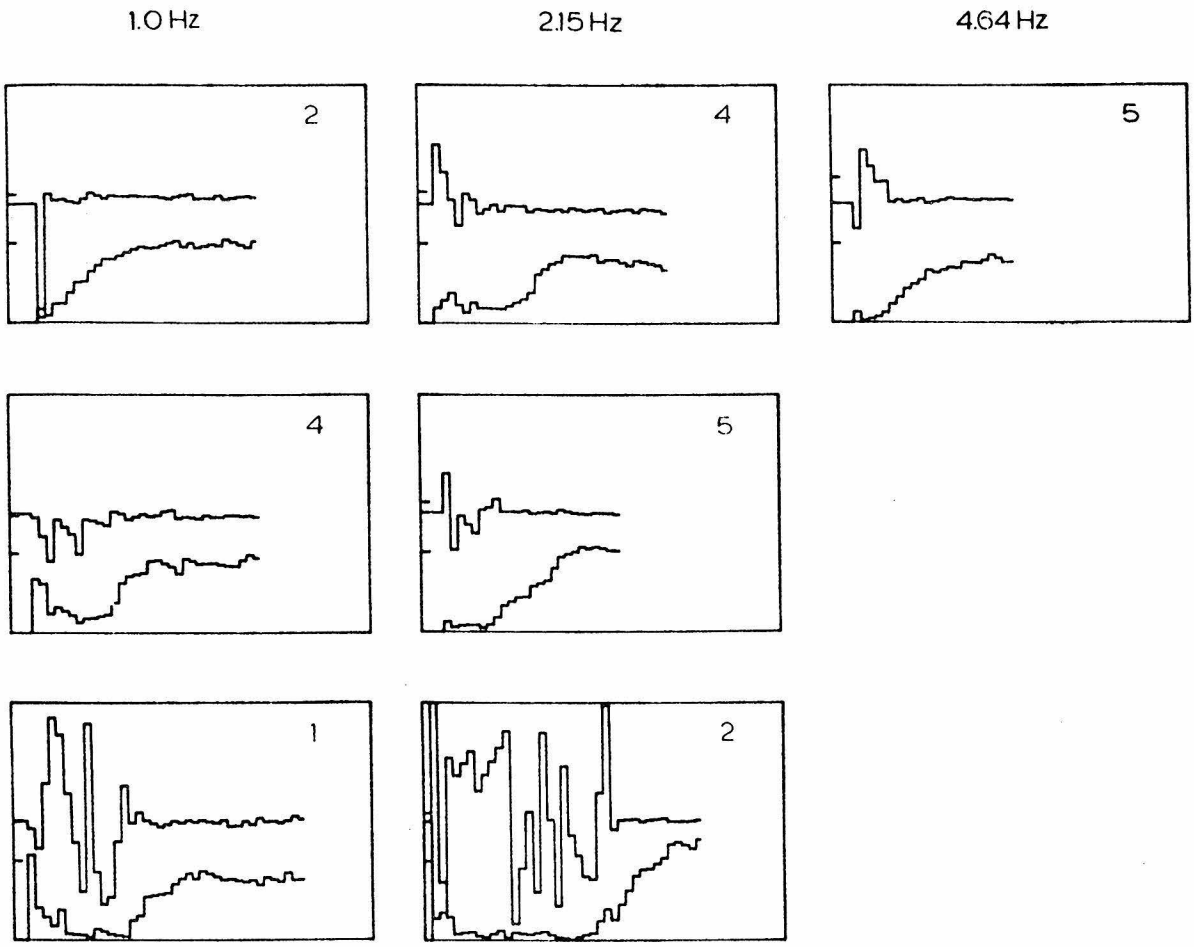

Figure 3.11. Wild type data at the lower frequencies, 1.0 Hz - 4.64 Hz. Each horizontal row is processed data for the same unit.

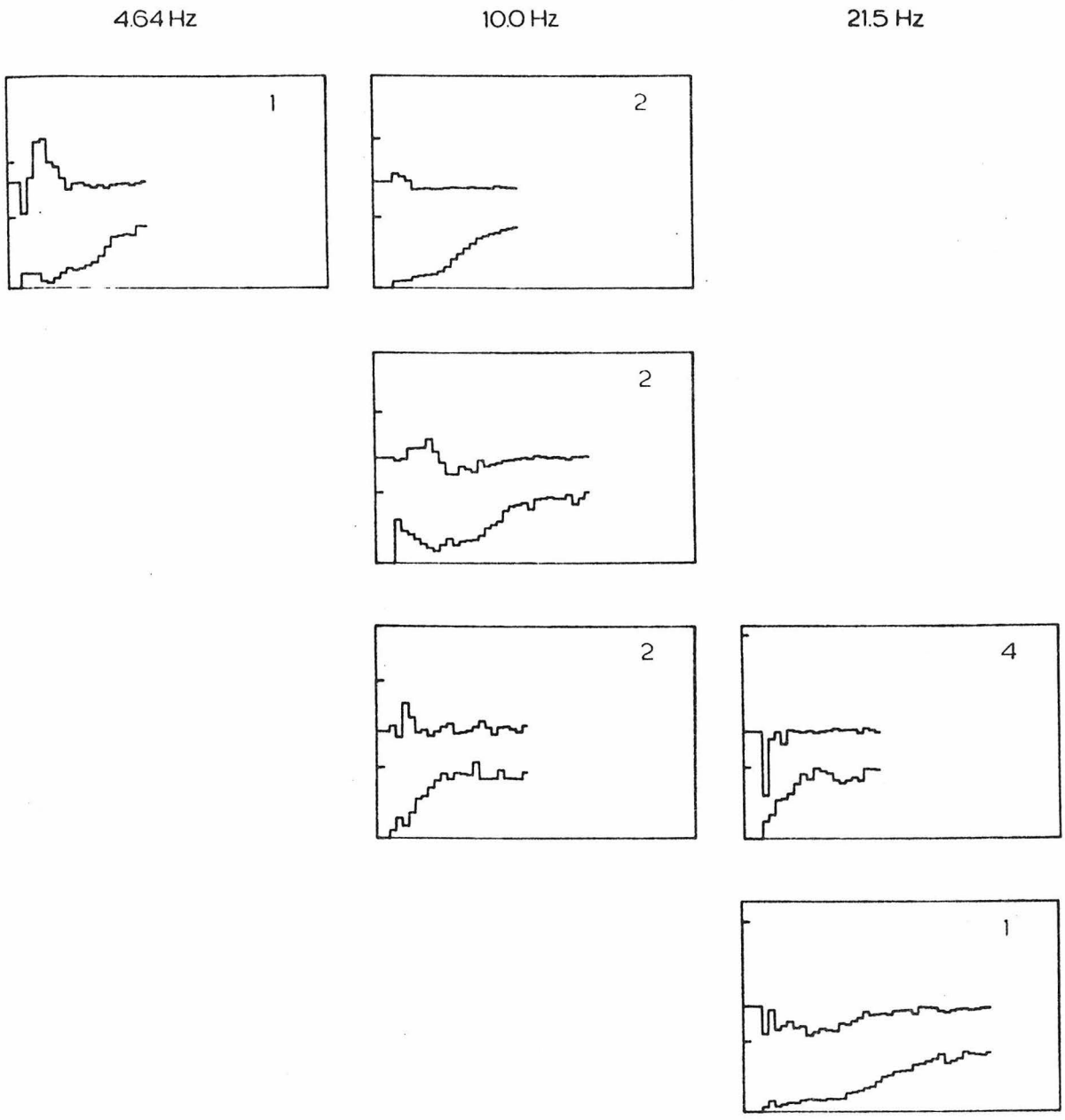

Figure 3.12. Wild type data at an intensity 0.9 log unit below that used for figs. 3.7 - 3.11. Each horizontal row is processed data for the same unit.

fig. 3.13. As was noted in 'Materials and Methods' all the data from this mutant were collected during the unaccommodating summer months. The top graph is the best indication obtained for a coherent result. Taken at 10.0 Hz, the pattern of recovery is similar to that obtained for the wild type. Gain is suppressed but not eliminated for 8 sec followed by a well defined recovery lasting 7 sec. Phase is delayed by -0.21 π at the time of initiation of gain advance and increases smoothly toward the control value. The other cells were selected on the basis that they each accepted two injections; however, the processed records are quite noisy. If any conclusion may be drawn from the norp A injections it is that the results of lowered intracellular pCa are similar to those for wild type. This conclusion will be utilized in formulating a model for phototransduction in the **next chapter.**

Injection into 'trp' Units

Figure 3.14 presents the results of Ca^{++} injections into trp photoreceptors. The top graph is from a cell that accepted only one **injection** recorded in the month of December from a very responsive fly. Visual activity in most trp flies recorded was suppressed at the maximum intensity used. However, the activity of this preparation was sufficient at this intensity to record sinusoidal responses. The four lower graphs are from another cell that seemed to accept nine injections, although the processed records for most of these were quite noisy, as for example the results at 21.5 Hz in the lower right of fig. 3.14b. Nevertheless, data for the spectrum of stimulation frequencies from 1.0 Hz to 21.5 Hz at an intensity 0.9 log unit below maximum were collected for this unit. This

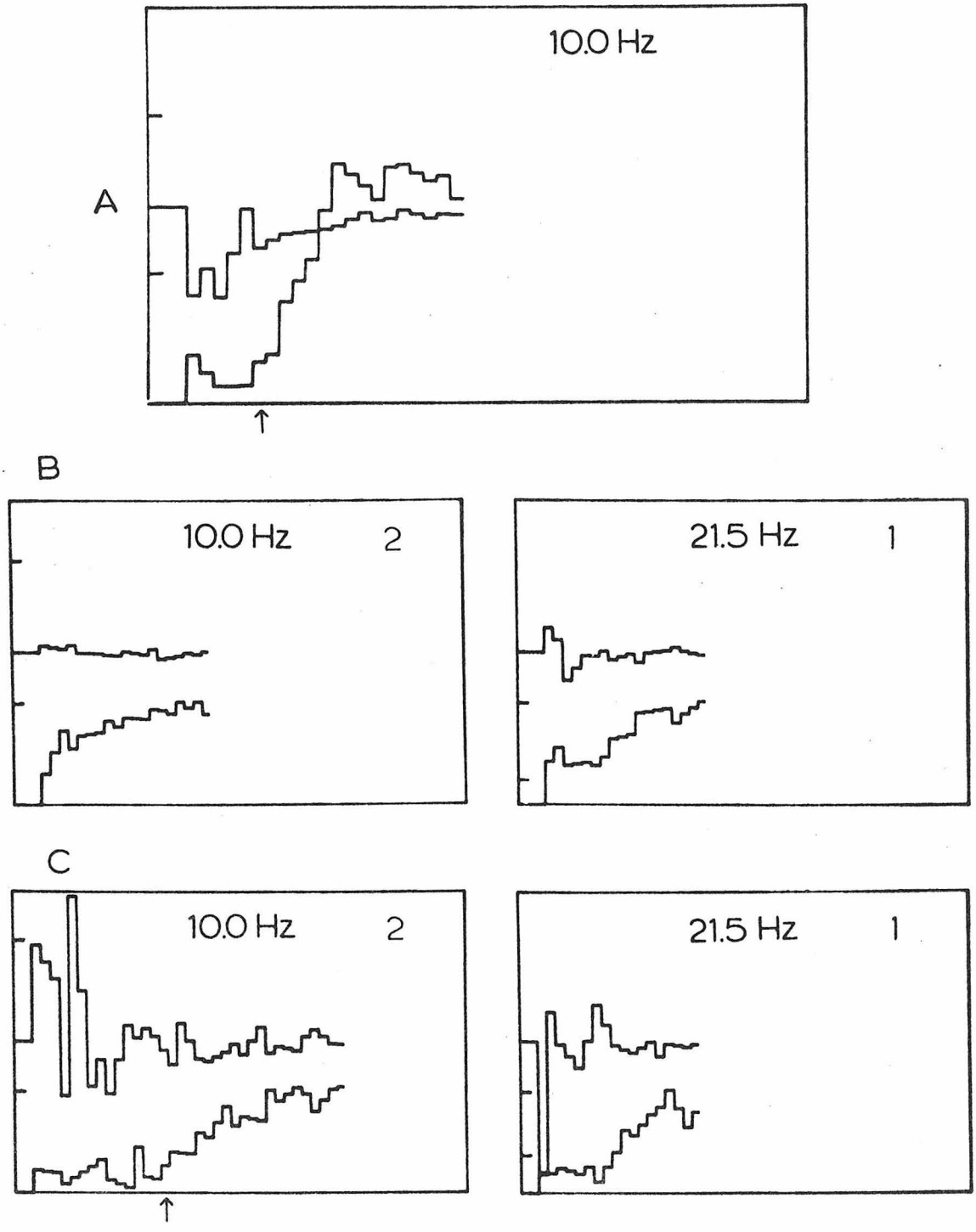

Figure 3.13. Ca^{++} injection results for three photoreceptors of the norp A^{H52} phototransduction mutant. A), B), and C) are data from three different units. The conditions are the same as those of figs. 3.6 - 3.11. Arrows in the 10.0 Hz records indicate the inception of gain recovery; data before the arrows are used in fig. 3.15.

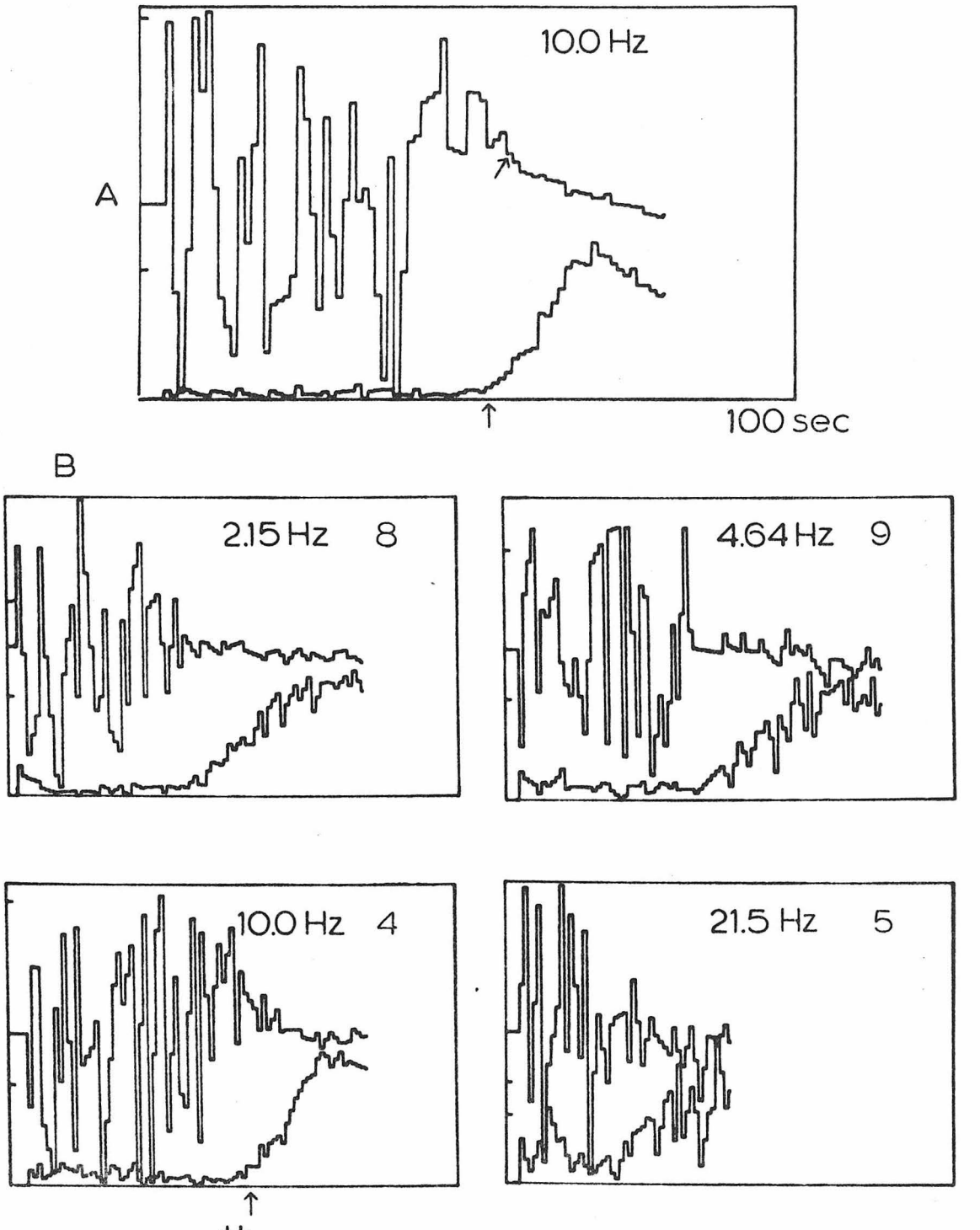

Figure 3.14. Ca^{++} **injection results for two photoreceptors of the** trp **phototransduction mutant. Light stimuli at 491 nm are A) 0.4 maximum intensity and B) 0.9 log unit below** this level. This graph is **100 sec in length. Otherwise the conditions are the same as those of figs. 3.6 - 3.11. Arrows in the 10.0 Hz records indicate the inception of gain recovery; data before the arrows are used in fig. 3.15.**

cell was recorded in the month of February.

Several observations may be made with respect to the trp data presented. The time course in the receptor potential recovery of both gain and phase are similar to that of wild type in that this period is of the order of 10 - 20 sec. This similarity is apparent despite the fact that the mutant recovery occurs after a much pronounced delay. Note in particular that this figure differs from the previous similar figures in that each graph is 100 sec in length instead of 50 sec. The time to inception of gain recovery of both the 10.0 Hz records shown is 53 sec, as contrasted with a typical delay to 10 sec for the wild type photoreceptors. Further, the phase data for trp during the gain quiescence are highly scattered. The histograms for wild type, norp A and trp phases during this period at 10.0 Hz stimulation are shown in figure 3.15. The data for this figure were developed from those sections of records prior to the beginning of gain recovery in the receptor potentials. Arrows in the previous gain and phase figures used for the histograms demarcate the data points collected for fig. 3.15. A much more uniform distribution of phase calculation between $-\pi$ and π is evident for the trp data. This result suggests that the trp photoresponse is completely absent during this period, whereas the wild type units typically maintain some light-coupled transmembrane activity. The source of this activity will be considered in the 'Discussion'. It should be emphasized here that both wild type and mutant preparations were handled identically in that the ERG has been subtracted from the data collected as described in 'Materials and Methods'. The gain of the trp data must then be dominated by noise from all the possible sources other than the cell response.

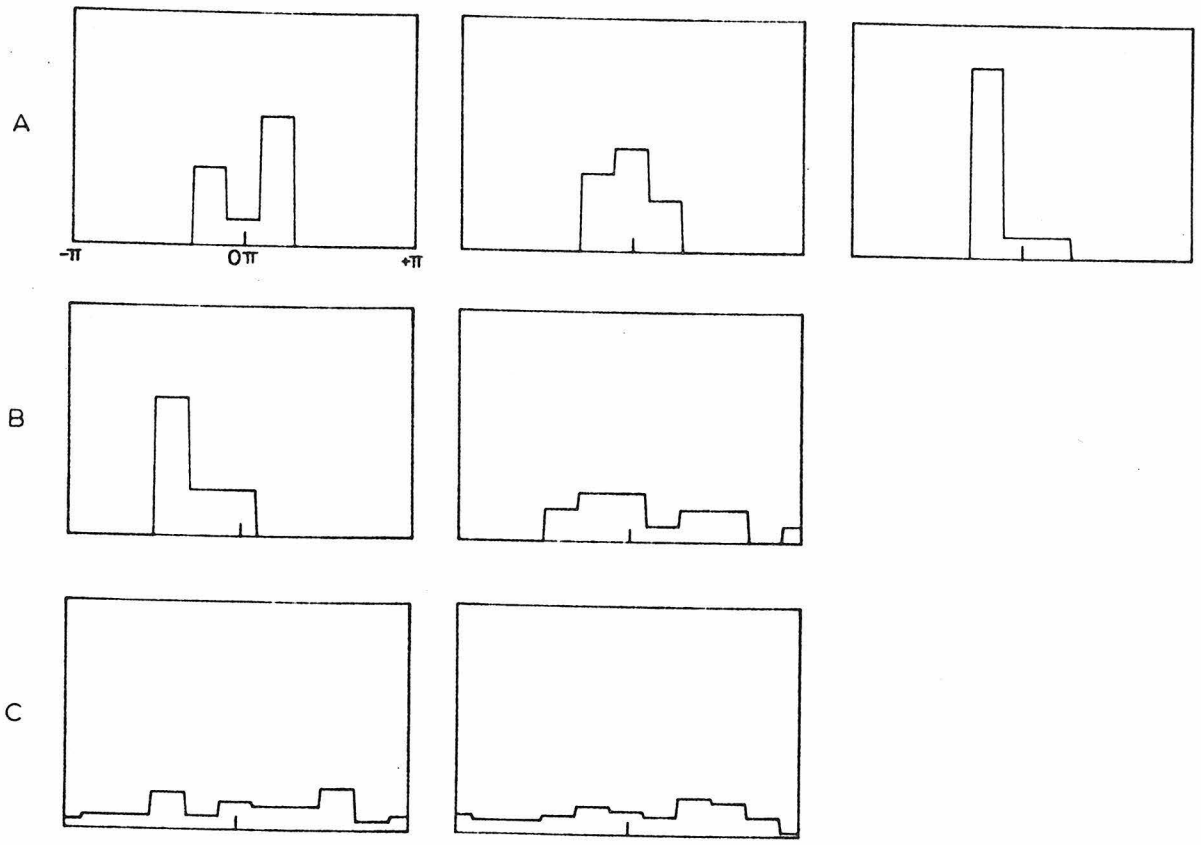

Figure 3.15. Phase histograms with respect to control of the receptor potential at 10.0 Hz following Ca^{++} injection and before inception of gain recovery. The three horizontal rows are A) wild type from fig. 3.8, B) norp A^{H52} from fig. 3.13, and C) trp from fig. 3.14. The vertical scale of each graph is normalized to 1.0. The horizontal scale of each graph is an excursion of $-\pi$ to $+\pi$. The tick marks at 0π identify the pre-injection control.

A further observation on the trp recovery of more significance to phototransduction is the apparent phase advance seen at 10.0 Hz, particularly for fig. 3.14a. While a few of the data points in the phase recovery are the results of averaging neighboring data due to avoiding the calibration pulses, the trend is clearly to a transient advance during gain recovery. Certainly by the time the data indicated an advance of +0.25 π at the time indicated on the phase plot, the efficacy of both Fourier records are well established. The phase shift corresponds formally to a relative advance of 12.5 msec. The phase advance for low intracellular pCa constitutes a new distinction of the trp photoresponse with respect to both wild type and norp A.

Conclusion

This chapter has described the data obtained from iontophoretic experiments on individual Drosophila photoreceptors. These results are the first to be obtained by manipulating directly the intracellular Ca^{++} concentration in this preparation. Among the important observations that have been made are the following:

(i) The effects of Ca^{++} iontophoresis are completely reversible.

(ii) For large Ca^{++} injections, the time to recovery is proportional to the amount of current passed by the microelectrode.

(iii) The maximal effect of Ca^{++} injection is engaged with a delay of a second or two.

(iv) There is an 'injection-insensitive' component of wild type response that is stimulus-coincident and is identical to the 'after-potential' recorded in these cells.

(v) Both wild type and norp A photoreceptors exhibit a quiescent period of approximately 10 sec for the injections used, followed by a receptor potential recovery that proceeds over approximately 10 sec. Both these cells show transient phase delay at 10.0 Hz and above that is maximal at the inception of recovery and advances back to the control or pre-injection value. A phase delay that corresponds formally to a physical delay of 7.8 msec has been demonstrated for a wild type unit. The quiescent period in wild type cells is characterized by a relative hyperpolarization with respect to the otherwise light-adapted average response.

(vi) The photoreceptors of the trp mutant have a quiescent period of approximately 50 sec for these injections. Nevertheless, the subsequent recovery proceeds at a rate comparable to that of the other two animals. Further, the phase recovery exibits a transient advance during the gain recovery. A phase advance that corresponds formally to a physical advance of 12.5 msec has been demonstrated in a trp unit.

To this author's knowledge this chapter describes the first demonstration of a phase advance in a visual cell potential that does not involve manipulation of the light stimulus.

Chapter IV

DISCUSSION

Introduction

This chapter discusses the results of the previous chapter. These results imply an involvement of Ca^{++} in photoreception prior to its blocking of light-coupled Na^{+}-conductance channels of the plasma membrane. A model of the phototransduction process is presented in which both free Ca^{++} and the mitochondrial energy complement of the cell play roles in quantum bump production. The mutant lesions are presented in terms of this model. Further, it is argued that the 'injection-insensitive' component identified in the previous chapter derives from cell coupling in the retina.

Constraints

Pak and Pinto (1976) have diagrammed the Dipteran phototransduction process as follows:

$$\text{Rhodopsin}_{480} \rightleftharpoons \text{Metarhodopsin}_{580}$$

$$\downarrow$$

internal transmitter (?)

$$\downarrow$$

bumps (Na^{+} ions)

$$\downarrow$$

receptor potential.

The simple nature of the scheme belies the weight of evidence that supports it. However, its simplicity also reflects the limits of our knowledge about sensory transduction. Phototransduction is probably the best understood and most extensively studied of all the primary sensory functions. The limitation is imposed by the variety and sophistication

of the techniques we are able to apply.

The constraints on technique arise from the fact that the entire mechanism is contained within living cells. In the case of Limulus ventral photoreceptor the available volume is of the order of $10^5\mu^3$; for the Drosophila it is of the order of $10^3\mu^3$. It is necessary to invade the cell's primary defenses, the bilipid layer forming the plasma membrane, while maintaining its viability. The invasion must be capable of conducting data out to an accessible location with as little noise as possible. The most elementary of the possible data types to be collected under these circumstances is intracellular potential. The technology for collecting other data types such as transmembrane current and intracellular ionic activity is not yet available for the Dipteran.

The dilemma inherent in being restricted to this single data type is that the transduction process is complete by the time the potential is specified. Thus only the final step is available for most photoreceptors, and hence the simplicity of our schemes. Many of the same limitations apply to other single cell transduction mechanisms. For example, excitation-secretion coupling is a field dominated by the concept of Ca^{++} as a 'second messenger'. The transduction schemes proposed for Calliphora salivary gland (Prince, Berridge & Rasmussen, 1972) are nearly as simple as that shown for the retina.

A secondary constraint on technique arises from the speed of the process itself. For no visual cell is there time to modulate any factor other than the light stimulus itself at an intermediate stage in the response. This is a less severe limitation on visual studies than that

imposed for single cell transduction. It is at least partly compensated by the fact that visual stimuli are easily applied. For example, stimuli for auditory studies at the most direct level are mediated by mechanical coupling to hair cells.

New Model for 'Drosophila' Phototransduction

The results presented in the last chapter do not support the Yoshikami-Hagins model as the exclusive vehicle of Ca^{++} involvement in photoreception. By this model only gain would be affected by injection; shifts in latency and phase cannot be explained by a simple blockage of plasma membrane conductance channels. A further elaboration of the Pak-Pinto model of transduction to include a Ca^{++} requirement is indicated.

The bump studies undertaken so far in the two mutants suggest immediately distinguishing two processes within 'bump production'. These may be termed accumulation and transformation. Bumps as recorded in the receptor potential appear to be the manifestation of singular events underlying the voltage noise (Wu & Pak, 1975). Therefore we will follow the linguistic convention of speaking of a precursor pool as a collection of individual items that are accumulated and transformed, created and destroyed. Accumulation of one precursor in the available pool readies it for utilization, yielding one bump. Rate- and gain-limiting factors are then conveniently described in these terms, with the explicit understanding that subcellular physical objects such as molecules or transmitter packets may or may not be the quantized substrate. The events could reflect conformational states of arrays of proteins just as well.

Since both phototransduction lesions affect the bump process, albeit in the differing aspects of latency and efficiency, it has not been necessary to subdivide 'production' itself. However, the results of the present chapter have made a new distinction between wild type and norp A transduction on the one hand and trp transduction on the other. Therefore let us write the fundamental scheme as indicated in fig. 4.1a. Photon capture by rhodopsin at the left induces isomerization of the chromophore, possible release of transmitter, and subsequent transformation of part of the precursor pool X, which in turn is filled by the accumulation process. Transformation of the precursor into its active state X^* is the last step before its expression at the membrane, on the right, as voltage noise. Since the figure is meant to illustrate a model for transduction only, all the usual processes of membrane function such as ion pumps and permeability sites are understood. The arrow from X^* to the membrane indicates activation of the primary light-coupled p_{Na^+} mechanism.

The norp A lesion codes for a protein which increases both latency and dispersion (Pak, Ostroy, Deland & Wu, 1976) of precursor transformation. The trp lesion on the other hand is expressed as inefficient production during steady light (Minke, Wu & Pak, 1975b). The dark adapted cells are fully sensitive and show nearly normal on-depolarization. Since the inefficiency is exhibited only after some seconds in the light, the obvious interpretation is that the reservoir X has been depleted, limiting the amount available to be transformed. The trp lesion somehow decouples a transformation-stimulated accumulation which in the wild type process sustains the available pool. The mutant lesions are presented in fig. 4.1b.

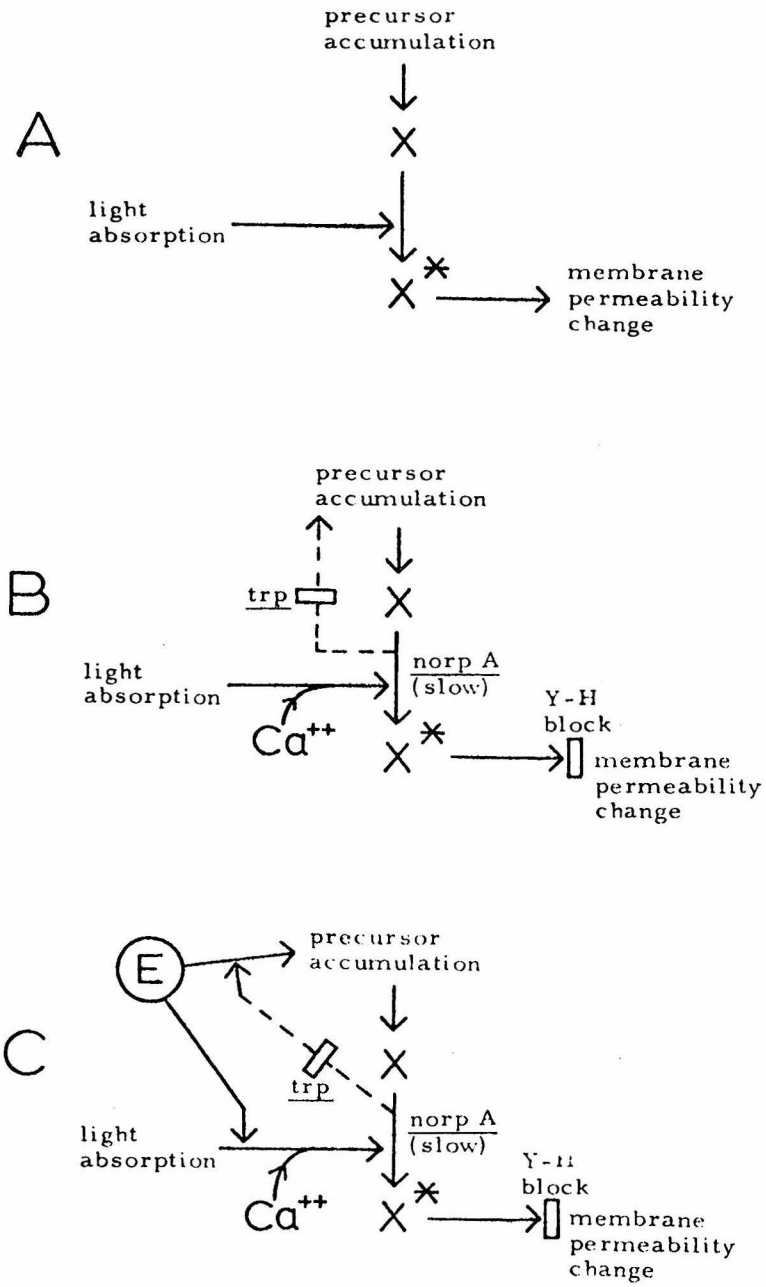

Figure 4.1. New model for Drosophila phototransduction. A) Bump production is represented as an event that transforms a precursor X into an active state X*. B) The mutant lesions are introduced. In norp A the transformation of X to X* is slow with respect to wild type following photon absorption by the pigment chromophore. In trp the accumulation of X is decoupled from its transformation. Also introduced is the location of the Yoshikami-Hagins blockage of membrane conductance channels by free intracellular Ca^{++}. C) The E pool is introduced. E is utilized both in bump production and in precursor accumulation. The trp lesion decouples the use of E for accumulation.

Also introduced in this figure is the Yoshikami-Hagins Ca^{++} blockage of the membrane conductance channels. Blockage of these channels from the inside of the cell is consistent with the relative hyperpolarization of the unit during its quiescent period. However, this simple blockage cannot account for either the phase delay seen in wild type or the phase advance seen in trp under conditions of low intracellular pCa. The trp phase advance is of particular significance; the same lesion must both decouple precursor accumulation from its transformation and provide for a faster response in the presence of high Ca^{++} concentration.

In fact, the phase advance seen for trp is precisely what one would expect for unlesioned phototransduction. Since lowered intracellular pCa should at least partially mimic the effects of light adaptation, the Fuortes-Hodgkin reduction of time scale requires phase advance. Some evidence has been obtained from Limulus ventral photoreceptor discrete wave latency that increased intracellular Ca^{++} may have this effect (Martinez & Srebro, 1976). A canonically determined latency with respect to light stimulation of this process and the attendant standard deviation vary directly with both external Ca^{++} concentration and temperature; increasing or decreasing either of these variables induces the opposite effect on the physiological measures. Further, the result of lowering both Ca^{++} and temperature simultaneously sums nonlinearly in the direction predicted by a model wherein Ca^{++} is involved in a chemical reaction whose rate determines the inverse of bump latency.

Therefore, Ca^{++} is very likely used directly in this photoreceptor prior to the activation of Na^{+} channels at the membrane by X^{*}. Present

technology does not allow us to either confirm or disprove this hypothesis in the Dipteran. However, both the ubiquity of the bump phenomenon in arthropods and the critical importance of Ca^{++} to the functioning of a huge variety of physiological systems (Carafoli & Crompton, 1978) render it unlikely that the role of Ca^{++} differs markedly between the two systems. Since we have defined X^* to be the last state of the precursor before p_{Na^+} activation, the alternative model of having Ca^{++} involved after creation of X^* instead of before may be disposed of immediately. In this case a new X^{**} is the active state so that the alternative collapses to the more economical original model.

The direct Ca^{++} requirement for bump production is pictured in fig. 4.1b as a requirement before transformation of the X pool. This is, however, inessential and may just as easily be written, analogously to Martinez and Srebro (1976),

$$X + Ca^{++} \rightleftharpoons X^*,$$

with an implicit light absorption requirement.

Increasing the availability of free Ca^{++} then should yield a phase advance in both the wild type and trp-lesioned systems. However, this is the case only for the system where accumulation of the precursor is decoupled from its transformation. Hence, further articulation of the model is necessary. Three things have been posited so far for the creation of X^*: light absorption, free Ca^{++}, and available X. Let us introduce one more factor, call it E as shown in fig. 4.1c. E is necessary for both accumulation and utilization. The lesion in trp is in coupling transformation to the use of E for accumulation. Further, excess free

Ca^{++} stimulates the depletion of E.

Now the following scenarios may be given. When Ca^{++} is injected into photoreceptors of wild type flies, it has three manifestations in the phototransduction process:

i) Ca^{++} sets up a temporary Yoshikami-Hagins blockage of light-coupled Na^{+}-conductance channels at the inside of the plasma membrane,

ii) an excess of Ca^{++} is available for the transformation of precursor, and

iii) E is depleted.

If the third manifestation is more critical than the second, phase delay results. As the Yoshikami-Hagins block is removed by extrusion of Ca^{++}, E is replenished by the cell enabling phase advance. During the entire time, a constant demand on the E pool has been made by precursor accumulation.

When Ca^{++} is injected into trp cells, the same three manifestations accrue. However, since the demand on the E pool by transformation has been decoupled, the E available for utilization is higher than would normally be the case in the unlesioned process. As the Yoshikami-Hagins block is being removed, this higher E pool enables the excess Ca^{++}, now at or near physiological levels, to be expressed as decreased latency in the process from light absorption to precursor utilization, hence a phase advance. As further Ca^{++} is extruded, the phase advance decays to the control level.

Energy Interpretation

The hypotheses concerning the E pool are the simplest with respect to the data presented. A reasonable candidate for E is the energy available to the cell as supplied by its mitochondrial complement. Energy is certainly required by any accumulation process the cell must undertake. Further, energy is required to complete the chain from photon capture to membrane resistance change. Alawi (1972) estimated the power amplification required of a Drosophila photoreceptor in its response to single quanta to be of the order of 10^4. Most of this amplification is attributable to continuous ion pumps at the plasma membrane. However, it is unlikely that the gain necessary to the receptor potential is achieved in one stage alone. To the extent that the response is subserved by an X to X^* transformation, some energy utilization is certainly involved.

The third property of E is the most suggestive, that its depletion be stimulated by high intracellular Ca^{++}. Mitochondria are the most likely organelles to sequester Ca^{++} in these cells, although endoplasmic reticulum may also be involved in its regulation (Carafoli & Crompton, 1978). The transmembrane potential of mitochondria is typically -180 mV, so free cation is driven inward. This resting potential is maintained either by respiration- or ATP hydrolysis-driven H^+ efflux.

An electron-microscopic study of the wild type Drosophila retina has demonstrated that the somas of the receptor cells are heavily populated by mitochondria (Mr. R. Fargason, Dr. R. Pierantoni, Mr. F. Hayes personal communication). With the interpretation of E as the mitochondrial supply of energy, the complete model is presented in fig. 4.2. Both E

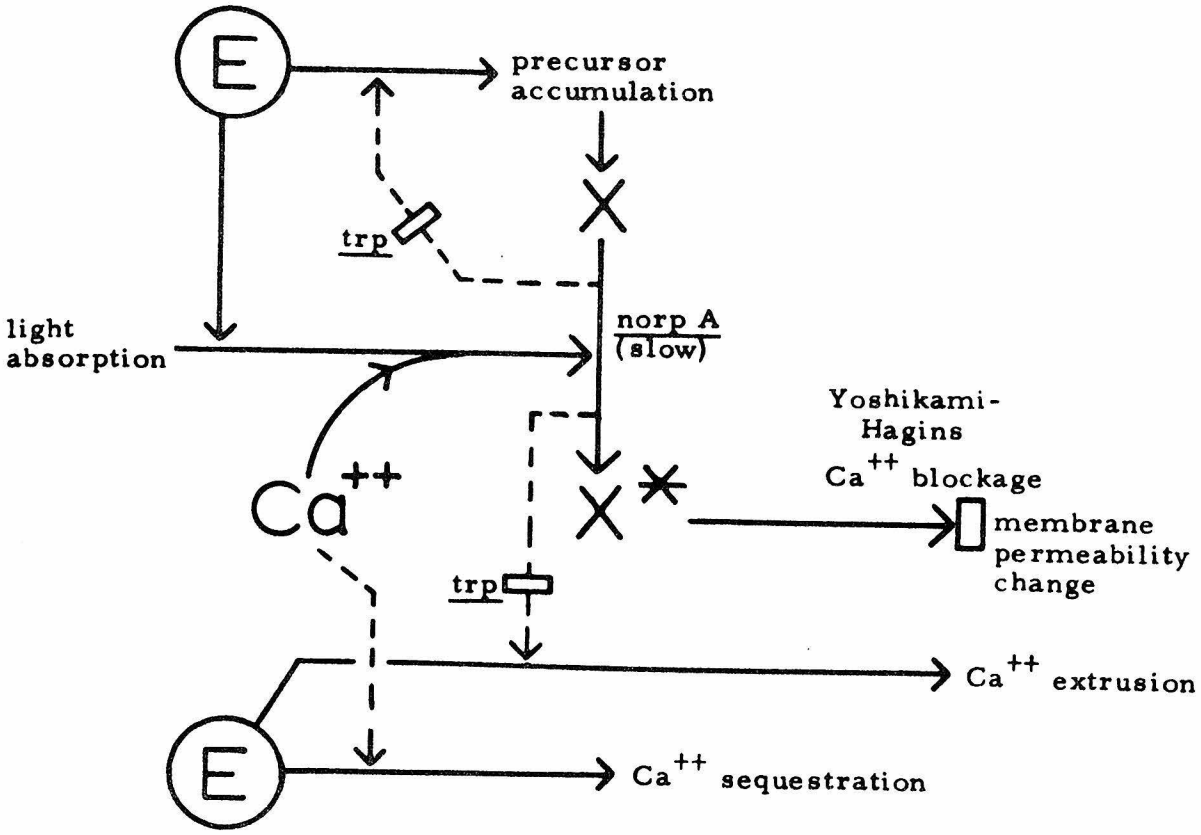

Figure 4.2. Transduction events in the Drosophila photoreceptor. Continuing the model development from fig. 4.1c, Ca^{++} is used directly in bump production. Mitochondrial energy E is used in both membrane Ca^{++} extrusion and in mitochondrial Ca^{++} sequestration. The 'second' trp lesion shown decouples the use of energy for extrusion from the transformation of precursor X. Hence the expression of the trp gene is interpreted as a decoupling of X transformation to the use of mitochondrial energy.

pools shown are meant to be the same one. Introduced in this figure are the two major energy-dependent Ca^{++} functions of the cell not specifically related to phototransduction. Ca^{++} stimulates both of the energy-dependent processes involved in its intracellular regulation, mitochondrial sequestration and extrusion through the plasma membrane. The observation that the trp cells take several times as long to initial receptor potential recovery as the wild type cells is interpreted as a trp lesion in the coupling of X transformation to the utilization of energy for Ca^{++} extrusion through the plasma membrane. This trp lesion is stated as a decoupling of X transformation to utilization of energy for any purpose.

With these interpretations for both the E pool and the trp lesion a model prediction may be offered here. The apparent heat of activation of the trp receptor potential should be larger than that of wild type for light intensities low enough to allow large trp response. Arguing analogously to Srebro and Behbehani (1972), all the energy-dependent processes that are ordinarily coupled to X transformation should contribute to a higher apparent thermal activation for trp. With the coupling intact, energy for these processes is supplied by the mitochondrial pool; with the decoupled system, activation should be more temperature-dependent.

If the E pool is interpreted as the cell's energy supply, then the power dissipated in Ca^{++} sequestration subsequent to injection should be a significant portion of the total power dissipated by the cell in the phototransduction process. Assuming that two moles H^{+} are extruded by the mitochondria for each mole Ca^{++} sequestered to the intra-mitochondrial space (Carafoli & Crompton, 1978), and assuming that the H^{+} are driven up an electrical potential of 180 mV, we may estimate the total energy

required to sequester all the iontophoresed Ca^{++} of a typical injection. With a transport number of $1^{o}/o$ and a total current passed of 4 ncoul, we have the estimated energy of sequestration,

$$E_{seq} = 180 \text{ mV} \cdot 4 \text{ ncoul} \cdot 1^{o}/o = 7.2 \cdot 10^{-12} \text{ joule} .$$

If the total resistance of the cell is $3.4 \cdot 10^{7} \Omega$ (Alawi, 1972), then the energy a single 1 mV quantum bump of duration 10 msec is

$$E_{bump} = \frac{(1 \text{ mV})^2}{3.4 \cdot 10^{7} \Omega} \cdot 10 \text{ msec} = 2.9 \cdot 10^{-16} \text{ joule}$$

Hence the energy of sequestration corresponds to the energy involved in $E_{seq}/E_{bump} = 2.5 \cdot 10^{4}$ bumps

Sequestration energy may also be compared to the energy required by the cell to maintain its resting potential. Assuming this potential to be -21.5 mV (Alawi, 1972), we have the power dissipated,

$$P_{rest} = \frac{(21.5 \text{ mV})^2}{3.4 \cdot 10^{7} \Omega} = 1.4 \cdot 10^{-11} \text{ watt.}$$

Hence the energy of sequestration is equivalent to the energy expended by the cell in maintaining its resting potential for $E_{seq}/P_{rest} = 0.5$ sec.

The results of the next chapter demonstrate that, if extrusion and sequestration of Ca^{++} ion are described by first-order rate reactions, then the rate of sequestration is at least as high as that of extrusion. Hence a large fraction of injected ion is expected to be sequestered. By the equivalences calculated above, the power dissipated in sequestering this fraction is deliverable by the cell, but is not negligible. Hence these estimates are consistent with our model that the energy available to the early steps of phototransduction is depleted by the demands of

mitochondrial Ca^{++} sequestration.

'Injection-Insensitive' Component

A number of possible interpretations may be offered for the continuing transmembrane activity of wild type units during maximally suppressed gain. The phase relationships of the response to the stimulus that reach into the unphysical region are attributable to noise. However, figs. 3.7 - 3.12 show that these periods of apparently unphysical phase for wild-type units are relatively infrequent. The origin of this activity during sinusoidal stimulation is probably identical to that of the after-potential of fig. 3.3, since a distinctive feature of each is relative injection-insensitivity.

Alawi (1972) first recorded the receptor potentials from both normally pigmented wild type and white eyes. The after-potentials from cells in the pigmented retina show a small transient relative depolarization followed by a longer relative hyperpolarization. While Alawi did not subtract the ERG, the after-potentials he obtained for white mutant photoreceptors agree qualitatively with those of the control responses presented in fig. 3.3. Since the genetic removal of screening pigment is expected to change only the optics of the retina, these after-potentials most likely derive from coupling to other cells. The site of this coupling may be either in the retina itself or in the first synaptic plexus below the basement membrane marking the proximal termination of the retina. That this component of the response is insensitive to Ca^{++} injection is consistent with this view. With this interpretation, the second and third post-injection pulse responses show that component of the transmembrane receptor potential derived strictly from cell coupling.

Ribi (1978) has identified symmetric gap junctions among the major receptor cell axons in both Musca and Calliphora. These junctions undoubtedly subserve receptor-receptor electrical coupling in the fly.

It is possible that the coupling itself has been altered in the experiments described in this chapter. Adjacent Chironomus salivary gland cells are electrically coupled. Pressure injection of Ca^{++}-EGTA buffers that lower intracellular pCa decouples these cells by increasing electrical resistance at the junction between them (Rose & Loewenstein, 1975). This decoupling occurs for free Ca^{++} concentration in excess of $5 - 8 \cdot 10^{-5}$ M. If an analogous decoupling were to apply to the Dipteran receptor system, and if our interpretation of the 'Ca^{++}-insensitive' component is correct, then this component might be diminished in the wild type response and hence remain undetected. However, the maximum Ca^{++} concentration at the electrode tip at the termination of injection may not reach this effective range. The kinetic model of the next chapter predicts this maximum to be $4.3 \cdot 10^{-6}$ M for the case of the slowest extrusion rate.

Conclusion

This chapter has presented a new model for Dipteran phototransduction consistent with the results obtained in the last chapter. The discussion has utilized some of the major results and hypotheses current in invertebrate visual physiology. Among these results and hypotheses, two are outstanding:

(i) The Yoshikami-Hagins model, and

(ii) The Fuortes-Hodgkin reduction of time scale.

These models are not immediately contradictory. If Ca^{++} enters the cell in increasing amounts with increasing light intensity stimulation, this does not imply that its intracellular concentration is primarily responsible for the attendant enhancement of the speed of response ubiquitous to visual sensory cells. That the Yoshikami-Hagins model calls for only plasma membrane Na^{+}-conductance channel blockage does not exclude other mechanisms earlier in phototransduction from mediating time scale changes in response independently of Ca^{++}. However, the results of Martinez and Srebro (1976) in Limulus ventral photoreceptor do recommend a further involvement of Ca^{++} that would serve to mediate these time scale changes.

The results of the previous chapter have demonstrated that time scale or phase changes in the receptor potential can be induced in both directions by increasing the intracellular Ca^{++} concentration, dependent upon the genotype of the retinal tissue. This extraordinary result has necessitated the introduction into our model of phototransduction of a kind of 'inverse' to Ca^{++} concentration. This inverse is the mitochondrial energy complement of the cell. Our interpretation of this inverse is consistent with both the known properties of mitochondria and the fact that the photoreceptor is required to provide power amplification of the light signal. This interpretation is consistent also with the quantitative results of the next chapter. Sequestration of free Ca^{++} is the most reasonable rate-limiting factor in the large time course of recovery of these units following Ca^{++} iontophoresis.

Chapter I of this thesis offered as a rationale for these experiments the fact that Ca^{++} injection into Drosophila photoreceptors should help to decompose the most fundamental process in which sensory transduction in these cells is now understood, quantum bump production. Given the established phenotypes at this level of norp A and of trp, the present chapter has articulated the genetic lesions in terms of our model. Hence, genetic dissection combined with intracellular technique has led us to address primary issues in phototransduction. We conclude that both intracellular Ca^{++} and mitochondrial energy are involved in early events in the sensory process of Drosophila photoreceptors.

Chapter V

DIFFUSIVE AND KINETIC MODELS

Introduction

In a classic paper in photoreceptor physiology Cone (1973) discussed some of the quantitative implications of the transmitter model of phototransduction. In particular, he concluded that diffusion of transmitter is a rapid enough mechanism over the necessary distances to mediate the response of both Limulus ventral photoreceptor and rat rod. This chapter seeks to follow a similar approach in discussing the quantitative implications of the typical Ca^{++} injection of Chapter III. Both diffusive and kinetic mechanisms are introduced in five models of the intracellular Ca^{++} concentration to account for the time scale of the wild type Drosophila receptor potential recovery. Recovery inception is approximately 10 sec after the current is turned off; full recovery is achieved approximately 20 sec after current termination. The theoretical results of this chapter indicate that intracellular sequestration of free Ca^{++} is an important function in the physiology of these cells.

Parameters

There are three processes which we shall take to govern the concentration profile of an ion inside a long cylindrical cell. While other processes could be considered, the three chosen here are probably the most significant in describing the time-varying gradient of injected cation into the intracellular space of biological cells. These processes with estimates of the constants associated with them are as follows.

i) Diffusion. This is the only process which applies to spatial movement of the ion along the length of the cell. Hagins (1972) and Cone

(1973) give an estimate of the diffusion coefficient of an ion or small molecule in the intracellular compartment of photoreceptors of $D = 10^{-5} cm^2\ sec^{-1} = 10^3 \mu^2\ sec^{-1}$. Baker and Crawford (1972) give the lower estimate of $D = 10^{-7} cm^2\ sec^{-1}$ for Loligo forbesi axon. However, the data supporting this number are not convincing. We will return to this point below in the discussion of sequestration and retain the former estimate for D.

ii) Extrusion through the plasma membrane. By extrusion we mean here the active transport of the ion out of the cell. Under equilibrium conditions the net rate of passive flow into the cell equals that of energy-dependent transport into the extracellular space. Let us assume with Hagins and Yoshikami (1974) that ion extrusion is governed by a first-order rate reaction. Thus, since both active transport and passive permeability are to be described this way they may be combined in the models to be presented into one expression. Rasmussen (1970) gives $0.01 - 0.1$ pmol $cm^{-2} sec^{-1}$ as a rate of passive influx of Ca^{++} ion in many systems. The rate of passive efflux must differ from that of passive influx by division by the Boltzmann factor, $e^{-E_m/2RT} \sim 0(10)$. Therefore in the interest of the simplicity of the models passive efflux may be ignored. Let us take the range offered by Rasmussen as a reasonable estimate for the equilibrium rates of influx and transport. If we assume with Hagins (1972) that the steady state intracellular Ca^{++} concentration of the light-adapted photoreceptor is about 10^{-7}M, and that the radius of the cylindrical cell is 3 μ, then the concentration per unit length is $9\pi \cdot 10^{-13}$ nmol/μ = $2.8 \cdot 10^{-12}$ nmol/μ. Taking Alawi's (1972) estimate of $2.4 \cdot 10^{-4} cm^2$ for the total membrane area of the Drosophila photoreceptor

excluding axon, and assuming a length of approximately 60 μ for the soma (Wolken, Capenos & Turano, 1957), the lower first-order rate k can be calculated from

$$k_{low} = 0.01\ \text{pmol}\ \text{cm}^{-2}\text{sec}^{-1} \cdot 2.4 \cdot 10^{-4}\text{cm}^2 [60\ \mu]^{-1} [9\pi \cdot 10^{-13}\text{nmol}/\mu]^{-1} = 14.1\ \text{sec}^{-1}.$$

Therefore we estimate the rate of extrusion to be $14\ \text{sec}^{-1} \leq k \leq 140\ \text{sec}^{-1}$.

The data from the cell described in 'Pulse Response Recovery A' of the previous chapter may be used to obtain an upper bound on the extrusive rate. Two numbers were calculated for this unit which average $7.7 \cdot 10^{-2}$ ncoul sec^{-1}. Assuming that this number reflects a constant extrusive rate, we calculate this rate in the following way. We have estimated in 'Materials and Methods' the transport number for the typical pipette to be 1°/o. However, as discussed in the previous chapter, this estimate is probably low for the pipette used. A transport of 10°/o, approaching that for the electrodes used in Limulus ventral photoreceptor (Fein & Lisman, 1975) would be an absolute upper bound. Hence, with the value of the Faraday constant $F = 9.65 \cdot 10^4$ coul/mol, recalling that Ca^{++} is divalent, and assuming a 10°/o transport, we have

$$7.7 \cdot 10^{-2}\ \frac{\text{ncoul}}{\text{sec}} \cdot \frac{1}{F} \cdot \frac{1}{2} \cdot 10\% = 4.0 \cdot 10^{-5}\text{pmol}\ \text{sec}^{-1}$$

for the total extrusion. When normalized by the membrane area of $2.4 \cdot 10^{-4}\text{cm}^2$, this is equivalent to 0.17 pmol $\text{cm}^{-2}\text{sec}^{-1}$. This upper bound is comparable to the upper bound for influx in other systems as reviewed by Rasmussen (1970).

iii) Sequestration and release from an internal substrate. This substrate may be either integral or peripheral to the phototransduction

process, and either membrane-associated or cytoplasmic. The rates of sequestration and release may be characterized by first-order rate reactions with constants λ and δ, respectively. Subcellular organelles, notably mitochondria, are known to sequester Ca^{++} ion at rates as high as 200 - 2000 pmol $cm^{-2} sec^{-1}$ (Rasmussen, 1970), the dimensions being normalized by the area of exposed organelle membrane.

The estimate for D given by Baker and Crawford (1972) was obtained by comparing a theoretical curve, equivalent in certain respects to the first model for Ca^{++} concentration given below, with the amount of $^{45}Ca^{++}$ label in axon segments $8\frac{1}{2}$ hr after a point deposition of ion inside the cell. However, the spatial resolution of the data (only three points are well above baseline) does not seem sufficient to support the hypothesis that this system is strictly diffusive. Sequestration of the label would tend to constrict its flow, greatly lowering its apparent diffusion. Indeed, a similarly low diffusion value in frog muscle fibre has been attributed to binding of free Ca^{++} to sarcoplasmic reticulum (Kushmerick, Podolsky 1969).

Assumptions

We seek to describe models of Ca^{++} ion concentration applicable to experiments reported for the Drosophila photoreceptor. While two are not solved explicitly, their demarcation will serve to show the relative importance of the three processes listed above in governing the recovery of the receptor potential following an injection. Thus it is the order of magnitude of the coefficients associated with each process that determines their significance to the data. Since the exact values of these numbers

are not measured in this system, we make the following assumption:

i) The processes by which this photoreceptor adjusts its internal Ca^{++} concentration have coefficients similar to those demonstrated in other biological systems. Other assumptions of more direct relevance to the models themselves are listed here:

ii) The electrode tip is assumed to be a point source. As discussed in 'Materials and Methods' the pipettes used for this study had tips of the order of 0.1 μ. Therefore a point source of material is a reasonable assumption for this situation.

iii) The injection of ion is presumed constant. Since the data taken that relate to material injected is the time integral of the current, for most records this assumption amounts to supposing that the transport number of the electrode remains constant during the injection. The vast majority of electrodes tried were unusable for injections. These had current integrals in which the current passed decayed through time. Most usable pipettes had current integrals in which the resistance remained the same during the course of current passage. An occasional usable pipette would have a current characteristic which was essentially bimodal, in that the resistance exhibited a rapid decrease or increase for some unknown reason. The transport number of these pipettes undoubtedly underwent a similar change. Nevertheless, the assumption of constant transport number for those injections with linear integrals is a reasonable one to make. These first three assumptions would be of paramount importance if the experimental data were being rate-limited by diffusion as opposed to both extrusion and sequestration.

iv) The photoreceptor is assumed to be of infinite length and zero radius. The problem is non-dimensionalized by taking 1 μ as the unit of length. If the electrode is placed halfway down the cell, then the ratio of the distance to the end of the soma to the radius is of the order of 10:1. It was decided that the advantage of simplicity in formulating the problem in one dimension exceed any advantage gained by posing it in a finite cylinder.

v) The membrane is assumed to be uniformly exposed to the injected Ca^{++} and the rate of extrusion uniform across its surface. Strictly speaking, this is an unrealistic condition due to the geometry of the rhabdomere. This portion of the cell extends nearly the entire length of the soma and consists of closely-spaced rod-shaped extension of the plasma membrane disposed perpendicularly to the axial direction. This system has been described for Musca at the level of electron microscopy by Boschek (1971). Further, since the primary function of the rhabdomere is that of absorption of light, its membrane acts as a substrate for the receptor's photopigment. It is therefore probably the case that the permeability and extrusive properties of the rhabdomere differ from those of the rest of the plasma membrane. However, in light of the fourth assumption made above, these membrane properties may be regarded as an average over a cross section.

vi) The extracellular space is assumed to be homogeneous in concentration. The photoreceptor is therefore presumed to be in a well-mixed bath with respect to ion movement so that no tight spaces close to the cell can accumulate excess ion, thereby lowering the apparent rate of extrusion. These last two assumptions would be of paramount importance if

the experimental data were being rate-limited by membrane extrusion. They may be concisely stated by saying that the extrusive process is assumed to be a simple two-compartment system.

Concentration Models

Having made these six assumptions with respect to the experimental situation, let us describe the models of the concentration profile.

i) Simple diffusion. Consider the concentration C(x,t) of an ion governed by diffusion in one dimension. We have

$$DC_{xx} = C_t, \tag{1}$$

where $D(\mu^2/sec)$ is the diffusion coefficient. The Green's function for equation (1) is given by Crank (1956) as

$$\frac{1}{2\sqrt{\pi Dt}} e^{-\frac{x^2}{4Dt}} . \tag{2}$$

Since all free space solutions of the diffusion equation are linear combinations of the Green's function, let us (following Crank) relate the constant to be multiplied with this solution, $A_1(mol/sec)$, with the parameter relevant to the source. The total amount of ion diffusing, M, from an instantaneous point source a x=0, t=0, is given by the integral over x of the Green's function,

$$M = \frac{A_1}{2\sqrt{\pi Dt}} \int_{-\infty}^{\infty} dx\, e^{-\frac{x^2}{4Dt}} = A_1. \tag{3}$$

The concentration $C_D^s(x,t)$ for such a source at t=0 is given by the integral over time of the Green's function,

$$\frac{1}{A_1} C_D^s(x,t) = \frac{1}{2\sqrt{\pi D}} \int_0^t d\tau \, \frac{1}{\sqrt{\tau}} \, e^{-\frac{x^2}{4D\tau}}$$

$$= \frac{|x|}{\sqrt{D}} \int_{\frac{|x|}{2\sqrt{Dt}}}^{\infty} d\eta \, \frac{1}{\eta^2} \, e^{-\eta^2} d\eta$$

$$= -\frac{1}{\eta} e^{-\eta^2} \Bigg|_{\frac{|x|}{2\sqrt{Dt}}}^{\infty} - 2 \int_{\frac{|x|}{2\sqrt{Dt}}}^{\infty} d\eta \, e^{-\eta^2}$$

$$= 2\sqrt{t} \, e^{-\frac{x^2}{4Dt}} - \sqrt{\frac{\pi}{D}} \, |x| \operatorname{erfc} \frac{|x|}{2\sqrt{Dt}}, \qquad (4)$$

where we have made the change of variable $\eta = \frac{|x|}{2\sqrt{Dt}}$ and have used the definition of the complementary error function,

$$\operatorname{erfc}(x) = \frac{2}{\sqrt{\pi}} \int_x^{\infty} e^{-\xi} \, d\xi.$$

If the source stops at $t=t_o$, then the problem may be solved either by considering $C_D^s(x,t_o)$ as an initial condition for equation (1), or by simply noting that the problem is entirely linear. Solutions with a time-dependent source are linear combinations of the solution with a constant source with time translations. Therefore the gradient $C_D(x,t)$, satisfying $C_D(x,0) = 0$, for a source turned on at $t=0$ and off at $t=t_o$ is given by

$$C_D(x,t) = \begin{cases} C_D^s(x,t), & 0 \le t \le t_o \\ C_D^s(x,t) - C_D^s(x,t - t_o), & t \ge t_o \end{cases} \qquad (5)$$

ii) First-order extrusion. Combined with diffusion, and writing the source explicitly in this case, we have for the concentration $C_k(x,t)$,

$$DC_{k;xx} - C_{k;t} - kC_k = - A_1\delta(x), \tag{6}$$

where $k(sec^{-1})$ is the extrusion coefficient and A_1 is the strength of the source at x=0. Let us first write explicitly the simple relations for the conditions of non-zero initial and external concentrations. If I, C_i', C_e' are the injected, initial, and external concentrations, respectively, and k' and p' the active transport and permeability rates, then the homogeneous equation is

$$C_t = DC_{xx} - k'C + p'(C_e' - C),$$

where $C=C_i' + I$ is the total interior concentration. Therefore, since the initial concentration is presumably a function of neither x nor t and must obey

$$k'C_i' = p'(C_e' - C_i'),$$

we have

$$I_t = DI_{xx} - (k' + p')I.$$

This is the homogeneous form of (6); so we proceed with its solution with the understanding that it is to be added to the initial concentration. Letting $\gamma_k(x,s)$ denote the Laplace transform in time of $C_k(x,t)$,

$$\gamma_k(x,s) = \int_o^\infty dt\ e^{-st}C_k(x,t)$$

we have (7)

$$D\gamma_{k;xx} - (s + k)\gamma_k = - \frac{1}{s} A_1\delta(x).$$

Integrating (7) over the source, and providing for continuity and an asymptotic condition,

$$\gamma_{k;x}(0^+,s) - \gamma_{k;x}(0^-,s) = - \frac{1}{Ds} A_1 \tag{8}$$

$$\gamma_k(0^+,s) = \gamma_k(0^-,s) \tag{9}$$

$$\gamma_k(x,s) \to 0, \quad |x| \to \infty \tag{10}$$

With the source at x=0 the solution to (7) - (10) is

$$\frac{1}{A_1}\gamma_k(x,s) = -\frac{1}{2s\sqrt{D(s+k)}} e^{-\sqrt{\frac{s+k}{D}}|x|}. \tag{11}$$

We need to invert (11). The inverse Fourier integral of Campbell and Foster (1931) is given by

$$G(t) = \int_{-\infty}^{\infty} F(f)e^{2\pi ift}\,df$$

$$= \frac{1}{2\pi i}\int_{-i\infty}^{i\infty} F_1(p)e^{pt}dp,$$

where $p=2\pi if$ and $F_1(p)=F(f)$. This is the inverse Laplace transform if there are no singularities of the integrand for $p\geq 0$. The relevant transform is given as

$$\frac{1}{p(p+\rho)^{\frac{1}{2}}} e^{-\sigma^{\frac{1}{2}}(p+\rho)^{\frac{1}{2}}} - \frac{1}{\rho^{\frac{1}{2}}p} e^{-\rho^{\frac{1}{2}}\sigma^{\frac{1}{2}}}$$

$$\to -\frac{1}{2\rho^{\frac{1}{2}}}\left[e^{\rho^{\frac{1}{2}}\sigma^{\frac{1}{2}}}\operatorname{erfc}\left(\rho^{\frac{1}{2}}t^{\frac{1}{2}} + \frac{\sigma^{\frac{1}{2}}}{2t^{\frac{1}{2}}}\right) + e^{-\rho^{\frac{1}{2}}\sigma^{\frac{1}{2}}}\operatorname{erfc}\left(\rho^{\frac{1}{2}}t^{\frac{1}{2}} - \frac{\sigma^{\frac{1}{2}}}{2t^{\frac{1}{2}}}\right)\right], \quad t > 0.$$

(C.F. 824.1 p. 97)* (12)

*Notations such as this at the end of transforms and integrals give the source of the expression.
A.S. ... Abramowitz & Stegun (1964)
C.F. ... Campbell & Foster (1931)

The second term on the left-hand side of (12) eliminates the singularity at p=0. Since there are no singularities for p>0, integration up any path in the right half plane equals that up the imaginary axis. Therefore the inverse transform of this second term may be added to both sides of the inversion given by (12) when the integration is to the right of the imaginary axis. Since by the transform

$$\frac{1}{\rho^{\frac{1}{2}}p}\, e^{-\rho^{\frac{1}{2}}\sigma^{\frac{1}{2}}} \rightarrow \frac{1}{\rho^{\frac{1}{2}}}\, e^{-\rho^{\frac{1}{2}}\sigma^{\frac{1}{2}}} ,$$

the procedure may be checked by confirming that this term equals the limit as $t\rightarrow 0$ of the right-hand side of (12). Changing variables with $\rho=k$, $\sigma^{\frac{1}{2}}=|x|/\sqrt{D}$, we have finally that the concentration profile for a constant source is given by

$$\frac{1}{A_1} C_k^s(x,t) = \frac{1}{2\sqrt{Dk}}\left[e^{-\sqrt{\frac{k}{D}}\,|x|} - \frac{1}{2} e^{\sqrt{\frac{k}{D}}\,|x|} \operatorname{erfc}\left(\sqrt{kt} + \frac{|x|}{2\sqrt{Dt}}\right) \right.$$

$$\left. - \frac{1}{2} e^{-\sqrt{\frac{k}{D}}\,|x|} \operatorname{erfc}\left(\sqrt{kt} - \frac{|x|}{2\sqrt{Dt}}\right)\right] . \qquad (13)$$

Since the problem is linear, an expression exactly analogous to (5) may be written for the case where the source is turned off at $t=t_o$.

iii) Saturated extrusion. This model has been developed in an attempt to retard the extensive rate of the previous model in a way consistent with the membrane ion pump behavior. When the models are evaluated later in this chapter, it will be seen that the second model proceeds too rapidly to equilibrium.

Let us suppose in this case that the first-

order rate extrusion of the previous problem saturates to a constant rate at some concentration, c_1. While the source is turned on the problem is identical to the one in the previous model until concentration at the source reaches c_1 at time $t=t_m$. Then two new problems arise, one in the 'exterior' where the first-order rate still applies, and one in the 'interior' where the rate has saturated. These solutions meet at some position which is a function of time, $x=X_m(t)$, which must grow monotonically from $X_m(t_m)=0$ to some constant value for a continuous source. This last is true since the source has finite strength. The problem is nonlinear after $t=t_m$, so the transform applied to the previous problem to accommodate non-zero initial and external concentrations does not work here.

Problems such as this one are known in the literature as free boundary problems since the boundary to which conditions are to be applied, $X_m(t)$, is an unknown function of time [Friedman, 1964 (chapter 8)]. The position of the boundary is frequently the most important part of the underlying physical problem. For example, when the system is regarded as the heat equation the boundary may describe the position of phase transition between liquid and solid state. Two versions of this problem have been considered by Boley (1961), the first in which a slab undergoes a melt at a surface which is constantly exposed, and the second in which a liquid undergoes a freeze. The situations are different in the sense that in the second case the heat sink is stationary, and so two regions of solution must be retained, whereas in the first the source moves with the phase transiton, so only the unmelted portion is required. Our case is more like the second than the first since the source remains at x=0 and both exterior and interior solutions coexist. We will follow closely Boley's formulation.

We are concerned primarily with that time after the source has been turned off. Boley's method provides a system of coupled integral equations in the phase transition position. Therefore we will obtain the appropriate equations in $X_m(t)$ for the time after the source has been turned on. The entire system must approach asymptotically through time a solution we will call the final one, with a constant boundary between exterior and interior, X_f. Using this final state as an initial condition, we then will obtain the equations for the boundary $X_r(t)$ governing the return of the system after the source has been turned off by a strict analogy to the previous situation. This indirect approach for the return has been chosen because it is easier to describe Boley's technique for a body that grows from the source than one which must shrink to zero in some finite time.

Since power series obtained about the initial conditions will necessarily diverge for times forward, a limiting case of the system for $X_r(t)$ will be evaluated at $t=t_r$, that time at which X_r is zero. This provides one equation in one unknown, that unknown being a time which will be an upper bound on t_r. It is the order of magnitude of this parameter that is of interest. To keep the problems as simple as possible, we will assume a zero initial condition in the problem for $X_m(t)$ and zero spatial asymptotic conditions for all exterior problems. Further, we will use the symmetry about $x=0$ and consider only the half plane for which $x\geq 0$.

For times $t\leq t_m$ the solution is just $C_k^s(x,t)$ as given by (13). The time to separation of solutions is governed by

$$c_1 = \frac{A_1}{2\sqrt{Dk}} \operatorname{erfc} \sqrt{kt_m} \tag{14}$$

since the concentration c_1 is achieved first at the source. For times $t \geq t_m$, Boley's method consists first of extending the new interior solution from its region of validity, $|x| \leq X_m(t)$, to the entire half plane, $t \geq t_m$, by introducing an unknown initial condition $T_m(x)$ at $t=t_m$. Likewise the exterior solution is extended from $|x| \geq X_m(t)$ to $t \geq t_m$ by introducing an unknown source $Q_m(t)$ at $x=0$. Both extended solutions are then constrained to meet all the boundary conditions at $X_m(t)$. The sources and initial conditions are shown in fig. 5.1a.

Consider first the problem for the extended exterior $C_{me}(x,t)$ with constant source as before. We have:

$$\begin{aligned}
&DC_{me;xx} - C_{me;t} = kC_{me} - A_1 H(0)\delta(x) - Q_m(t)\delta(x) \\
&C_{me}(X_m(t),t) = c_1; C_{me;x}(X_m(t),t) = Q_1(t) \\
&C_{me}(x,o) = 0; C_{me}(x,t) \to 0, |x| \to \infty \\
&Q_m(t) = 0, \; t \leq t_m \; ,
\end{aligned} \tag{15}$$

where H(t) is the Heaviside function of time introduced to emphasize that the exterior separates from the source at $t_m > 0$. $Q_1(t)$ is introduced in Boley's problem as an unknown heat exchange across the transition boundary. It is necessary in the case where the transition itself requires a nonzero flux, for example, the latent heat of melting. Although our case does not require such a flux for transition to saturated extrusion, Q_1 is retained to preserve a useful separation between the exterior and interior problems and will be eliminated immediately when the boundary constraints are imposed.

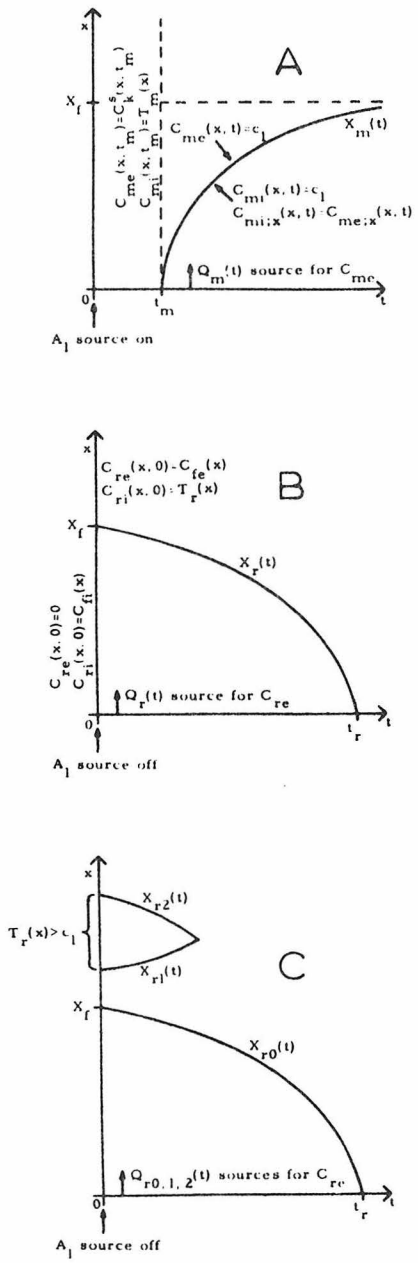

Figure 5.1. Sources and initial and boundary conditions for the saturated extrusion model. Distance from the real A_1 source is the ordinate, time the abscissa. The 'interior' is beneath the curves $X_m(t)$, $X_r(t)$, and $X_{r0}(t)$, the 'exterior' above them. A) The interior grows from the A_1 source. B) The interior disappears after A_1 is turned off. C) An hypothetical situation for the return system if the fictitious initial condition $T_r(x)$ were not maximized by the concentration c_1 on $X_{r0}(t)$.

The transform of the equation in (15) is given by

$$D\gamma_{me;xx} - (s + k)\gamma_{me} = - \left[\frac{A_1}{s} + q_m(s)\right] \delta(x) \tag{16}$$

$$\gamma_{me}(x,s) = - \frac{1}{2\sqrt{D(s + k)}} e^{-\sqrt{\frac{s + k}{D}}\,|x|}\left[\frac{A_1}{s} + q_m(s)\right] , \tag{17}$$

where $q_m(s)$ is the transform of $Q_m(t)$. The first term of the sum transforms back into $C_k^s(x,t)$, $x \geq 0$. The second term yields a convolution in time. By the Campbell and Foster inversion,

$$\frac{1}{(p + \rho)^{\frac{1}{2}}} e^{-\sigma^{\frac{1}{2}}(p + \rho)^{\frac{1}{2}}} \rightarrow \frac{1}{(\pi t)^{\frac{1}{2}}} e^{-\rho t - \frac{\sigma}{4t}} , \quad t>0, \quad \text{(C.F. 823 p. 96)}$$

the extended exterior solution is given by the inversion of (17),

$$C_{me}(x,t) = C_k^s(x,t) + \frac{1}{2\sqrt{\pi D}} \int_0^{t-t_m} d\tau Q_m(t - \tau) \frac{1}{\sqrt{\tau}} e^{-k\tau - \frac{x^2}{4D\tau}} . \tag{18}$$

We will need its spatial derivative as well.

$$\begin{aligned} C_{me;x}(x,t) = - \frac{A_1}{2D\sqrt{k}} \Bigg[& \sqrt{k}\; e^{-\sqrt{\frac{k}{D}}\,|x|} \\ & + \frac{1}{2}\left[\sqrt{k}\ \text{erfc}\left(\sqrt{kt} + \frac{|x|}{2\sqrt{Dt}}\right) - \frac{1}{\sqrt{\pi t}} e^{-\left(\sqrt{kt} + \frac{|x|}{2\sqrt{Dt}}\right)^2}\right] e^{\sqrt{\frac{k}{D}}\,|x|} \\ & - \frac{1}{2}\left[\sqrt{k}\ \text{erfc}\left(\sqrt{kt} - \frac{|x|}{2\sqrt{Dt}}\right) - \frac{1}{\sqrt{\pi t}} e^{-\left(\sqrt{kt} - \frac{|x|}{2\sqrt{Dt}}\right)^2}\right] e^{-\sqrt{\frac{k}{D}}\,|x|} \Bigg] \\ & - \frac{|x|}{4\sqrt{\pi}\ D^{3/2}} \int_0^{t-t_m} d\tau Q_m(t - \tau) \frac{1}{\tau^{3/2}} e^{-k\tau - \frac{x^2}{4D\tau}} , \quad x \neq 0. \end{aligned} \tag{19}$$

Considering next the extended interior $C_{mi}(x,t)$, it is simplest to

decompose this problem into two parts and then sum. The first part satisfies the diffusion equation with saturated extrusion, with constant source and a zero initial condition at $t=t_m$. The second part satisfies the diffusion equation without extrusion with the unknown initial condition, $T_m(x)$ at $t=t_m$. To the sum is applied the matching constraints at $X_m(t)$. Thus,

$$DC^{(1)}_{mi;xx} - C^{(1)}_{mi;t} = kc_1 - A_1\delta(x);\ C^{(1)}_{mi}(x,t_m) = 0 \tag{20}$$

$$DC^{(2)}_{mi;xx} - C^{(2)}_{mi;t} = 0;\ C^{(2)}_{mi}(x,t_m) = T_m(x) \tag{21}$$

$$C_{mi}(X_m(t),t) = c_1; C_{mi;x}(X_m(t),t) = Q_1(t);\ C_{mi}(x,t) \to 0,\ |x|\to\infty\ . \tag{22}$$

Note that the choice of problems in which the extrusive term appears is entirely arbitrary. The derivative boundary conditions at $X_m(t)$ of (15) and (22) may now be understood. Together they require that the amount of material for the two extended regions diffusing across the boundary be equal. The expressions for the interior may be written directly as

$$C^{(1)}_{mi}(x,t) = - kc_1(t - t_m) + C^{s}_{D}(x,t - t_m) \tag{23}$$

$$C^{(2)}_{mi}(x,t) = \frac{1}{2\sqrt{\pi D(t - t_m)}} \int_0^\infty d\xi\, e^{-\frac{|x - \xi|^2}{4D(t - t_m)}} T_m(\xi) \tag{24}$$

$$C_{mi;x}(x,t) = - A_1\sqrt{\frac{\pi}{D}}\ \operatorname{erfc}\frac{|x|}{2\sqrt{D(t - t_m)}}$$

$$- \frac{1}{4\sqrt{\pi}\ D^{3/2}(t - t_m)^{3/2}} \int_0^\infty d\xi \left[(x - \xi) e^{- \frac{(x - \xi)^2}{4D(t - t_m)}} \right.$$

$$\left. + (x + \xi) e^{- \frac{(x + \xi)^2}{4D(t - t_m)}} \right] T_m(\xi) \ . \qquad (25)$$

Applying the three boundary conditions at $x=X_m(t)$ results in three coupled integral equations in the three unknowns, $X_m(t)$, $Q_m(t)$, and $T_m(x)$. These may be written as follows:

$$\frac{1}{2\sqrt{\pi D}} \int_0^{t-t_m} d\tau\, Q_m(t-\tau) \frac{1}{\sqrt{\tau}} e^{-k - \frac{X_m^2(t)}{4D\tau}}$$

$$= c_1 - \frac{A_1}{2\sqrt{Dk}} \left[e^{-\sqrt{\frac{k}{D}} X_m(t)} - \frac{1}{2} e^{\sqrt{\frac{k}{D}} X_m(t)} \operatorname{erfc}\left(\sqrt{kt} + \frac{X_m(t)}{2\sqrt{Dt}}\right) \right.$$

$$\left. - \frac{1}{2} e^{-\sqrt{\frac{k}{D}} X_m(t)} \operatorname{erfc}\left(\sqrt{kt} - \frac{X_m(t)}{2\sqrt{Dt}}\right) \right] \qquad (26)$$

$$\frac{1}{2\sqrt{\pi D(t-t_m)}} \int_0^{\infty} d\xi e^{-\frac{|X_m(t)-\xi|^2}{4D(t-t_m)}} T_m(\xi) = c_1 + kc_1(t-t_m)$$

$$- A_1 \left[2\sqrt{t-t_m}\, e^{-\frac{X_m^2(t)}{4D(t-t_m)}} - \sqrt{\frac{\pi}{D}} X_m(t) \operatorname{erfc} \frac{X_m(t)}{2\sqrt{D(t-t_m)}} \right] \qquad (27)$$

$$- \frac{X_m(t)}{4\sqrt{\pi}\, D^{3/2}} \int_0^{t-t_m} d\tau\, Q_m(t-\tau) \frac{1}{\tau^{3/2}} e^{-k\tau - \frac{X_m(t)}{4D\tau}}$$

$$+ \frac{1}{4\sqrt{\pi}\, D^{3/2}(t-t_m)^{3/2}} \int_0^{\infty} d\xi |X_m(t) - \xi| e^{-\frac{|X_m(t)-\xi|^2}{4D(t-t_m)}} T_m(\xi)$$

$$= \frac{A_1}{2D\sqrt{k}} \left\{ \sqrt{k}\, e^{-\sqrt{\frac{k}{D}} X_m(t)} \right.$$

$$+ \frac{1}{2} \left[\sqrt{k} \operatorname{erfc}\left(\sqrt{kt} + \frac{X_m(t)}{2\sqrt{Dt}}\right) - \frac{1}{\sqrt{\pi t}} e^{-\left(\sqrt{kt} + \frac{X_m(t)}{2\sqrt{Dt}}\right)^2} \right] e^{\sqrt{\frac{k}{D}} X_m(t)}$$

$$\left. - \frac{1}{2} \left[\sqrt{k} \operatorname{erfc}\left(\sqrt{kt} - \frac{X_m(t)}{2\sqrt{Dt}}\right) - \frac{1}{\sqrt{\pi t}} e^{-\left(\sqrt{kt} - \frac{X_m(t)}{2\sqrt{Dt}}\right)^2} \right] e^{-\sqrt{\frac{k}{D}} X_m(t)} \right\}$$

$$- A_1 \sqrt{\frac{\pi}{D}} \operatorname{erfc} \frac{X_m(t)}{2\sqrt{D(t-t_m)}} \quad . \qquad (28)$$

While this system may be solved asymptotically as $t \to t_m$ or as $t \to \infty$, these calculations would not serve to estimate the approximate time to the final state. Therefore it remains undetermined whether a given source turned on for some specified time would bring an extrusive system saturating at a concentration c_1 close to an equilibrium gradient. However, since our interest is primarily in the time to the original state after the source has been turned off, it is necessary to assume some initial condition at that time when the source is terminated. It suits the conclusions to be reached below that this extreme case be computed.

Therefore we proceed to calculate the asymptotic state, $C_f(x)$, for the problem with the source on. Again the problem is decomposed into exterior and interior regions separated at $|x|=X_f$, the final boundary. The problems are, respectively,

$$DC_{fe;xx} = kC_{fe}; \quad C_{fe}(X_f) = c_1 \tag{29}$$

$$DC_{fi;xx} = kc_1 - A_1\delta(x); \quad C_{fi}(X_f) = c_1; \; C_{fe;x}(X_f) = C_{fi;x}(X_f) \tag{30}$$

with solutions:

$$C_{fe}(x) = c_1 e^{-\sqrt{\frac{k}{D}}\left||x| - X_f\right|} \tag{31}$$

$$C_{fi}(x) = \frac{kc_1}{2D}(x^2 - X_f^2) - \frac{A_1}{2D}(|x| - X_f) + c_1 \; . \tag{32}$$

X_f itself is obtained from the derivative boundary condition in (30) and is written immediately as

$$X_f = \frac{A_1}{2kc_1} - \sqrt{\frac{D}{k}} \; . \tag{33}$$

If $C_{fi}(x)$ is negative then saturated extrusion is not obtained in any region about the tip. A convenient check on the solution is provided by the conservation of material diffusing. The source strength must equal the total amount extruded in the interior plus the amount diffusing across the boundaries,

$$\frac{A_1}{2} = kc_1X_f - DC_{fi;x}(X_f).$$

We are now prepared to consider the return of the system to zero concentration from this final state. It is convenient to translate the time axis here so that zero coincides with the time that the source is turned off. The exterior and interior regions are again extended to the entire half plane, $t \leq t_r$. The exterior is extended by an unknown source, $Q_r(t)$ at x=0, and the interior is extended by an unknown initial concentration profile, $T_r(x)$ at t=0. The source and initial condition are shown in fig. 5.1b.

It should be noted that $T_r(x)=0$, $|x| \leq X_f$, since these data apply to the actual interior and not the extended part. The actual initial condition $C_f(x)$ at t=0 still applies to both extended problems, albeit only on the 'nonextended' side of each. For specificity let us write the extended return equations.

$$
\begin{aligned}
&DC_{re;xx} - C_{re;t} = kC_{re} - Q_r(t)\delta(x) \\
&C_{re}(X_r(t),t) = c_1 \\
&C_{re}(x,o) = \begin{cases} 0 & , \ |x|<X_f \\ C_{fe}(x), & |x|\geq X_f \end{cases} \\
&C_{re}(x,t) \to 0, \ |x| \to \infty
\end{aligned}
\tag{34}
$$

$$
\begin{aligned}
&DC_{ri;xx} - C_{ri;t} = kc_1 \\
&C_{ri}(X_r(t),t) = c_i; C_{ri;x}(X_r(t),t) = C_{re;x}(X_r(t),t) \\
&C_{ri}(x,0) = \begin{cases} C_{fi}(x) & |x|<X_f \\ T_r(x) & |x|\geq X_f \end{cases} \\
&C_{ri}(x,t) \to 0, \ |x| \to \infty
\end{aligned}
\tag{35}
$$

For clarity it suffices for our purposes to solve (35) in terms of $C_{fi}(x)$ for now, not solving the integrals for the initial condition explicitly by (32). With a single exception the three boundary conditions at $X_r(t)$ as given by (34) and (35) may be derived from those already calculated for the case with the source on.

Let us dispose of the exception now. The extended exterior must be provided with a non-zero initial condition, $C_{fe}(x)$ for $x\geq X_f$. Since the problem is linear, that part of the extended exterior owing to this initial condition is independent of that part owing to the unknown source $Q_r(t)$. Therefore, if $\gamma_{e2}(x,s)$ is the Laplace transform of the former term, the inversion of γ_{e2} will be added to that part resulting from the

source. We have:

$$D\gamma_{e2;xx} - (s + k)\gamma_{e2} = - C_f(x) \tag{36}$$

Using expression (31) for $C_{fe}(x)$ we have immediately

$$\gamma_{e2}(x,s) = \frac{c_1}{2\sqrt{D}(s + k)} \int_{X_f}^{\infty} d\xi \; e^{-\sqrt{\frac{s + k}{D}} \left| \xi - |x| \right|} e^{-\sqrt{\frac{k}{D}} (\xi - X_f)}$$

$$= \frac{c_1}{2\sqrt{s + k}} \left[\frac{1}{\sqrt{s + k} - \sqrt{k}} + \frac{1}{\sqrt{s + k} + \sqrt{k}} \right] e^{-\sqrt{\frac{k}{D}} (|x| - X_f)}$$

$$- \frac{c_1}{2\sqrt{s + k}\,(\sqrt{s + k} - \sqrt{k})} \; e^{-\sqrt{\frac{s + k}{D}} (|x| - X_f)} . \tag{37}$$

Making use of the following two inversions, the second being one of Campbell and Foster,

$$\frac{1}{\sqrt{s}\,(\sqrt{s} + a)} \rightarrow e^{a^2 t} \operatorname{erfc} a\sqrt{t} \qquad \text{(A.S. 29.3.43 p. 1024)}$$

$$\frac{1}{(p + \rho)^{\frac{1}{2}}[\lambda + (p + \rho)^{\frac{1}{2}}]} \; e^{-\sigma^2 (p + \rho)^{\frac{1}{2}}} \longrightarrow$$

$$e^{\lambda\sigma^{\frac{1}{2}} + \lambda^2 t - \rho t} \operatorname{erfc}\left(\lambda t^{\frac{1}{2}} + \frac{\sigma^{\frac{1}{2}}}{2t^{\frac{1}{2}}} \right), \; t>0, \text{ (C.F. 830.0 p.99)}$$

we obtain finally the inversion of $\gamma_{e2}(x,s)$,

$$C_{e2}(x,t) = c_1 e^{-\sqrt{\frac{k}{D}} (|x| - X_f)} \left[1 - \frac{1}{2} \operatorname{erfc}\left(- \sqrt{kt} + \frac{(|x| - X_f)}{2\sqrt{Dt}} \right) \right] . \tag{38}$$

We will need also its spatial derivative:

$$C_{e2;x}(x,t) = -\frac{c_1}{\sqrt{D}}\, e^{-\sqrt{\frac{k}{D}}\,(|x| - X_f)}\left[\sqrt{k}\left[1 - \frac{1}{2}\,\mathrm{erfc}\left(-\sqrt{kt} + \frac{|x| - X_f}{2\sqrt{Dt}}\right)\right]\right.$$
$$\left. - \frac{1}{2\sqrt{\pi t}}\, e^{-\left(-\sqrt{kt} + \frac{(|x| - X_f)}{2\sqrt{Dt}}\right)^2}\right]. \qquad (39)$$

With these terms calculated we may now return to writing the coupled integral equations for the boundary conditions at $X_r(t)$. These are written in strict analogy with those given by (26) - (28), with several simple changes. Explicity, set $A_1=0$ since the physical source is off, replace all occurrences of $X_m(t)$ by $X_r(t)$, replace the unknown source $Q_m(t)$ by $Q_r(t)$, and replace the unknown initial condition $T_m(x)$ by $C_{fi}(x)$, $|x|\leq X_f$, and by $T_r(x)$, $|x|\geq X_f$. Further, time is now measured from 0 and not from some positive t_m. Finally, $C_{e2}\{X_r(t),t\}$ and $C_{e2;x}\{X_r(t),t\}$ must be included in the exterior and derivative boundary conditions, respectively. Therefore we have:

$$\frac{1}{2\sqrt{\pi}D}\int_o^t d\tau Q_r(t-\tau)\,\frac{1}{\sqrt{\tau}}\,e^{-k\tau-\frac{X_r^2(t)}{4D\tau}}$$

$$+\,c_1 e^{-\sqrt{\frac{k}{D}}\,(X_r(t)-X_f)}\left[1-\frac{1}{2}\,\mathrm{erfc}\left(-\sqrt{kt}+\frac{X_r(t)-X_f}{2\sqrt{Dt}}\right)\right]=c_1 \qquad (40)$$

$$\frac{1}{2\sqrt{\pi}Dt}\left[\int_o^{X_f} d\xi e^{-\frac{|X_r(t)-\xi|^2}{4Dt}}\,C_{fi}(\xi)\right.$$

$$\left.+\int_{X_f}^{\infty} d\xi e^{-\frac{|X_r(t)-\xi|^2}{4Dt}}\,T_r(\xi)\right] = c_1(1+kt) \qquad (41)$$

$$-\frac{X_r(t)}{4\sqrt{\pi}\,D^{3/2}}\int_o^t d\tau\, Q_r(t-\tau)\,\frac{1}{\tau^{3/2}}\,e^{-k\tau-\frac{X_r^2(t)}{4D\tau}}$$

$$-\,c_1\sqrt{\frac{k}{D}}\,e^{-\sqrt{\frac{k}{D}}\,(X_r(t)-X_f)}\left[1-\frac{1}{2}\,\mathrm{erfc}\left(-\sqrt{kt}+\frac{(X_r(t)-X_f)}{2\sqrt{Dt}}\right)\right]$$

$$+\frac{c_1}{\sqrt{\pi Dt}}\,e^{-\sqrt{\frac{k}{D}}\,(X_r(t)-X_f)}e^{-\left(-\sqrt{kt}+\frac{(X_r(t)-X_f)}{2\sqrt{Dt}}\right)^2}$$

$$+\frac{1}{4\sqrt{\pi}\,D^{3/2}t^{3/2}}\left[\int_o^{X_f} d\xi|X_r(t)-\xi|e^{-\frac{|X_r(t)-\xi|^2}{4Dt}}\,C_{fi}(\xi)\right.$$

$$\left.+\int_{X_f}^{\infty} d\xi|X_r(t)-\xi|e^{-\frac{|X_r(t)-\xi|^2}{4Dt}}\right]T_r(\xi) \quad = 0\ . \qquad (42)$$

These are the integral equations for the return in terms of the three unknowns $X_r(t)$, $Q_r(t)$, and $T_r(x)$. As given they present essentially the same difficulties as do those for the physical source on in that they are amenable only to short time power series expansion and long time asymptotics. Even this last treatment might prove unworkable since both $X_r(t)$ and $Q_r(t)$ are destined to be identically zero after some time, $t \geq t_r$.

It may now be apparent why the situation with the physical source on and a growing interior solution has been described first. The extended interior has two distinct initial conditions, one real and one fictitious. The situation with a homogeneous fictitious initial condition seems conceptually simpler. In this regard $T_r(x)$ cannot be extended to $|x| \leq X_f$, and the initial condition for the non-extended part is restricted by definition to just this region.

Regardless of the fact that equations (40) - (42) are not solved here explicitly, we may obtain an upper limit on the time to disappearance of the saturated region. This is fortunate since t_r is probably the most useful physical parameter for this system. The reader should be cautioned that the next steps of this model rest upon an heuristic which, while eminently reasonable and convincing, is not demonstrated rigorously. The systems of coupled equations (26) - (28) and (40) - (42) are correct for their respective applications of Boley's method to the saturated extrusion model. The expedient taken in obtaining an equation for an upper limit on t_r is pointed out without affecting the validity of the model up to this point.

The heuristic posited is that $T_r(x) \leq c_1$, $|x| \geq X_f$. That this is a perfectly reasonable assumption may be seen from the following considerations. If it is assumed that the fictitious initial condition for the extended interior were for some region greater than the transitional concentration c_1, as depicted in fig. 5.1c, then it is likely that the solution of the coupled equations would not be unique. New X_r's and Q_r's may arise for each extended interior region that propagates forward from regions of the x axis where $T_r(x)$ exceeds c_1. Since the full problem is nonlinear, even while it has been decomposed into two linear subproblems, it cannot be said that the solution for $X_r(t)$ must be unique. However from a purely physical point of view it could not be otherwise. It would be untenable to hold that the interior and exterior regions have more than one boundary when only one is specified in the actual initial condition.

If on the other hand it is assumed that the boundary $X_r(t)$ and the fictitious source $Q_r(t)$ for the exterior are in fact the unique and correct functions, that is, the least in absolute value, then the extended interior diffusion equation would apply to regions of concentration greater than c_1. However, all physical sources are off. Since the actual concentration profile is decaying everywhere there is nothing in the physical problem that would tend to pull the boundary $X_r(t)$ farther out on the x axis than X_f. A region of the initial condition greater than c_1 would tend to do just this. Therefore this upper limit on the extended interior initial condition is a reasonably convincing hypothesis. The validity of the limit is most likely demonstrable by the maximum

principles of partial differential equations [Dr. D. Cohen, personal communication, Friedman, 1964 (chapter 2)].

With the rationale for the heuristic in place we may now proceed to use it in determining an upper bound on t_r. That $T_r(x)$ is bounded above should imply that t_r is bounded above as well. Evaluating the second of the integral equations (41) at $t=t_r$, we obtain the simplification that $X_r(t_r) = 0$. The first integral of (41) may now be evaluated by the use of (32). With the following definitions of 'known', 'maximal', and 'correct' functions,

$$K(t) = 2\sqrt{\pi D}\, c_1 \sqrt{t}\,(1 + kt) - \int_0^{X_f} d\xi\, e^{-\frac{\xi^2}{4Dt}}\, C_{fi}(\xi)$$

$$= 2\sqrt{\pi D}\, c_1 \sqrt{t}\,(1 + kt)$$

$$- \sqrt{\pi D t}\left[kc_1 t - \frac{kc_1}{2D} X_f^2 + \frac{A_1}{2D} X_f + c_1\right] \operatorname{erf} \frac{X_f}{2\sqrt{Dt}}$$

$$+ (A_1 - kc_1 X_f)t\, e^{-\frac{X_f^2}{4Dt}} - A_1 t \qquad (43)$$

$$M(t) = c_1 \int_{X_f}^{\infty} d\xi\, e^{-\frac{\xi^2}{4Dt}}$$

$$= \sqrt{\pi D t}\, c_1 \operatorname{erfc} \frac{X_f}{2\sqrt{Dt}} \qquad (44)$$

$$C(t) = \int_{X_f}^{\infty} d\xi\, T_r(\xi) e^{-\frac{\xi^2}{4Dt}}, \qquad (45)$$

the boundary condition reduces to $K(t_r) = C(t_r)$, where $C(t)$ is maximized by $C(t) < M(t)$. The correct t_r must be maximized by t_{rm}, where $K(t_{rm}) = M(t_{rm})$. The number t_{rm} should exist by consideration of the asymptotic

derivatives. Up to constant positive multipliers, $K(t) \sim t^{3/2}$, $M(t) \sim t^{1/2}$ as $t \to \infty$. Thus, $K(t) = M(t)$, where $K'(t) > M'(t)$, provides an upper bound on the return time t_r.

iv) Sequestration to an unlimited substrate. For clarity, let us first write the equations for the case of limited substrate. We assume the same source and diffusive and first-order extrusive conditions as in the non-saturating model above. In addition, the ion is assumed to be bound to an inactivating and immobile chemical site S which is hence altered to an S^*. Both forward and backward reactions are assumed to be governed by first-order kinetics with rates λ and δ, respectively. This is written as

$$C + S \underset{\delta}{\overset{\lambda}{\rightleftharpoons}} S^* .$$

We obtain the coupled equations,

$$DC_{xx} - C_t = kC - S_t^* - A_1\delta(x) \tag{46}$$

$$S_t^* = \lambda CS - \delta S^* . \tag{47}$$

Equation (47) is nonlinear, so let us consider the linear case of an unlimited substrate. Since S is constant, we have now,

$$C \underset{\delta}{\overset{\lambda}{\rightleftharpoons}} S^* ,$$

$$S_t^* = \lambda C - \delta S^* \tag{48}$$

replacing (47). Transforming (46) and (48) in the usual way,

$$D\gamma_{xx} + C_0 - s\gamma - S_0^* + s\Gamma^* - k\gamma = -\frac{1}{s} A\delta \tag{49}$$

$$- S_0^* + s\Gamma^* = \lambda\gamma - \delta\Gamma^* , \tag{50}$$

where $\gamma(x,s)$ and $\Gamma^*(x,s)$ are the transforms of $C(x,t)$ and $S^*(x,t)$,

respectively, and C_0, S_0^* are the initial conditions. Eliminating Γ^* we have,

$$D\gamma_{xx} - \left[s + k - \frac{\lambda s}{s + \delta}\right]\gamma + \frac{sS_0^*}{s + \delta} + (C_0 - S_0^*) = -\frac{1}{s} A_1 \delta(x) \qquad (51)$$

$$\gamma(x,s) = \frac{s + \delta}{(s + k)(s + \delta) - \lambda s}\left[\frac{sS_0^*}{s + \delta} + C_0 - S_0^*\right]$$

$$- \frac{A_1}{2s\sqrt{D}} \sqrt{\frac{s + \delta}{(s + k)(s + \delta) - \lambda s}}\; e^{-\sqrt{\frac{1}{D}\left(s + k - \frac{\lambda s}{s + \delta}\right)}|x|} . \qquad (52)$$

The inversion of the second term in (52) is unavailable to this author. However, several points may be made about the solution. The problem is linear, so an expression analogous to (5) may be written for the case where the source is turned off at $t=t_0$. Since the ion is to be sequestered sufficiently to perturb the solution from that without substrate, we assume at least that $\lambda \geq \delta$. If the rate of sequestration is small, $\lambda \sim o(1)$ and (52) reduces in the limit to (11) for zero initial conditions. If $\lambda \sim 0(1)$, the discrepancy between the cases with and without sequestration will probably not be large since we have already determined that $k \gtrsim 0(10)$. The solution should differ markedly however if $\lambda \sim 0(k)$.

v) Sequestration with diffusion eliminated. The fact that the x-dependent term in (52) is not inverted precludes either eliminating or accepting this model. Hence the problem may be restated with the diffusive term eliminated. Although the nondimensionalized diffusion constant $D = 10^3$ is large, the time scale on which the model is to be used may be large enough so that the concentration gradient becomes spatially uniform. This

strictly kinetic system may be solved explicitly with all initial conditions included. Since the problem is simpler we also distinguish a first-order permeability p of the plasma membrane which permits a small ionic flow back into the cell from the constant extracellular concentration C_{out}. If the intracellular concentration exceeds C_{out} then the permeability allows net flow out of the cell. Therefore the intracellular concentration $C_{\lambda de}(t)$ is in dynamic equilibrium with both the exterior of the cell and the inactivating unlimited substrate S according to

$$C_{out} \underset{k}{\overset{\overbrace{(C_{out} - C_{\lambda de})}^{p}}{\rightleftharpoons}} C_{\lambda de} \underset{\delta}{\overset{\lambda}{\rightleftharpoons}} S^{*}.$$

Since the problem no longer admits x-dependence, the system with the continuous source starting at t=0 is written in matrix notation as

$$\frac{d}{dt}\begin{pmatrix} C_{\lambda de} \\ S^{*} \end{pmatrix} + \begin{pmatrix} -(\lambda + k + p) & \delta \\ \lambda & -\delta \end{pmatrix}\begin{pmatrix} C_{\lambda de} \\ S^{*} \end{pmatrix} + \begin{pmatrix} A_1 H(t) + pC_{out} \\ 0 \end{pmatrix} \tag{53}$$

$$\begin{pmatrix} C_{\lambda de} \\ S^{*} \end{pmatrix}_{t=0} = \begin{pmatrix} C_0 \\ S_0^{*} \end{pmatrix}, \tag{54}$$

where H(t) is the Heaviside function. The initial condition reduces to $C_o = \frac{p}{k + p} C_{out}$, $S_0^{*} = \frac{\lambda}{\delta} C_0$. Following the notation of Boyce and DiPrima (1969), the fundamental solution matrix $\underline{\Psi}(t)$ and its inverse are given by

$$\underline{\Psi}(t) = \begin{pmatrix} (\delta + \beta_+)e^{\beta_+ t} & (\delta + \beta_-)e^{\beta_- t} \\ \lambda\, e^{\beta_+ t} & \lambda\, e^{\beta_- t} \end{pmatrix} \tag{55}$$

$$\underline{\Psi}^{-1}(t) = \frac{1}{\lambda(\beta_+ - \beta_-)} e^{-(\beta_+ + \beta_-)t} \begin{pmatrix} \lambda e^{\beta_- t} & -(\delta + \beta_-)e^{\beta_- t} \\ -\lambda e^{\beta_+ t} & (\delta + \beta_+)e^{\beta_+ t} \end{pmatrix}, \tag{56}$$

where

$$\beta_{\pm} = \frac{1}{2}\left[-\alpha \pm \sqrt{\alpha^2 - 4(k+p)\delta}\right], \tag{57}$$

$$\alpha = k + p + \lambda + \delta\ , \tag{58}$$

assuming distinct roots. Since no oscillatory components are expected, we anticipate that the discriminant in (57) is positive. If $\underline{U}'(t)$ is the product of the integrating factor $\underline{\Psi}^{-1}(t)$ and the forcing term of (53),

$$\underline{U}'(t) = \underline{\Psi}^{-1}(t) \begin{pmatrix} A_1 H(t) + pC_{out} \\ 0 \end{pmatrix}$$

$$= \frac{A_1 H(t) + pC_{out}}{(\beta_+ - \beta_-)} \begin{pmatrix} e^{-\beta_+ t} \\ -e^{-\beta_- t} \end{pmatrix} \tag{59}$$

then its integral $\underline{U}(t)$ for times $t \geq t_o$ after the source is turned off is given by

$$\underline{U}(t) = \frac{1}{(\beta_+ - \beta_-)} \begin{pmatrix} -\frac{1}{\beta_+}\left[A_1 e^{-\beta_+ t} - pC_{out}\left(1 - e^{-\beta_+ t}\right)\right] \\ \frac{1}{\beta_-}\left[A_1 e^{-\beta_- t_o} - pC_{out}\left(1 - e^{-\beta_- t}\right)\right] \end{pmatrix}, t \geq t_o, \tag{60}$$

where we have specified $\underline{U}(0) = \underline{0}$. With the initial condition matrix $\underline{c}$ defined by

$$\underline{c} = \underline{\Psi}^{-1}(0) \begin{pmatrix} C_0 \\ S_0^* \end{pmatrix}$$

$$= \frac{1}{\lambda(\beta_+ - \beta_-)} \begin{pmatrix} \lambda C_0 - (\delta + \beta_-)S_0^* \\ -\lambda C_0 + (\delta + \beta_+)S_0^* \end{pmatrix}, \tag{61}$$

$$\begin{pmatrix} C_{\lambda de} \\ S^* \end{pmatrix} = \underline{\Psi}(t)\underline{c} + \underline{\Psi}(t)\underline{U}(t)$$

$$= \begin{pmatrix} C_0 \\ S_0^* \end{pmatrix} + \frac{1}{(\beta_+ - \beta_-)} \begin{pmatrix} (\delta + \beta_+)z_-\left(e^{\beta_+ t} - 1\right) - \frac{1}{\beta_+}(\delta + \beta_+)r_+(t) \\ \quad + (\delta + \beta_-)z_+\left(e^{\beta_- t} - 1\right) + \frac{1}{\beta_-}(\delta + \beta_-)r_-(t) \\ \lambda z_-\left(e^{\beta_+ t} - 1\right) - \frac{\lambda}{\beta_+} r_+(t) \\ \quad + \lambda z_+\left(e^{\beta_- t} - 1\right) + \frac{\lambda}{\beta_-} r_-(t) \end{pmatrix}, \quad (62)$$

where

$$z_{\pm} = \mp C_0 \pm \frac{1}{\lambda}(\delta + \beta_{\pm})S_0^* \quad (63)$$

$$r_{\pm}(t) = A_1 e^{\beta_{\pm}(t - t_0)} + pC_{out}\left(1 - e^{\beta_{\pm} t}\right) . \quad (64)$$

Evaluation of the Models

These five models constitute different hypotheses regarding the Ca^{++} concentration up and down the photoreceptor in the experiments reported in Chapter III. Their applicability is subject to the several assumptions we have made above. The time course of the recovery data will be used to eliminate the first three hypotheses. The first two models have been solved exactly, so their time scale to equilibrium conditions is explicit. For the case of saturated extrusion however, we offer here an upper limit on that time to the disappearance of the saturated region, and therefore a strong heuristic argument. Though nonlinear, this model presents a degree of symmetry between the time when the source is turned on and

the time following its cessation in the sense that the time scale to equilibrium must approximate the time scale to maximum X_f. This property is not shared by the sequestration model even though it is linear, since the presence of unlimited substrate with low dissociation provides an essential asymmetry between these times. The substrate is able to buffer the concentration for periods long with respect to the injection time.

Let us check each of these models in turn. We first repeat that the problem is to be nondimensionalized by μ, sec, and the estimate we have given of 10^{-7} M for the initial intracellular Ca^{++} concentration of the light-adapted photoreceptor. We need now the nondimensionalized value of A_1, the strength of the source. For this we require strictly the transport number of the electrode, which we have estimated in 'Materials and Methods' to be approximately $1^{o}/o$. Therefore, assuming a typical 2 nA injection, and taking into account the value of the Faraday constant $F = 9.65 \cdot 10^4$ coul/mol and the fact that Ca^{++} is a divalent cation, we have

$$A_1 = 2\ nA \cdot \frac{1}{2} \cdot \frac{1}{F} \cdot 10^7 M^{-1} \cdot \frac{1}{1.7} \cdot 10^{12} \ell^{-1} \cdot 1\%$$

$$= 6.1 \cdot 10^2 sec^{-1}$$

Let us further suppose that the injection lasts for a typical time of 2 sec, and that the recovery proceeds on a time scale of 10 - 20 sec. This is a typical value for the experimental recovery of the wild type receptor potential at all frequencies tested. The assumption inherent in using the experimental value in checking the models, while perhaps obvious, should be made explicit. The receptor potential generated at any point along the

photoreceptor is a function of either the free Ca^{++} concentration there or of some local variable coupled to it, such as the concentration of inactived substrate S^* in the fourth and fifth models. The approach taken in applying this assumption should be clear from the estimates which follow.

i) Check on simple diffusion. The concentration predicted for a system without extrusion or sequestration is too large to be of use in modeling a return to equilibrium on the order of 10-20 sec. At 30 μ distance from the source, the maximum for the soma in the experimental situation if the electrode is positioned halfway along it, and with $t_0=2$, t=12, the right-hand side of equation (5) is approximately

$$C_D(30,12)\Big|_{t_0=2} = 3.64\cdot 10^3 .$$

This lower bound is therefore about three log units too high.

ii) Check on first-order extrusion. The concentration predicted for this system is too small, even for the slowest extrusion rate, k=14. At the source, only 1 sec after it is turned off an estimate given by equation (13) in analogy with (5) is

$$C_{k=14}(0,3)\Big|_{t_0=2} = 3.13\cdot 10^{-6}$$

The value of $C_k(x,t)$ is normalized by the initial concentration, so that the increment predicted for injected material is negligible.

iii) Check on saturated extrusion. Values of t_{rm2} in fig. 5.2 were calculated by a zero-seeking subroutine applied to the function K(t) - M(t) as defined by equations (43) and (44). With values for k of 4.2, 14 and 42, the results are presented in Table V.1.

Table V.1. $X_f(\mu)$ and $t_{rm}(sec)$ as functions of $c_1(10^{-7}\ M)$ and $k(10^{-7}\ M/sec)$ for the saturated extrusion model.

X_f	c_1=1	3	10
k=4.2	57.2	8.8	<0
14	13.3	<0	
42	2.4	<0	
140	< 0		

t_{rm}	c_1=1	3
k=4.2	17.9	0.308
14	0.417	
42	$<10^{-3}$	

In order to keep the integral equations (40) - (42) as simple as possible the saturation model was stated with a zero initial condition. Therefore the values obtained are somewhat distorted from those which would be obtained with a unity initial condition. Assuming the former case should yield an overestimate of the values obtained for t_{rm}. This error should decrease with increasing c_1.

Recalling that x = ±30 are the approximate physical limits of the soma, the results for X_f show that the case represented by k=4.2, c_1=1 exceeds this limit. Assuming an infinite one-dimensional space instead of a finite narrow cylinder should yield an underestimate of the concentration and therefore an underestimate of t_{rm}. This error should decrease with increasing k.

The results for t_{rm} show that for the two cases for which kc_1=14 the maximized time to return is still over an order of magnitude too short. Both values of X_f for these two cases are well within the soma. The only case remaining is that for which kc_1=4.2, corresponding to a dimensional extrusive rate of 0.003 pmol $cm^{-2}sec^{-1}$. For the cell described in 'Pulse Response Recovery A' of the previous chapter we have estimated a maximum rate of 0.17 pmol $cm^{-2}sec^{-1}$, which is close to the range 0.1 - 0.01 pmol $cm^{-2}sec^{-1}$ of passive influx for other systems. It is unlikely that a photoreceptor with its Ca^{++} extrusion rate saturated would exhibit a rate lower than 0.01 pmol $cm^{-2}sec^{-1}$.

Hence, while introducing saturation in the extrusive rate extends the time course with respect to that of the second model, it does not extend it far enough for parameter values applicable to the present biological system. What is required is a model in which a system is

introduced which can govern total membrane extrusion by competing with it for ions.

iv) Sequestration to an unlimited substrate. Since equation (52) is not inverted, quantitative estimates are not obtained for this model.

v) Check on sequestration with diffusion eliminated. The time that $C_{\lambda de}(t)$ from equation (62) crosses twice the initial concentration was computed for values of k=14, 42, and 140, with λ varying from 10 to 3000, and $\delta \leq \lambda$. The results are presented in Table V.2. The time so obtained is an estimate of that time required to bring the concentration close to the initial concentration. Values of the slower of the two time constants, β_+ from equation (57), are presented in Table V.3 for the same parameter ranges. It is reasonable to assume that the receptor potential begins its recovery when the Ca^{++} concentration is of the order of small multiples of the initial light-adapted concentration. Therefore, the time elapsed to two times initial concentration should be approximately 10 sec after the source is turned off. The tiers of parameters consistent with this requirement are indicated in Table V.2 for the time, and the same tiers are indicated in Table V.3 for the time constants. For each of the cases k=42 and k=140 two tiers are indicated defining the parameter limits.

The dimensional time constants obtained at the tiers indicated decreases in absolute value with increasing k. In particular, the time constants are between $-0.41\ sec^{-1}$ and $-0.12\ sec^{-1}$ for the limiting tiers for the case k=42. Therefore, on the assumption that the receptor potential recovery begins at a small multiple of initial concentration and that the concentration decays with a time constant approaching $-0.1\ sec^{-1}$, comparable to the negative of the inverse of the time from

Table V.2. Time (sec) that $C_{\lambda de}(t) = 2(\cdot 10^{-7}M)$, as a function of k, λ, and δ (10^{-7} M/sec) for the kinetic sequestration model.

λ=10	30	100	300	1000	3000	k = 14
5.11	10.8	29.6	83.1			δ = 1
	3.75	10.1	27.9	89.9		3
		3.20	8.6	27.3	82.3	10
			3.04	9.3	27.2	30
				2.98	8.3	100
					2.96	300

λ=30	100	300	1000	3000	k = 42
3.05	7.64	19.9	61.8		δ = 1
	2.65	6.77	20.9	60.4	3
		2.12	6.44	18.5	10
			2.22	6.33	30
				1.98	100

λ=300	1000	3000	k = 140
2.55	7.35	21.0	δ = 1
	2.97	7.45	3
		2.74	10

Table V.3. $\beta_+(sec^{-1})$ as a function of k, λ, and δ (10^{-7} M/sec) for the kinetic sequestration model.

λ=10	30	100	300	1000	3000	k = 14
-0.573	-0.313	-0.122	-0.045			δ = 1
	-0.911	-0.360	-0.133	-0.041		3
		-1.14	-0.433	-0.137	-0.046	10
			-1.23	-0.402	-0.138	30
				-1.26	-0.449	100
					-1.27	300

λ=30	100	300	1000	3000	k = 42
-0.580	-0.294	-0.122	-0.040		δ = 1
	-0.874	-0.366	-0.120	-0.042	3
		-1.20	-0.399	-0.138	10
			-1.18	-0.410	30
				-0.34	100

λ=300	1000	3000	k = 140
-0.318	-0.122	-0.044	δ = 1
	-0.368	-0.134	3
		-0.444	10

inception of recovery to full recovery, then the case with k=42 is the best choice among the three extrusive rates. This corresponds to a membrane extrusion rate of 0.03 pmol $cm^{-2}sec^{-1}$. The ratio of sequestration to release rates therefore is approximately 100 - 300.

It is known that mitochondria from many systems display saturation kinetics with respect to Ca^{++} influx. However, the half-maximal rates have been demonstrated to occur at external free Ca^{++} concentration of 2 - 70 μM (Carafoli & Crompton, 1978). This range, nondimensionalized by our initial concentration of 10^{-7} M, is 20 - 700. The maximal theoretical concentration produced by iontophoresis for the limiting case of k=14, λ=1, and δ=1 is $C_{\lambda de}(2) = 42.6$. This is within the above range. However, if saturation of the Ca^{++} sequestering capacity of the sensory cells had been occurring for the experiments of Chapter III, this saturation probably would be short-lived and would not extend far from the electrode tip.

Conclusion

This chapter has considered five models of the Ca^{++} concentration within the Drosophila photoreceptor following iontophoresis from a microelectrode. Four of these models have been evaluated on the basis of the time course to recovery of the wild type units described in Chapter III. Diffusion itself is too slow to subserve this recovery. Introducing membrane extrusion yields a model concentration that proceeds too quickly to equilibrium. This progress is slowed by an extrusive rate that saturates in the third model; however, near equilibrium concentration is achieved still too rapidly.

Introducing sequestration that obeys first-order kinetics does account for the time course to recovery of the wild type Drosophila receptor potential following Ca^{++} injection. The ratio of sequestering to release rates is predicted to be large, at least 30 for the case of the lowest plasma membrane extrusion rate.

The previous chapter concluded on the basis of the genetically dissected phototransduction in Drosophila that mitochondrial sequestration of intracellular Ca^{++} is an important mechanism in accounting for the transient receptor potential phase shifts demonstrated in Chapter III. This chapter has considered the time course of the receptor potential recovery and has by quite different methods arrived at a similar conclusion. The biological and mathematical endeavors of the 'Discussion' and of the present chapter have been pursued independently. Their agreement is substantial evidence that the results of the intracellular study undertaken in this thesis have been interpreted correctly.

Chapter VI

IONTOPHORETIC STUDIES IN PHOTORECEPTORS AND SECOND-ORDER UNITS

Introduction

This chapter begins with a review of the white noise method of characterizing stationary temporal dynamic systems. This method is then used to characterize the light responses of both photoreceptors and second order monopolar units of the Drosophia retina during continuous iontophoresis from the recording micropipette. The results of this chapter show distinct properties of the responses from these two classes of neuron. Light-coupled conductance changes of the photoreceptor membrane are approximately linear functions of light intensity input for the Gaussian white noise stimulus used. The monopolar unit response is primarily hyperpolarizing to light and exhibits an active voltage dependence.

Analytical Review

The use of random or white noise inputs to define the temporal dynamics of visual systems has been pioneered by McCann, P. Marmarelis, and Naka. Among the systems studied with this technique have been Calliphora photoreceptors (McCann, Fargason & Shantz, 1977), Musca and Phaenicia motion detection units (Marmarelis & McCann, 1973), and neurons of the catfish retina (Marmarelis, 1971; Marmarelis & Naka, 1973a,b). Visual neurons are particularly well suited for the application of white noise theory since the input required is complex. Intensity modulation of light is probably the most easily applied of the stimuli to which sensory neuronal systems respond.

White noise theory itself has been given wide review. Our purpose here is to discuss the limited case of a third-order stationary system whose input has Gaussian probability distribution and zero mean.

Wiener (1958) characterized such a system to be a sum of functionals whose terms are each orthogonal with respect to time averaging to all previous terms. Let x(t) be a given random input with Gaussian probability distribution and zero mean such that

$$\int_{-\infty}^{\infty} d\tau\ x(\tau)x(\sigma - \tau) = P\delta(\sigma),$$

and let y(t) be the output. Then the Wiener formulation to third order is given by a sum of functionals,

$$y(t) = \sum_{0}^{3} G_n[h_n;x(t)]\ ,$$

where

$$G_n[h_n;x(t)] = \int_0^\infty d\tau_1 \cdots \int_0^\infty d\tau_n h_n(\tau_1,\ldots,\tau_n)x(t - \tau_1)\ldots x(t - \tau_n)$$

$$+ \sum_{m=0}^{n-1} \int_0^\infty d\tau_1 \cdots \int_0^\infty d\tau_m k_{mn}(\tau_1,\ldots,\tau_m)x(t - \tau_1)\ldots x(t - \tau_m).$$

The $h_n(\tau_1,\ldots,\tau n)$ are known as the Wiener kernels of the system; the $k_{mn}(\tau_1,\ldots,\tau_m)$ are terms dependent upon the Wiener kernels so as to orthogonalize the series. We require

$$\lim_{T\to\infty} \frac{1}{2T} \int_{-T}^{T} dt\ G_m[h_m;x(t)]G_n[h_n;x(t)] = 0;\ 0\leq m\leq 3,\ 0\leq n\leq m.$$

Hence (Marmarelis, 1971),

$$k_{10} = k_{30} = k_{21}(\tau) = k_{32}(\tau_1,\tau_2) = 0$$

$$k_{20} = -P \int_0^\infty d\tau\ h_2(\tau,\tau)$$

$$k_{31}(\tau) = -3P \int_0^\infty d\tau \int_0^\infty d\tau_1 h_3(\tau,\tau_1,\tau_1)x(t - \tau)\ .$$

Lee and Schetzen (1961; Marmarelis, 1971) have provided a convenient method of calculating the Wiener kernels that exploits the randomness of the input. In general,

$$h_n(\tau_1,\ldots,\tau_n) = \frac{1}{n!P^n} \lim_{T\to\infty} \frac{1}{2T} \int_{-T}^{T} dt \left\{ y(t) - \sum_{m=0}^{n-1} G_m[h_m;x(t)] \right\} x(t-\tau_1)\ldots x(t-\tau_n).$$

Hence,

$$h_0 = \lim_{T\to\infty} \frac{1}{2T} \int_{-T}^{T} dt\, y(t)$$

$$h_1(\tau) = \frac{1}{P} \lim_{T\to\infty} \frac{1}{2T} \int_{-T}^{T} dt\, y(t)x(t-\tau)$$

$$h_2(\tau_1,\tau_2) = \frac{1}{2P^2} \lim_{T\to\infty} \frac{1}{2T} \int_{-T}^{T} dt\{y(t) - h_0\}x(t-\tau_1)x(t-\tau_2)$$

$$h_3(\tau_1,\tau_2,\tau_3) = \frac{1}{3!P^3} \lim_{T\to\infty} \frac{1}{2T} \int_{-T}^{T} dt \left\{ y(t) - \int_0^{\infty} d\tau h_1(\tau)x(t-\tau) \right\} x(t-\tau_1)x(t-\tau_2)x(t-\tau_3).$$

The lowest order term h_0 is the time average of the output. With input $x(t) = \delta(t)$, $h_1(t)$ is the linear contribution to the system response. The term involving $h_2(\tau_1,\tau_2)$ is the lowest order nonlinear term. With input $x(t) = \delta(t + \Delta\tau_1 + \Delta\tau_2) + \delta(t + \Delta\tau_1) + \delta(t)$, $\Delta\tau_1,\Delta\tau_2 \geq 0$, the total system response is given by

$$\begin{aligned} y(t) = {} & h_o + h_1(t + \Delta\tau_1 + \Delta\tau_2) + h_1(t + \Delta\tau_1) + h_1(t) \\ & + h_2(t + \Delta\tau_1 + \Delta\tau_2, t + \Delta\tau_1) + h_2(t + \Delta\tau_1, t) \\ & + h_3(t + \Delta\tau_1 + \Delta\tau_2, t + \Delta\tau_1, t). \end{aligned}$$

With the change of variables,

$$\tau = \min\{\tau_1, \tau_2\}$$

$$\Delta\tau = |\tau_1 - \tau_2|,$$

we may define an alternate version of the second-order kernel,

$$h_2'(\tau, \Delta\tau) = h_2(\tau, \tau + \Delta\tau) .$$

The alternate version will henceforth be designated as a primed variable. With input $x(t) = \delta(t + \Delta\tau) + \delta(t)$, the total system response of a second-order system is given by

$$y(t) = h_0 + h_1(t + \Delta\tau) + h_1(t) + h_2'(t, \Delta\tau).$$

Consider a system which is composed of a linear subsystem with kernel $h_1(\tau)$ followed by a nonlinear subsystem whose output depends only on the present value of its input, a so-called 'zero-memory nonlinearity'. Then the second-order kernel $h_2(\tau_1, \tau_2)$ of the entire system is proportional to $h_1(\tau_1)h_1(\tau_2)$, and the third-order kernel $h_3(\tau_1, \tau_2, \tau_3)$ is proportional to $h_1(\tau_1)h_1(\tau_2)h_1(\tau_3)$.

Since the convolutions used in calculating kernels are time averages, the white noise technique is especially useful in noisy data collection enviroments, such as that implied by intracellular recording in neurons. Further, since the Wiener power level of the stimulus is constant, every data point of stimulus and response is utilized the maximum number of times in the calculations. The set of kernels computed for the physical system provides a series of measures on the response characteristics that is both canonical and rationally decomposed.

Photoreceptor Iontophoretic Study

In order to investigate the effects of continuous current passage on the receptor potential, white noise experiments were conducted during continuous iontophoresis from microelectrodes containing 2 M KCl. These neurons depolarize to light stimuli via nonregenerative membrane resistance changes. Therefore, current that hyperpolarizes the neuron should increase the response, and current that depolarizes the neuron should decrease the response. These properties should be expressed ideally without changes in the time scale of the receptor potential.

Gradual degradation of response during current passage is an inherent problem in these experiments. This degradation may be due as much to continuous loading of the intracellular space with ions as to excess current handled by the membrane channels. This loading would make increased demands on membrane ion pumps.

Data from the best receptor are presented in fig. 6.1 under the three conditions of no current and of 0.5 nA current of both polarities. The maxima of the first-order kernels are in the expected order for the different recording conditions; response is enhanced or suppressed dependent upon negative or positive iontophoresis, respectively. The fact that the first-order kernel for the case of positive iontophoresis goes in the depolarizing direction indicates that the transmembrane potential has not been driven beyond zero by the current alone. Assuming the total resistance of the cell to be $3.4 \cdot 10^7$ Ω in the dark (Alawi, 1972), these currents would yield 17 mV changes from resting potential.

There is a slight delay to maximum for each of the kernels for current

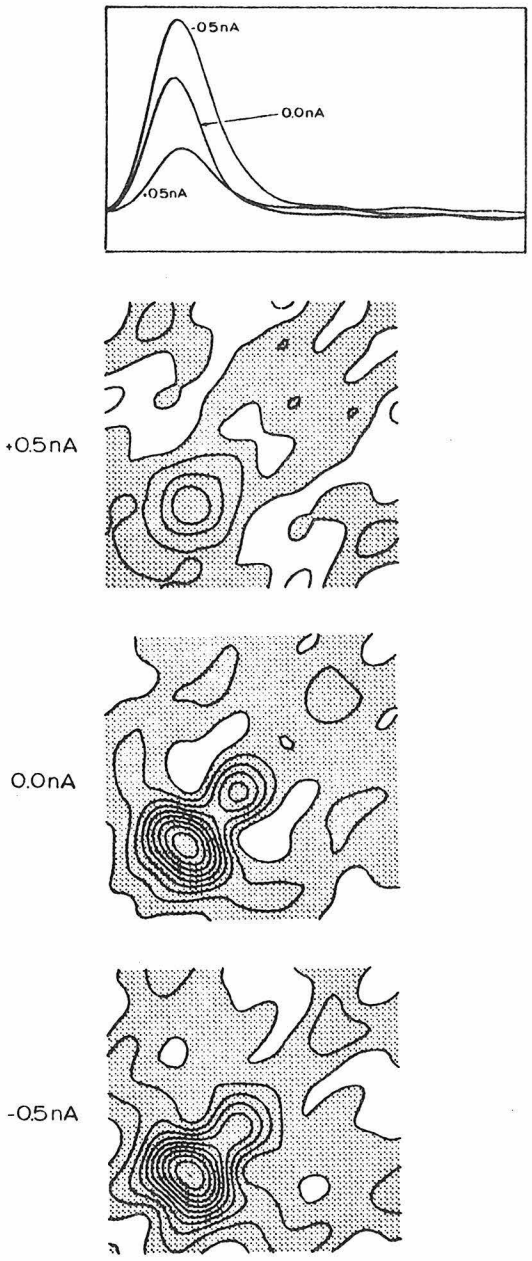

Figure 6.1. First- and second-order kernels of the wild type receptor potential during iontophoresis from the recording microelectrode, with the current values indicated. The horizontal excursions of the first-order kernels is 72 msec, those of the second-order kernels is 50 msec. On these scales the first- and second-order kernels may be compared as presented. The vertical scale for the first-order kernels is $-6.34 \cdot 10^{-11}$ to $+3.16 \cdot 10^{-10}$ mV phot^{-1} cm^{-2}. The second-order kernels are shown as contour plots. Speckled areas are negative, white areas positive. Each contour line represents a division of $1.26 \cdot 10^{-19}$ mV phot^{-2} cm^{-4}.

passage with respect to the control. As shown in Table IV.1, these delays are approximately 0.2 msec and 1.2 msec for negative or positive current, respectively.

For visual clarity, all the second-order kernels in fig. 6.1 are plotted within the same range of dependent values. Therefore the contour lines counted away from zero correspond among the three kernels shown. The speckled areas denote negative regions, the white areas positive regions. The ranges of the independent parameters τ_1 and τ_2 are each from 0 to 50 msec. Time along the horizontal axes of the second-order kernels is to the same scale as the abscissa for the first-order kernel. Therefore the kernels may be compared vertically just as they are presented (Mr. R. M. Larkin, personal communication).

The second-order kernels for this receptor all have on-diagonal negative maxima at positions which are each delayed with respect to the time to peak of the respective first-order kernels. As shown in Table VI.1, these delays are approximately 2.1 msec, 1.3 msec, and 1.1 msec for the cases -0.5 nA, 0.0 nA, and +0.5 nA, respectively.

The third-order kernel for this receptor with no current injection is displayed in fig. 6.2. Its absolute maximum is positive and is attained at an on-diagonal delay of 12 msec. Each graph is a cut taken through the kernel at $\tau_3 = 0,4,8,\ldots,20$ msec. The ranges of τ_1 and τ_2 are each 0 to 30 msec. Three positive regions migrate perpendicularly from each of the axes, maintaining a 12 msec distance from the plane at 0 msec. Only two of these regions are readily discernible in fig. 6.2 because of the method of display. All three regions meet at $\tau_1 = \tau_2 = \tau_3 = 12$ msec to form the

Table VI.1. Data for the wild type photoreceptor of figs. 6.1 and 6.2. Normalizations are with respect to the case of no current.

i_e	τ (msec); $h_1(\tau)$max	τ_1(msec); $\lvert h_2(\tau_1,\tau_2)\rvert$max	τ_1(msec); $h_3(\tau_1,\tau_2,\tau_3)$max
-0.5 nA	11.9	14	12
0.0 nA	11.7	13	12
+0.5 nA	12.9	15	12

i_e	normalized $(i_m + i_e)^{-1}$	normalized $h_{2;max}/h_{1;max}^2$
-0.5 nA	0.56	0.56
0.0 nA	1.0	1.0
+0.5 nA	4.8	2.1

i_e	normalized $(i_m + i_e)^{-2}$	normalized $h_{3;max}/h_{1;max}^3$
-0.5 nA	0.31	0.49
0.0 nA	1.0	1.0
+0.5 nA	23.5	5.0

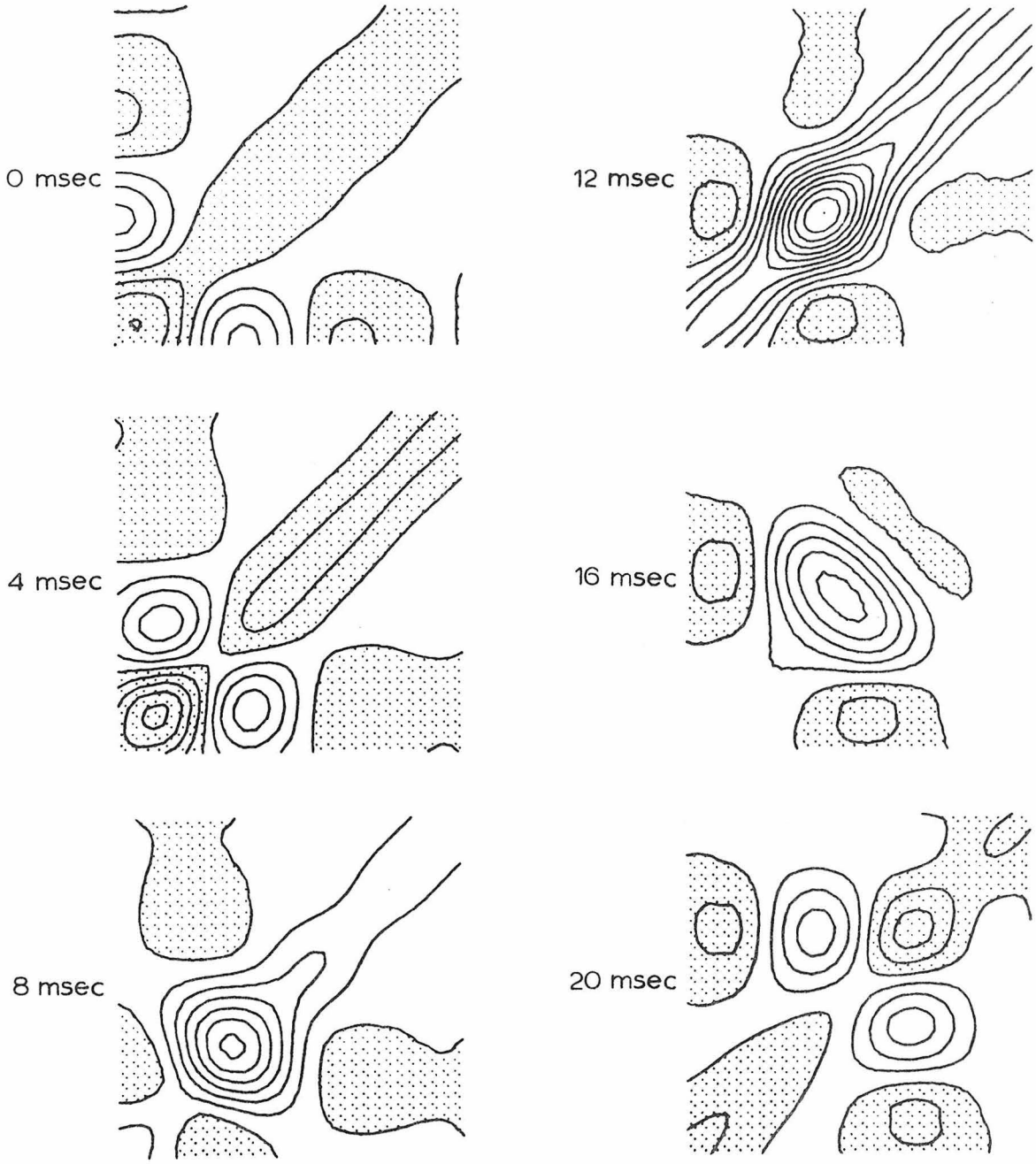

Figure 6.2. Third-order kernel for the photoreceptor of fig. 6.1 for the case of no current. Each graph is a contour plot, 50 msec square, of a cut through the cubic data at $\tau_3 = 0,4,\ldots,20$ msec. Each contour line represents a division of $1.97 \cdot 10^{-26}$ mV phot^{-3} cm^{-6}.

maximum of the whole kernel; each region proceeds at a 45° angle with respect to the axes of the plane to which its progress is parallel. These observations hold for the third-order kernels during the current injections as well.

The delays we have demonstrated in the kernels are real but are not remarkable. They are all less than the time shift at half maximal autocorrelation of the stimulus. In particular, the second- and third-order kernels are all close to those that would be exhibited by a zero-memory nonlinearity following the corresponding linear kernel. Ideally in this case the third-order kernel should have contour surfaces which all cross the diagonal. While this is not the case, the strength of the on-diagonal component at 12 msec with respect to the 'individual' off-diagonal components indicates that the approximation to the ideal is close. Fargason and McCann (1978) first showed the 'zero-memory' property of the second-order kernels for Drosophila photoreceptors stimulated by Gaussian white noise light intensity.

We may offer the hypothesis that the source of this zero-memory nonlinearity derives solely from the ohmic properties of the plasma membrane. Consider the diagram below as a simple electrical model of the membrane.

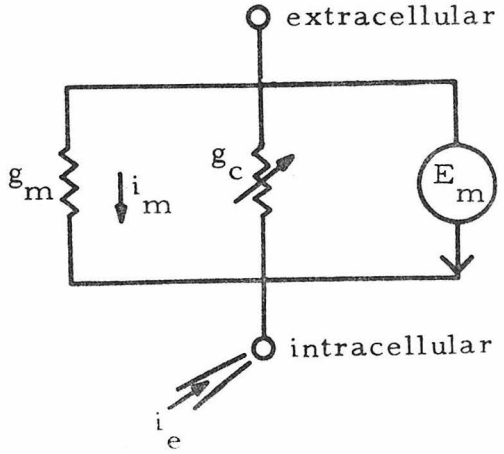

Resting potential is maintained by the electromotive force E_m acting across the membrane conductance g_m in the dark. The light-coupled conductance $g_c(t)$ is zero in the dark. The membrane current i_m passes through both g_m and $g_c(t)$. Assuming a resting potential of -21.5 mV and and a membrane resistance of $3.4 \cdot 10^7$ Ω, $i_m = -0.63$ nA. Electrode iontophoresis is expressed as a current i_e which is added to i_m to yield the total membrane current. If the potential change due to light stimulation is V(t), then we have

$$E_m + V(t) = \frac{i_m + i_e}{g_m + g_c(t)} .$$

Suppose that at a given average level of light stimulation the average of $g_c(t)$ is g_{c0}, and suppose further that $g_c(t)$ is a linear function of intensity with first-order kernel $g_{c1}(\tau)$. This is a reasonable approximation, particularly for light stimuli which are distributed in Gaussian fashion and hence are heavily distributed close to the mean. Let us write the first-, second-, and third-order kernels for V(t).

$$h_1(\tau) = - \frac{i_m + i_e}{(g_m + g_{c0})^2} g_{c1}(\tau)$$

$$h_2(\tau_1,\tau_2) = \frac{i_m + i_e}{(g_m + g_{c0})^3} g_{c1}(\tau_1) g_{c1}(\tau_2)$$

$$h_3(\tau_1,\tau_2,\tau_3) = - \frac{i_m + i_e}{(g_m + g_{c0})^4} g_{c1}(\tau_1) g_{c1}(\tau_2) g_{c1}(\tau_3) .$$

Consider the following ratios:

$$\frac{h_2(\tau_1,\tau_2)}{h_1(\tau_1) h_1(\tau_2)} = \frac{g_m + g_{c0}}{i_m + i_e}$$

$$\frac{h_3(\tau_1,\tau_2,\tau_3)}{h_1(\tau_1)h_1(\tau_2)h_1(\tau_3)} = \left[\frac{g_m + g_{c0}}{i_m + i_e}\right]^2 .$$

If our membrane model is correct and $g_c(t)$ is linear then these ratios predict the dependence of both the second- and third-order kernels on both the first-order kernel and the injected current. For convenience, the maxima of each of these kernels may be used; this will minimize the error.

As Table VI.1 shows, the agreement of the expected ratios with those measured is good for the case of negative iontophoresis. For the case of positive electrode current the nonlinearities are weaker than the model predicts, but nevertheless increase in value with the increasing order of nonlinearity. The positive current data were taken last in the experiment, and so loss of viability of the cell may be a factor here.

Therefore, a linear light-coupled conductance mechanism of the plasma membrane is consistent with the maxima of the nonlinearities of the receptor potential during current injection.

Monopolar Iontophoretic Study

The investigation of Drosophila vision reported in this thesis has been concerned up to this point with the physiology of the primary sensory cells. During experiments seeking responses from these neurons it was very occasionally the case that intracellular hyperpolarizing responses to light pulses were recorded, as shown in fig. 6.3. Superimposed upon the primary hyperpolarizing potential of these units is a high frequency wave shape. These responses are similar to those reported in larger flies as

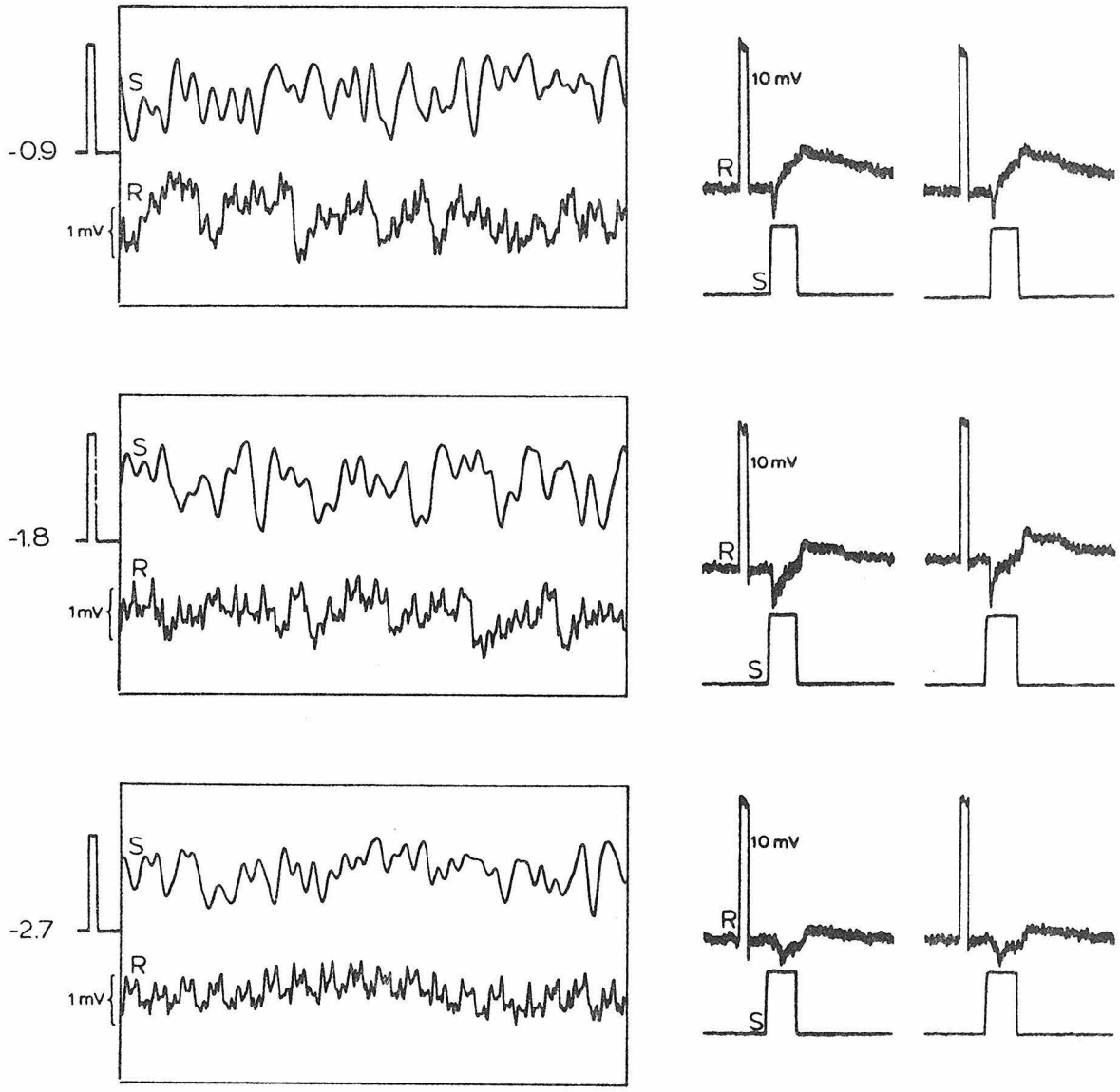

Figure 6.3. Raw data for a monopolar neuron response from the Drosophila retina. Log unit intensity differences from maximum are documented at the left. Traces (S) and (R) are light stimulus and cell response, respectively. The left-hand side shows white noise data. The extent of the full stimulus range is represented as a pulse next to the (S) traces. The right-hand side shows pulse response data to pulses 180 msec in duration. Each response is preceeded by a 10 mV calibration pulse.

deriving from second-order units, the monopolar neurons of the Dipteran retina (Järvilehto & Zettler, 1971; Zettler & Järvilehto, 1971; Arnett, 1972).

Plate I shows four monopolar neurons of the Phaenicia sericata retina stained with the Golgi technique of Strausfeld and Blest (1970). All four of these neurons may be classified as 'stratified radial diffuse' monopolar cells, or of the class L1 (Strausfeld, 1971). The vertical extent of the photograph is approximately the radial extent of the lamina. The cells are capped distally by the large cell bodies which lie just beneath the basal membrane. The laterally disposed processes of these cells are postsynaptic to the retinula cell endings. The L1 and L2 monopolar neurons are the two large types among five monopolar classifications in the Dipteran. The relatively large size of these neurons makes it likely that these are the monopolars that have been penetrated and characterized in this chapter.

Zettler and Järvilehto (1971) demonstrated that the response of the monopolar in Calliphora is conducted without decrement down the axon across the first optic chiasm to the surface of the second optic ganglion, or medulla. This is a distance of 400 - 800 μ in Calliphora. That slow potential responses should be conducted without significant change in size, shape, or latency across this distance in a fibre 1.5 μ in diameter is a relatively unusual property of these cells. This observation led these authors to propose that the response is propagated down the cell by an active mechanism in the axonal membrane.

Further evidence for an active mechanism was obtained from current

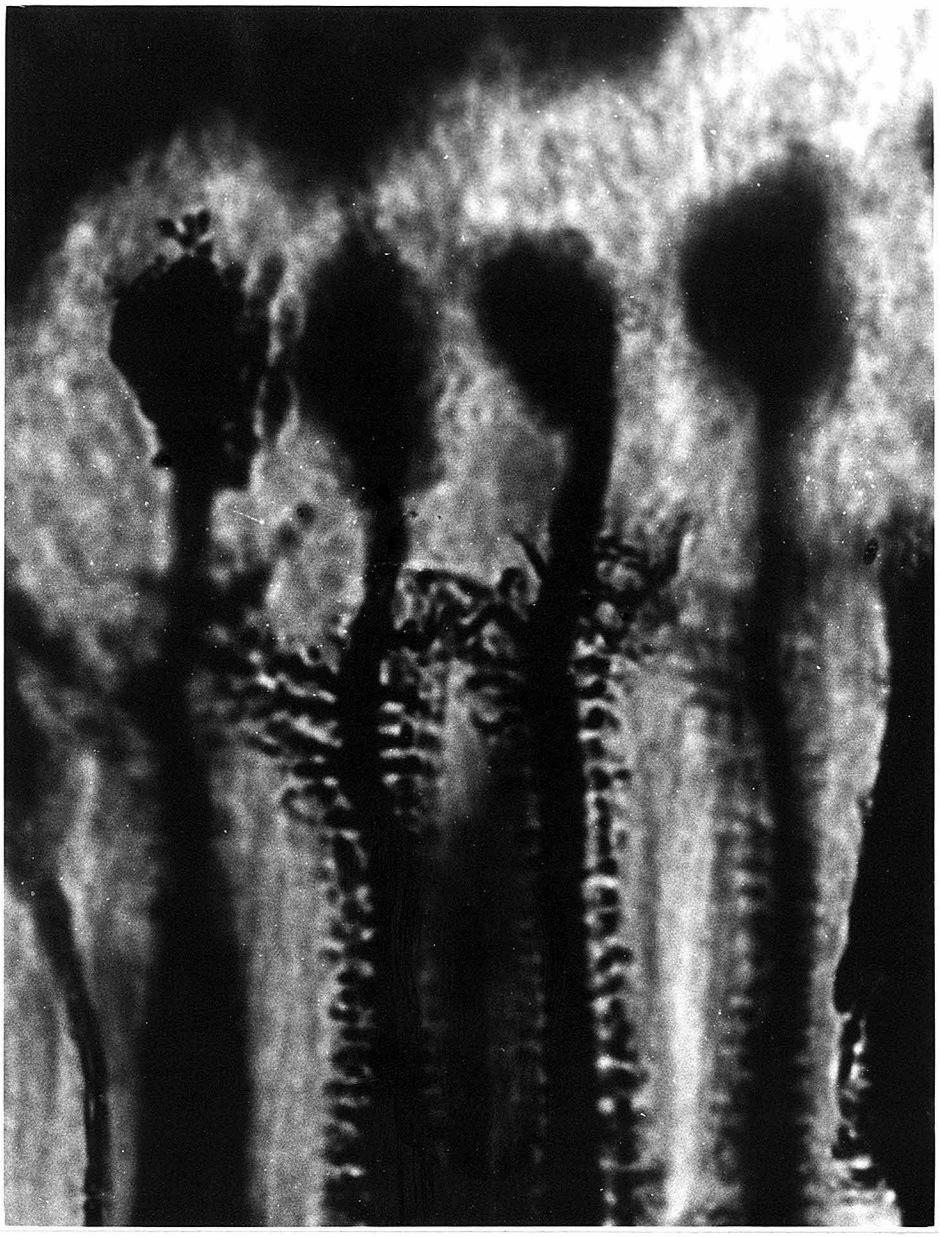

Plate I. Stratified radial diffuse monopolar neurons of the Phaenicia sericata retina stained with the Golgi technique of Straufeld and Blest (1970). The vertical extent of the plate is approximately the radial extent of the lamina or first synaptic plexus.

injection experiments. Current that depolarizes the membrane reduces the response amplitude to 10 Hz flicker light stimulation; current that hyperpolarizes the membrane enhances the response amplitude. The authors argued that, if the response were being generated by a passive resistance change mechanism, then the amplitude changes induced by the currents used would not be as large as the experimental results indicate.

In order to investigate the hypothesis of an active membrane mechanism, when monopolar-like responses were encountered, data were collected during continuous iontophoresis and simultaneous white noise light stimulation. Further, series of white noise experiments were conducted with different positions of the neutral density filter intervening in the optical path. The results of three cells are reported here, two with varying neutral density filter conditions and one with a series of current injections.

All three units were recorded with Ca^{++}-EGTA pipettes prepared as described in 'Materials and Methods'. Currents passed from the pipette into the monopolar were between -0.1 nA and +0.2 nA. It is unlikely that these small currents would pass significant amounts of either Ca^{++} or EGTA.

In order not to disturb the penetration stability, the indifferent electrode was left contacting the retina. Hence the responses recorded are those of the hyperpolarizing neuron minus the ERG. Since these units were obtained while seeking photoreceptor responses, they most likely represent penetrations in the lamina, just below the retina. Changes in extracellular potential that characteristically accompanied crossing of the basal membrane and entry into the lamina were observable but not large.

Further, the kernels obtained for the monopolar-like responses under the present recording conditions in Drosophila are much like those obtained from monopolars of Calliphora without the ERG subtracted (Mr. R. D. Fargason, Dr. G. D. McCann, personal communication). Therefore, this discussion will proceed on the supposition that the data collected closely reflect the monopolar neuron transmembrane potential up to DC shifts. Indeed, the results of the current injection experiment would be unobtainable if the data were not dominated by the intracellular hyperpolarizing response.

Figure 6.4 shows the first- and second-order kernels obtained from the two units for which the neutral density wedge position was varied. The first-order kernels are initially hyperpolarizing, then return to zero and cross it to form a small depolarizing component. At the lowest intensity stimulation there is no obvious overshoot. Increasing the amount of light stimulus passed through the neutral density filter shortens the time scale of the response of these units.

The second-order kernels show a consistent on-diagonal negative peak and an off-diagonal positive component. These are not apparent at the lowest intensity stimulation. With increasing stimulus level, both peaks increase in absolute value and move toward shorter times along with the first-order kernels. The positive peak in particular moves further off-diagonal and closer to the negative component.

Figure 6.5 shows the first- and second-order kernels for the unit into which currents were passed. In chronological order these were 0.0 nA, +0.1 nA, -0.1 nA, and +0.2 nA, the same order as the peak negative

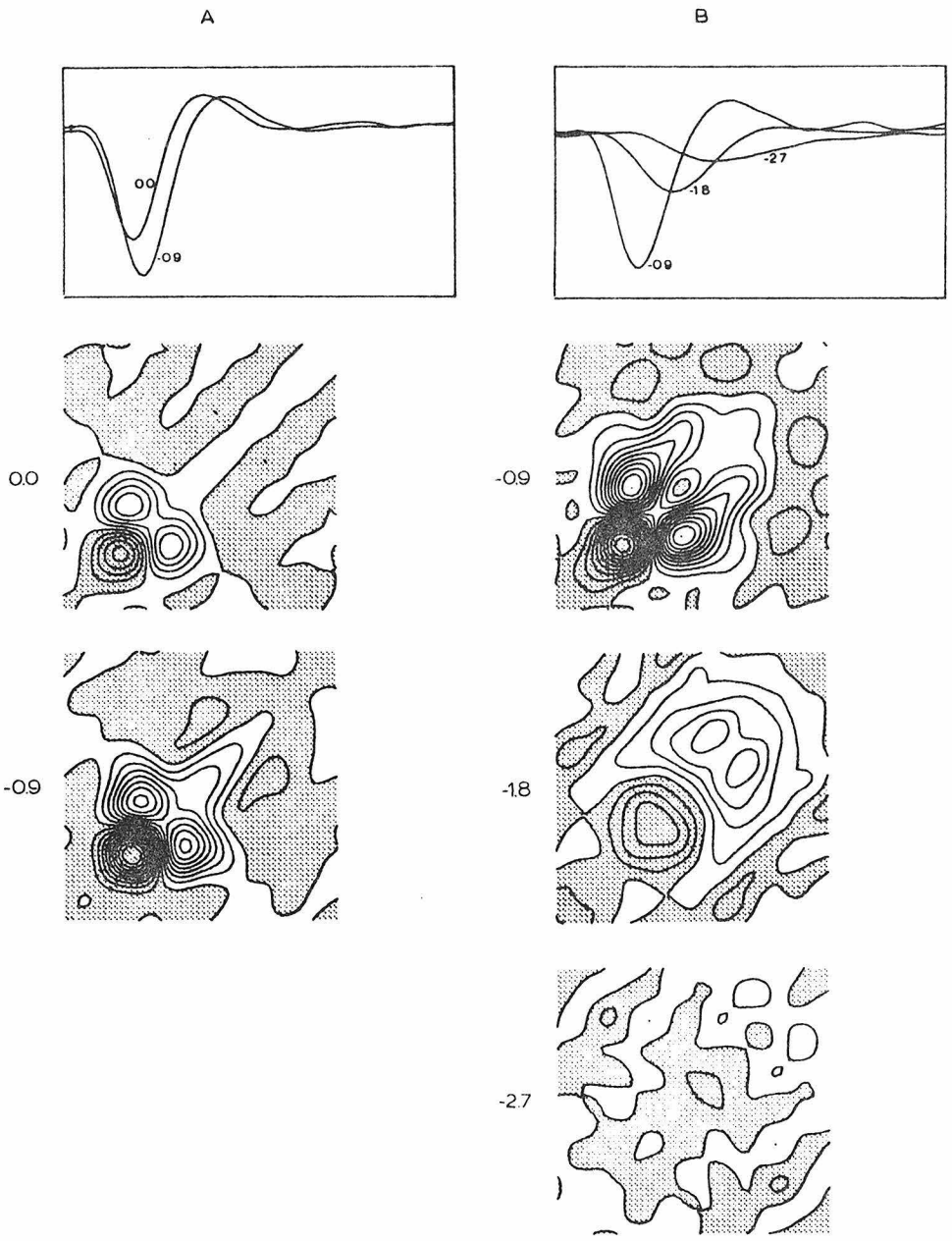

Figure 6.4. First- and second-order kernels from two monopolar neurons. Log light intensity differences from maximum are shown for each kernel. B) is the same cell as shown in fig. 6.3. The timing format is the same as that for fig. 6.1. First-order kernel vertical scales are A) $-5.42 \cdot 10^{-10}$ to $+2.03 \cdot 10^{-10}$ mV phot^{-1} cm^{-2} and B) $-2.99 \cdot 10^{-10}$ to $+ 1.19 \cdot 10^{-10}$ mV phot^{-1} cm^{-2}. Second-order kernel contours are A) $4.16 \cdot 10^{-19}$ mV phot^{-2} cm^{-4}, and B) $1.91 \cdot 10^{-19}$ mV phot^{-2} cm^{-4}.

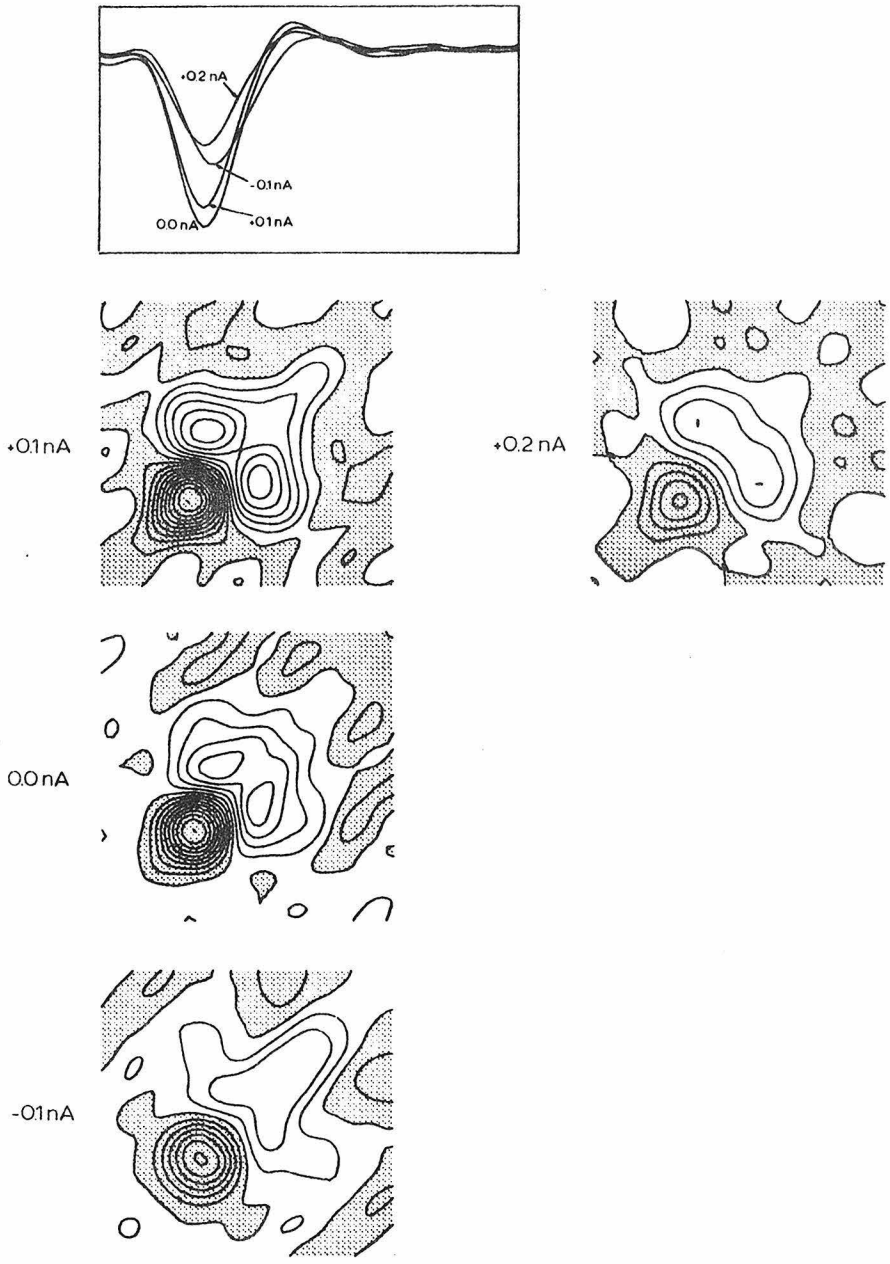

Figure 6.5. First- and second-order kernels from a monopolar neuron into which current was passed. The timing format is the same as that of figs. 6.1 and 6.4. First-order kernel vertical scales are $-2.54 \cdot 10^{-10}$ to $+6.35 \cdot 10^{-11}$ mV phot^{-1} cm^{-2}. Second-order contours are $2.12 \cdot 10^{-19}$ mV phot^{-2} cm^{-4}.

components of the first-order kernels. Loss of cell viability is evident, particularly for the final iontophoresis. Nevertheless, the increased delay to both the negative and positive peaks in the first-order kernel induced by hyperpolarizing current is eliminated in the final case by depolarizing current. The time course of response is re-established by positive current even as the magnitude of response is being lost.

The second-order kernels show coherent changes to iontophoresis as well. Current that hyperpolarizes the neuron diminishes the positive peak and brings it closer to the diagonal; current that depolarizes the neuron enhances the positive peak and brings it farther off-diagonal and closer to the negative peak. Even for the final iontophoresis of +0.2 nA, when the absolute value of both peaks is diminished, the positive peak has been translated farther off-diagonal than that for the first iontophoresis of +0.1 nA.

Table VI.2 tabulates the time delays and peaks of the first- and second-order kernels. The second-order kernels are now the primed variables $h_2'(\tau,\Delta\tau) = h_2(\tau,\tau + \Delta\tau)$, for convenience. In all cases the following order of timing is preserved, in increasing order:

i) time τ of $h_2'(\tau,0)$ on-diagonal negative peak

ii) time τ of $h_1(\tau)$ negative peak

iii) time τ of $h_2'(\tau,\Delta\tau)$ off-diagonal positive peak

iv) time τ of $h_1(\tau)$ positive peak.

Therefore the effect of the second-order kernel is to advance the timing of both the hyperpolarization and the repolarization of the first-order kernel in the presence of a second light pulse. Both increasing the level

Table VI.2. Times of peaks in msec of the negative and positive components of the kernels of figs. 6.4 and 6.5.

Cell figure		Negative Peaks		Positive Peaks			
		$\tau; \lvert h_1(\tau) \rvert_{max}$	$\tau; \lvert h_2'(\tau,0) \rvert_{max}$	$\tau; h_1(\tau)_{max}$	$\tau; h_2'(\tau,\Delta\tau)_{max}$	$\Delta\tau; h_2'(\tau,\Delta\tau)_{max}$	$h_{2;max}/h_{1;max}^2$
	log intensity						
6.4a	0.0	12.8	11	26.0	20	8	3.59
	-0.9	14.6	12	29.6	22	8	5.83
6.4b	-0.9	15.1	12	32.2	23	9	6.95
	-1.8	21.6	18	41.3	35	6	95.7
	-2.7	30.0	27	49.7(?)	45	9	*
	current (nA)						
6.5	-0.1	19.6	17	38.9	31	2	15.2
	0.0	18.2	16	34.1	27	6	11.2
	+0.1	17.96	15	33.2	27	9	9.35
	+0.2	18.0	15	33.6	29	11	9.40

of light stimulation and decreasing the transmembrane potential decrease these times and hence advance the response. Analogously, increasing the light and depolarizing the cell both increase the strength of both positive and negative peaks in the second-order kernels. Finally, the ratio for the positive peaks, $h_{2;max}/h^2_{1;max}$, decreases under both these conditions. Exceptions to these observations are evident, but they are limited to the extreme cases of light stimulation and to the case of +0.2 nA iontophoresis. The log light intensity level for the current-injected cell was -1.5, within the range -1.8 to -0.9 for which all of these observations hold.

A direct relation between response amplitude and current passage, as has been shown in Calliphora monopolars (Zettler & Järvilehto, 1971), has not been demonstrated in the present study. However, in order to preserve the Drosophila unit recording stability, very low currents were used. The range used by Zettler and Järvilehto was -5 nA to +0.7 nA. Their data for -0.2 nA to +0.1 nA do not show significant change.

The function of the neutral density filter as used in this series of experiments should be carefully explained. Decreasing the filter intervention in the light stimulus increases both the average light intensity and the Wiener power level of the white noise stimulus. Increasing the light intensity further hyperpolarizes the neuron; increasing the Wiener stimulus power increases the dynamic range of response. However, as seen in fig. 6.3, the steady state hyperpolarization to light pulses of increasing intensity is not large. This contrasts with the ranges of the first-order kernels, which are sensitive to neutral density filter change.

The results presented here help confirm the hypothesis of Zettler and

Järvilehto that the monopolar membrane potential exhibits an active or voltage-dependent component. As the Wiener power of the stimulus is increased, the first- and second-order kernels undergo characteristic shifts in the timing of their peaks. The direction of change of all of these shifts is mimicked by progressing from hyperpolarizing to depolarizing current. If the membrane were electrically passive, no change in the timing of the peaks would be seen. The consistency of the changes demonstrated is evidence that they reflect the voltage dependence of the membrane resistance dynamics. The voltage dependence must in turn subserve the regenerative nature of the monopolar axonal response.

Conclusion

This chapter has described experiments using random light intensity stimuli with Gaussian probability distribution to characterize the responses of retinal neurons in Drosophila during continuous iontophoresis. Since recording stability in these neurons is difficult to maintain, currents used in iontophoresis must be kept small. This in turn renders only subtle changes in response, particularly evident for the monopolar data presented here. It is to the experimental advantage to extract the most information from the neuron in the shortest possible time. The white noise method is undoubtedly the most sensitive available to detect subtle differences in stationary dynamics.

The photoreceptor is, for light input heavily distributed about a mean level, a linear conductance-modulating cell. The nonlinearities of the receptor potential detected by second- and third-order Wiener kernels derive largely from the resistive character of the plasma membrane.

The monopolar hyperpolarizing response is mediated by an electrically active membrane. As the cell is progressed from being artifically hyperpolarized to artifically depolarized, the response dynamics mimic removal of neutral density filter intervention in the light stimulus. Hence, decreasing membrane polarization mimics increasing the Wiener power of the light stimulus. This characterization contributes to our understanding of an unusual slow-potential, regenerative neuron.

The conclusions attained in this chapter depend upon the use of both white noise stimuli and iontophoresis. Either of these methodologies applied alone to the Drosophila visual system would not enable these results. The membrane physiology of Drosophila visual neurons has been addressed by a new combination of techniques.

References

Abramowitz, M., I. A. Stegun, Eds.; Handbook of Mathematical Functions with Formulas, Graphs, and Mathematical Tables. Washington, D.C.: National Bureau of Standards, Applied Mathematics Series No. 55 (1964).

Adolph, A. R.; Spontaneous slow potential fluctuations in the Limulus photoreceptor. J. Gen. Physiol. 48, 297-322 (1964).

Agin, D. P.; Electrochemical properties of glass microelectrodes. In: Lavalle'e, M., O. F. Schanne, N. C. He'bert, Eds. Glass Microelectrodes. p. 62-75, New York: John Wiley and Sons, Inc. (1969).

Alawi, A. A.-S.; Electrophysiological Investigation of Genetically Dissected Visual Processes in 'Drosophila melanogaster'. Thesis, Purdue University (1972).

Alawi, A. A., V. Jennings, J. Grossfield, W. L. Pak; Phototransduction mutants of Drosophila melanogaster. In: Arden, G. B., Ed. The Visual System; Neurophysiology, Biophysics and Their Clinical Applications. p. 1-21, New York: Plenum Press (1972).

Arnett, D. W.; Information Processing by the First Optic Ganglion in Dipterans. Thesis, California Institute of Technology (1971).

Arnett, D. W.; Spatial and temporal integration properties of units in first optic ganglion of Dipterans. J. Neurophysiol. 35, 429-44 (1972).

Bader, C. R., F. Baumann, D. Bertrand; Role of intracellular calcium and sodium in light adaptation in the retina of the honey bee drone (Apis mellifera L.). J. Gen. Physiol. 67, 475-91 (1976).

Baker, P. F.; Transport and metabolism of calcium ions in nerve. Prog. Biophys. Molec. Biol. 24, 177-223 (1972).

Baker, P. F., A. C. Crawford; Mobility and transport of magnesium in squid giant axons. J. Physiol. 227, 855-74 (1972).

Baylor, D. A., A. L. Hodgkin, T. D. Lamb; Reconstruction of the electrical responses of turtle cones to flashes and steps of light. J. Physiol. 242, 759-91 (1974).

Behbehani, M., R. Srebro; Discrete waves and phototransduction in voltage-clamped ventral photoreceptors. J. Gen. Physiol. 64, 186-200 (1974).

Behrens, M., W. Krebs; The effect of light-dark adaptation on the ultra-structure of Limulus lateral eye retinular cells. J. Comp. Physiol. 107, 77-96 (1976).

Benzer, S.; Behavioral mutants of Drosophila isolated by countercurrent distribution. Proc. Nat. Acad. Sci. 58, 1112-9 (1967).

Boley, B. A.; A method of heat conduction analysis of melting and solidification problems. J. Mathematics Physics 40, 300-13 (1961).

Borsellino, A. I., M. G. F. Fuortes; Interpretation of responses of visual cells of Limulus. Proc. I.E.E.E. 56, 1024-32 (1968).

Boschek, C. B.; On the fine structure of the peripheral retina and Lamina ganglionaris of the fly, Musca domestica. Z. Zellforsch. 118, 369-409 (1971).

Bownds, D., A. E. Brodie; Light-sensitive swelling of isolated frog rod outer segments as an in vitro assay for visual transduction and dark adaptation. J. Gen. Physiol. 66, 407-25 (1975).

Bownds, D., J. Dawes, J. Miller, M. Stahlman; Phosphorylation of frog photoreceptor membranes induced by light. Nature New Biol. 237, 125-7 (1972).

Boyce, W. E., R. C. DiPrima ; Elementary Differential Equations and Boundary Value Problems. New York: John Wiley and Sons, Inc. (1969).

Brown, A. M., P. S. Baur, Jr., F. H. Tuley, Jr.; Phototransduction in Aplysia neurons: Calcium release from pigmented granules is essential. Science 188, 157-60 (1975).

Brown, J. E., J. R. Blinks; Changes in intracellular free calcium concentration during illumination of invertebrate photoreceptors; Detection with aequorin. J. Gen. Physiol. 64, 643-65 (1974).

Brown, A. M., H. M. Brown; Light response of a giant Aplysia neuron. J. Gen. Physiol. 62, 239-54 (1973).

Brown, H. M., S. Hagiwara, H. Koike, R. M. Meech; Membrane properties of a barnacle photoreceptor examined by the voltage clamp technique. J. Physiol. 208, 385-413 (1970).

Brown, J. E., J. E. Lisman; Intracellular Ca modulates sensitivity and time scale in Limulus ventral photoreceptors. Nature 258, 252-4 (1975).

Brown, J. E., M. I. Mote; Ionic dependence of reversal voltage of the light response in Limulus ventral photoreceptors. J. Gen. Physiol. 63, 337-50 (1974).

Campbell, G. A., R. M. Foster; Fourier Integrals for Practical Applications. American Telephone and Telegraph Company (1931).

Carafoli, E., M. Crompton; The regulation of intracellular calcium. In: Bronner, F., A. Kleinzeller, Eds. Current Topics in Membranes and Transport, V. 10, p. 151-216, New York: Academic Press (1978).

Chowdhury, T. K.; Techniques of intracellular microinjection. In: Lavalle'e, M., O. F. Schanne, N. C. He'bert, Eds. Glass Microelectrodes. p. 404-23, New York: John Wiley and Sons, Inc. (1969).

Cone, R. A.; Rotational diffusion of rhodopsin in the visual receptor membrane. Nature New Biol. 236, 39-43 (1972).

Cone, R. A.; The internal transmitter model for visual excitation: Some quantitative implications. In: Langer, H., Ed. Biochemistry and Physiology of Visual Pigments. p. 275-82, New York: Springer-Verlag (1973).

Cosens, D. J., A. Manning; Abnormal electroretinogram from a Drosophila mutant. Nature 224, 285-7 (1969).

Crank, J.; The Mathematics of Diffusion. Oxford: The Clarendon Press (1956).

Deland, M. C., W. L. Pak; Reversibly temperature sensitive phototransduction mutant of Drosophila melanogaster. Nature New Biol. 244, 184-6 (1973).

Dodge, F. A., Jr., B. W. Knight, J. Toyoda; Voltage noise in Limulus visual cells. Science 160, 88-90 (1968).

Dowling, J. E.; Discrete potentials in the dark-adapted eye of the crab Limulus. Nature 217, 28-31 (1968).

Ephrussi, B., G. W. Beadle; A technique of transplantation for Drosophila. Am. Nat. 70, 218-25 (1936).

Fargason, R. D., G. D. McCann; Response properties of the peripheral retinula cells within Drosophila visual mutants to monochromatic Gaussian white-noise stimuli. Vis. Res. 18, 809-13 (1978).

Fein, A., J. Lisman; Localized desensitization of Limulus photoreceptors produced by light or intracellular calcium ion injection. Science 187, 1094-6 (1975).

Ferris, G. F.; External morphology of the adult. In: Demerec, M., Ed. Biology of Drosophila. p. 368-419, New York: John Wiley and Sons, Inc. (1950).

Fischbach, G. D., P. G. Nelson; Cell culture in neurobiology. In: Brookhart, J. M., V. B. Mountcastle, E. R. Kandel, S. R. Geiger, Eds. Handbook of Physiology, Sect. 1.The Nervous System. Vol. 1. Cellular Biology of Neurons, Part 2. p. 719-74, Bethesda: American Physiological Society (1977).

Friedman, A.; Partial Differential Equations of Parabolic Type. Englewood Cliffs, N. J.: Prentice-Hall, Inc. (1964).

Fulpius, B., F. Baumann; Effects of sodium, potassium, and calcium ions on slow and spike potentials in single photoreceptor cells. J. Gen. Physiol. 53, 541-61 (1969).

Fuortes, M. G. F., A. L. Hodgkin; Changes in time scale and sensitivity in the ommatidia of Limulus. J. Physiol. 172, 239-63 (1964).

Fuortes, M. G. F., S. Yeandle; Probability of occurrence of discrete potential waves in the eye of Limulus. J. Gen. Physiol. 47, 443-63 (1964).

Gorman, A. L. F., J. S. McReynolds; Control of membrane K^+ permeability in a hyperpolarizing photoreceptor: Similar effects of light and metabolic inhibitors. Science 185, 620-1 (1974).

Gradshteyn, I. S., I. M. Ryzhik; Table of Integrals, Series, and Products. New York: Academic Press (1965).

Hagins, W. A.; Electrical signs of information flow in photoreceptors. Cold Spring Harb. Symp. Quant. Biol. 30, 403-18 (1965).

Hagins, W. A.; The visual process: Excitatory mechanisms in the primary receptor cells. Ann. Rev. Biophys. Bioeng. 1, 131-58 (1972).

Hagins, W. A., S. Yoshikami; A role for Ca^{2+} in excitation of retinal rods and cones. Exp. Eye Res. 18, 299-305 (1974)..

Hanani, M., P. Hillman; Adaptation and facilitation in the barnacle photoreceptor. J. Gen. Physiol. 67, 235-49 (1976).

Harris, W. A., W. S. Stark, J. A. Walker; Genetic dissection of the photoreceptor system in the compound eye of Drosophila melanogaster. J. Physiol. 256, 415-39 (1976).

Hecht, S.; Photochemistry of visual purple. II. The effect of temperature on the bleaching of visual purple by light. J. Gen. Physiol. 3, 285-90 (1921).

Heisenberg, M., K. G. Götz; The use of mutations for the partial degradation of vision in Drosophila melanogaster. J. Comp. Physiol. 98, 217-41 (1975).

Hochstein, S., B. Minke, P. Hillman; Antagonistic components of the late receptor potential in the barnacle photoreceptor arising from different stages of the pigment process. J. Gen. Physiol. 62, 105-28 (1973).

Hotta, Y., S. Benzer; Abnormal electroretinograms in visual mutants of Drosophila. Nature 222, 354-6 (1969).

Hotta, Y., S. Benzer; Genetic dissection of the Drosophila nervous system by means of mosaics. Proc. Nat. Acad. Sci. 67, 1156-63 (1970).

Hotta, Y., S. Benzer; Mapping of behavior in Drosophila mosaics. Nature 240, 527-35 (1972).

Ikeda, K., W. D. Kaplan; Patterned neural activity of a mutant Drosophila melanogaster. Proc. Nat. Acad. Sci. 66, 765-72 (1970a).

Ikeda, K., W. D. Kaplan; Unilaterally patterned neural activity of gynandromorphs, mosaic for a neurological mutant of Drosophila melanogaster. Proc. Nat. Acad. Sci. 67, 1480-7 (1970b).

Ikeda, K., S. Ozawa, S. Hagiwara; Synaptic transmission reversibly conditioned by single-gene mutation in Drosophila melanogaster. Nature 259, 489-91 (1976).

Jan, Y. N., L. Y. Jan; Two mutations of synaptic transmission in Drosophila. Proc. Roy. Soc. Lond. B 198, 87-108 (1977).

Järvilehto, M., F. Zettler; Localized intracellular potentials from pre- and post-synaptic components in the external plexiform layer of an insect retina. Z. Vergl. Physiol. 75, 422-40 (1971).

Katz, B.; Nerve, Muscle, and Synapse. New York: McGraw-Hill Book Company (1966).

Kirschfeld, K.; Discrete and graded receptor potentials in the compound eye of the fly (Musca). In: Bernhard, C. G., Ed. The Functional Organization of the Compound Eye. p. 291-307, Oxford: Permagon Press (1966).

Kühn, H., J. H. Cook, W. J. Dreyer; Phosphorylation of rhodopsin in bovine photoreceptor membranes. A dark reaction after illumination. Biochem. 12, 2495-502 (1973).

Kushmerick, M. J., R. J. Podolsky; Ionic mobility in muscle cells. Science 166, 1297-8 (1969).

Lee, Y. W., M. Schetzen; Measurement of the kernels of a nonlinear system by crosscorrelation. Quart. Prog. Rept. No. 60, Res. Lab. Elect., M.I.T. (1961).

Lettvin, J. Y., W. F. Pickard, W. S. McCulloch, W. Pitts; A theory of passive ion flux through axon membranes. Nature 202, 1338-9 (1964).

Lisman, J. E., J. E. Brown; The effects of intracellular Ca^{2+} on the light response and on light adaptation in Limulus ventral photoreceptors. In: Arden, G. B., Ed. The Visual System;Neurophysiology, Biophysics, and their Clinical Applications. p. 23-33, New York: Plenum Press (1972a).

Lisman, J. E., J. E. Brown; The effects of intracellular iontophoretic injection of calcium and sodium ions on the light response of Limulus ventral photoreceptors. J. Gen. Physiol. 59, 701-19 (1972b).

Lisman, J. E., J. E. Brown: Light-induced changes of sensitivity in Limulus ventral photoreceptors. J. Gen. Physiol. 66, 473-88 (1975a).

Lisman, J. E., J. E. Brown; Effects of intracellular injection of calcium buffers on light adaptation in Limulus ventral photoreceptors. J. Gen. Physiol. 66, 489-506 (1975b).

Lindsley, D. L., E. H. Grell; Genetic Variations of 'Drosophila melanogaster'. Washington, D.C.: Carnegie Institution of Washington Publication No. 627 (1967).

Marmarelis, P. Z.; Nonlinear Dynamic Transfer Functions for Certain Retinal Neuronal Systems. Thesis, California Institute of Technology (1971).

Marmarelis, P. Z., G. D. McCann; Development and application of white-noise modeling techniques for studies of insect visual nervous system. Kybernetik 12, 74-89 (1973).

Marmarelis, P. Z., K.-I. Naka; Nonlinear analysis and synthesis of receptive-field responses in the catfish retina. I. Horizontal cell to ganglion cell chain. J. Neurophysiol. 36, 605-18 (1973a).

Marmarelis, P. Z., K.-I. Naka; Nonlinear analysis and synthesis of receptive-field responses in the catfish retina. II. One-input white-noise analysis. J. Neurophysiol. 36, 619-33 (1973b).

Martinez, J. M., II, R. Srebro; Calcium and the control of discrete wave latency in the ventral photoreceptor of Limulus. J. Physiol. 261, 535-62 (1976).

McCann, G. D., R. D. Fargason, V. T. Shantz; The response properties of retinula cells in the fly Calliphora erythrocephala as a function of the wavelength and polarization properties of visible and ultraviolet light. Biol Cybernetics 26, 93-107 (1977).

McDonald, H. S.; Note on the use of glow modulator lamps for studies of vision. J. Opt. Soc. Am. 50, 1138 (1960).

Millecchia, R., A. Mauro; The ventral photorecepor cells of Limulus. II. The basic photoresponse. J. Gen. Physiol. 54, 310-30 (1969a).

Millecchia, R., A. Mauro; The ventral photoreceptor cells of Limulus. III. A voltage-clamp study. J. Gen. Physiol. 54, 331-51 (1969b).

Miller, W. H.; Cyclic nucleotides and photoreception. Exp. Eye Res. 16, 357-63 (1973).

Miller, W. H., R. E. Gorman, M. W. Bitensky; Cyclic adenosine monophosphate: Function in photoreceptors. Science 174, 295-7 (1971).

Minke, B., Ch.-F. Wu, W. L. Pak; Isolation of light-induced response of the central retinula cells from the electroretinogram of Drosophila. J. Comp. Physiol. 98, 345-55 (1975a).

Minke, B., Ch.-F. Wu, W. L. Pak; Induction of photoreceptor voltage noise in the dark in Drosophila mutant. Nature 258, 84-7 (1975b).

Mullins, L. J., F. J. Brinley, Jr.; Calcium binding and regulation in nerve fibers. In: Wasserman, R. H., R. A. Carradino, E. Carafoli, R. H. Kretsinger, D. H. MacLennan, F. L. Siegel, Eds. Calcium-Binding Proteins and Calcium Function. p. 87-96, New York: Elsevier North-Holland, Inc. (1977).

Naka, K.-I., S. Inoma, Y. Kosugi, Ch.-W. Tong; Recording of action potentials from single cells in the frog retina. Jap. J. Physiol. 10, 436-42 (1960).

Ostroy, S. E., W. L. Pak; Protein differences associated with a phototransduction mutant of Drosophila. Nature New Biol. 243, 120-1 (1973).

Ostroy, S. E., W. L. Pak; Protein and electroretinogram changes in the alleles of the norp A^{P12} Drosophila phototransduction mutant. Biochim. Biophys. Acta 368, 259-68 (1974).

Ostroy, S. E., M. Wilson, W. L. Pak; Drosophila rhodopsin: Photochemistry, extraction and differences in the norp A^{P12} phototransduction mutant. Biochem. Biophys. Res. Comm. 59, 960-6 (1974).

Pak, W. L., J. Grossfield, K. S. Arnold; Mutants of the visual pathway of Drosophila melanogaster. Nature 227, 518-20 (1970).

Pak, W. L., J. Grossfield, N. V. White; Nonphototactic mutants in a study of vision of Drosophila. Nature 222, 351-4 (1969).

Pak, W. L., D. Hartl, K. G. Götz;'Neurobiology of Drosophila'. Cold Spring Harbor Laboratory of Quantitative Biology, Cold Spring Harbor, New York (1974).

Pak, W. L., S. E. Ostroy, M. C. Deland, C.-F. Wu; Photoreceptor mutant of Drosophila: Is protein involved in intermediate steps of phototransduction? Science 194, 956-9 (1976).

Pak, W. L., L. H. Pinto; Genetic approach to the study of the nervous system. Ann. Rev. Biophys. Bioeng. 5, 397-448 (1976).

Prince, W. T., M. J. Berridge, H. Rasmussen; Role of calcium and adenosine-3':5'-cyclic monophosphate in controlling fly salivary gland secretion. Proc. Nat. Acad. Sci. 69, 553-7 (1972).

Rasmussen, H.; Cell communication, calcium ion, and cyclic adenosine monophosphate. Science 170, 404-12 (1970).

Reuben, J. P., P. W. Brandt, H. Grundfest; Regulation of myoplasmic calcium concentration in intact crayfish muscle fibers. J. Mechanochem. Cell Motility 2, 269-85 (1974).

Ribi, W. A.; Gap junctions coupling photoreceptor axons in the first optic ganglion of the fly. Cell Tiss. Res. 195, 299-308 (1978).

Rose, B., W. R. Loewenstein; Permeability of cell junction depends on local cytoplasmic calcium activity. Nature 254, 250-2 (1975).

Schmid, R. W., C. N. Reilley; New complexon for titration of calcium in the presence of magnesium. Anal. Chem. 29, 264-8 (1957).

Scholes, J. H.; Discrete subthreshold potentials from the dimly lit insect eye. Nature 202, 572-3 (1964).

Srebro, R.; A thermal component of excitation in the lateral eye of Limulus. J. Physiol. 187, 417-25 (1966).

Srebro, R., M. Behbehani; A stochastic model for discrete waves in the Limulus photoreceptor. J. Gen. Physiol. 58, 267-86 (1971).

Srebro, R., M. Behbehani; The thermal origin of spontaneous activity in the Limulus photoreceptor. J. Physiol. 224, 349-61 (1972).

Srebro, R., M. Behbehani; Light adaptation in the ventral photoreceptor of Limulus. J. Gen. Physiol. 64, 166-85 (1974).

Strausfeld, N. J.; The organization of the insect visual system (light microscopy). I. Projections and arrangements of neurons in the Lamina ganglionaris of Dipterans. Z. Zellforsch. 121, 377-441 (1971).

Strausfeld, N. J., A. D. Blest; Golgi studies on insects. Part I. The optic lobes of Lepidoptera. Proc. Roy. Soc. Lond. B 258, 81-134 (1970).

Tomita, T.; Single and coaxial microelectrodes in the study of the retina. In: Lavalle'e, M., O. F. Schanne, N. C. He'bert, Eds. Glass Microelectrodes. p. 124-53, New York: John Wiley and Sons, Inc. (1969).

Wald, G., P. K. Brown, I. R. Gibbons; The problem of visual excitation. J. Opt. Soc. Am. 53, 20-35 (1963).

Walker, J. L., Jr.; Ion specific liquid ion exchanger microelectrodes. Anal. Chem. 43 (3), 89A-93A (1971).

Walker, J. L.; Ion-selective liquid ion exchanger microelectrodes. In: Kessler, M., L. C. Clark, Jr., D. W. Lübbers, I. A. Silver, W. Simon, Eds. Ion and Enzyme Electrodes in Biology and Medicine. p. 116-8, Baltimore: University Park Press (1976).

Wiener, N.; Nonlinear Problems in Random Theory. Cambridge, Massachusetts: The M.I.T. Press (1958).

Williams, R. J. P.; Calcium chemistry and its relation to protein binding. In: Wasserman, R. H., R. A. Carradino, E. Carafoli, R. H. Kretsinger, D. H. MacLennan, F. L. Siegel, Eds. Calcium-Binding Proteins and Calcium Function. p. 3-12, New York: Elsevier North-Holland, Inc. (1977).

Wolken, J. J., J. Capenos, A. Turano; Photoreceptor structures. III. Drosophila melanogaster. J. Biophys. Biochem. Cytol. 3, 441-7 (1957).

Wu, Ch.-F., W. L. Pak; Quantal basis of photoreceptor spectral sensitivity of Drosophila melanogaster. J. Gen. Physiol. 66, 149-68 (1975).

Wulff, V. J.; The effect of cyclic AMP on Limulus lateral eye retinular cells. Vis. Res. 11, 1493-5 (1971).

Yeandle, S., J. B. Spiegler; Light-evoked and spontaneous discrete waves in the ventral nerve photoreceptor of Limulus. J. Gen. Physiol. 61, 552-71 (1973).

Yoshikami, S., W. A. Hagins; Light, calcium, & the photocurrent of rods & cones. Biophys. Soc. Abstr. 15, 47A (1971).

Yoshikami, S., W. A. Hagins; Control of the dark current in vertebrate rods and cones. In: Langer, H., Ed. Biochemistry and Physiology of Visual Pigments. p. 245-55, New York: Springer-Verlag (1973).

Zettler, F., M. Järvilehto; Decrement-free conduction of graded potentials along the axon of a monopolar neuron. Z. Vergl. Physiol. 75, 402-21 (1971).